NATIONAL ADVISORY COMMITTEE FOR AERONAUTICS

TECHNICAL NOTE 3781

HANDBOOK OF STRUCTURAL STABILITY

PART I - BUCKLING OF FLAT PLATES

By George Gerard and Herbert Becker

New York University

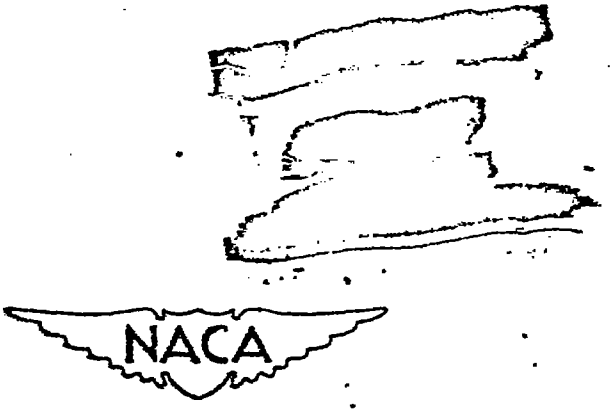

Washington
July 1957

TABLE OF CONTENTS

NATIONAL ADVISORY COMMITTEE FOR AERONAUTICS

TECHNICAL NOTE 3781

HANDBOOK OF STRUCTURAL STABILITY

PART I - BUCKLING OF FLAT PLATES

By George Gerard and Herbert Becker

SUMMARY

The various factors governing buckling of flat plates are critically reviewed and the results are summarized in a comprehensive series of charts and tables. Numerical values are presented for buckling coefficients of flat plates with various boundary conditions and applied loadings. The effects of plasticity are incorporated in nondimensional buckling charts utilizing the three-parameter description of stress-strain curves.

INTRODUCTION

This "Handbook of Structural Stability" presents a rather comprehensive review and compilation of theories and experimental data relating to the buckling and failure of plate elements encountered in the airframe. To meet the anticipated needs of those who would use this review and compilation, it appeared best to adopt a handbook style of presentation. The material is not intended as a textbook in which the emphasis is often on the mathematical development of different types of related problems. Neither is it intended to compete with the familiar aircraft-company structures manuals which generally present design information, empirical data, and methods of extending results beyond the scope of the original report.

This handbook attempts to cover the generally neglected area between the textbook and the structures manual. No attempt is made to present an exhaustive coverage of mathematical techniques which are of great importance in the solution of buckling problems. This material has been well presented in several excellent books and papers which are included in the reference list. The subject of columns is comprehensively treated in several books and, therefore, the inclusion of such material in this review did not appear to be warranted.

This presentation primarily constitutes a critical review of developments concerning buckling and failure of plate elements since the early 1940's. This date has been selected since the last comprehensive review of this nature (ref. 1) appeared at that time.

In order to meet the varying needs of airframe designers and analysts, structures methods, and research engineers, it appears best to organize this handbook as follows: The main text discusses assumptions, limitations, and background of the available literature; the appendix contains a summary of this material and indicates the manner in which this information is to be used in analysis and design. It is anticipated that, after the material in the main text has been reviewed, reference to only the appendix will be made in a majority of routine applications. The duplication in these two main parts has been held to a minimum consistent with completeness and intelligibility.

In the main text of this report, the various factors appearing in the general buckling-stress equation

$$\sigma_{cr}(\text{or } \tau_{cr}) = \eta\bar{\eta}\frac{k\pi^2 E}{12\left(1 - \nu_e^2\right)}\left(\frac{t}{b}\right)^2 \qquad (1)$$

are critically examined from the standpoint of their theoretical development and the agreement of theory with test data.

In the section entitled "Basic Principles" a brief review of the basic mathematical principles involved in solution of buckling problems is given. The primary objective in presenting this material is to acquaint the reader with the approximate methods used in order to be able to indicate the accuracy of the results of particular solutions discussed in subsequent sections.

In the section entitled "Boundary Conditions" the influence of the geometric boundary conditions upon the buckling stress is discussed at some length. It is indicated that the use of a free unloaded edge in a plate involves Poisson's ratio in the compressive buckling coefficient. As an example, the buckling coefficients for plate columns, flanges, and simply supported plates are determined from theory to demonstrate the effect of various boundary conditions upon the behavior of such elements.

Also, the three-parameter method of mathematically describing stress-strain relations is presented in an introductory manner in the section entitled "Stress-Strain Relations in the Yield Region." Use of this method affords a considerable simplification in the presentation of results of inelastic buckling theories.

The effects of exceeding the proportional limit of a material are incorporated in a plasticity-reduction factor η. Because of the various theories that have been recently advanced together with the fact that no one publication has reviewed the conflicting assumptions of

these theories from the standpoint of engineering results, a rather comprehensive treatment of this subject is presented in the section entitled "Plasticity-Reduction Factors."

The effect of cladding upon the buckling stress of flat plates has been treated by an extension of inelastic-buckling theory. In the section entitled "Cladding Reduction Factors" a simplified treatment of buckling of clad plates is presented in which values for the cladding correction factor $\bar{\eta}$ are derived.

The background for determining the elastic-buckling coefficient k has been well documented. Therefore, the last sections are concerned with the buckling coefficients for a large number of cases. The presentation consists, for the most part, of a straightforward cataloging of results in the form of buckling-coefficient charts.

The appendix has been organized for unimpeded use in analysis and design and for this reason no references appear in this portion of the report. The references are examined in detail in the pertinent part of the main text. The literature is reviewed and discussed both as to content and application to the particular problem. Experimental evidence is presented where it tends to substantiate one theory among several which may have been advanced on a particular phase of the buckling problem; plasticity-reduction factors are perhaps the most conspicuous example of this. Thus, the recommendation for a particular theory is generally supported by experimental data.

The main text also contains some new material developed during the course of this compilation. Although such material is important to the unification of prior results, it has not been considered of sufficient consequence to merit separate publication. Therefore, when such material does appear in this handbook it is in a detailed form.

This survey was conducted under the sponsorship and with the financial assistance of the National Advisory Committee for Aeronautics.

SYMBOLS

A_r	area of rib cross section, sq in.
a	long dimension of plate, usually unloaded edge in uniaxial compression, in.
b	short dimension of plate, usually loaded edge in uniaxial compression, in.

$C_1 \ldots C_5$	coefficients in general inelastic-plate-buckling equation (see section entitled "Basic Principles")
$c_1 \ldots c_4$	coefficients in elastic-plate-buckling equation to be determined by geometrical boundary conditions along unloaded edges of plate
D	plate cross-section rigidity, $Et^3/12(1 - \nu^2)$, lb-in.
D'	plastic plate cross-section rigidity, $E_s t^3/9$, lb-in.
E	Young's modulus, psi
E_s	secant modulus, σ/ϵ
E_t	tangent modulus, $d\sigma/d\epsilon$
$\bar{E}_s, \bar{E}_t$	secant and tangent modulus for clad plates, respectively
f	ratio of total cladding thickness to total plate thickness
G	shear modulus
$g = \log_e \beta$	
I	moment of inertia
$j = (E_s/E)\left(1 - \nu_e^2\right)(1 - \nu^2)$	
K	modified buckling coefficient, $k\pi^2/12(1 - \nu^2)$
k	buckling coefficient
L	length of plate, in.
M	bending moment applied in plane of plate, in-lb
N	axial load, lb/in.
n	number of longitudinal half waves in buckled plate; also, shape parameter for stress-strain curve
P	normal load applied in plane of plate, σtb, lb
p	normal pressure, psi

$\bar{p} = \bar{\alpha}^2 - \nu_e(\pi b/\lambda)^2$

q shear loading, lb/in.

$\bar{q} = \bar{\beta}^2 + \nu_e(\pi b/\lambda)^2$

R stress ratio

t thickness of plate, in.

$u = \left(k_{s_+} - k_{s_-}\right) \Big/ \left(k_{s_+} + k_{s_-}\right)$

W potential energy, in-lb

w displacement normal to plane of plate, in.

x,y,z coordinates

$Y = 1 + 3\beta f$

α edge angle, deg; also, $12M/(Pb + 6M)$

$\bar{\alpha} = \pi(b/\lambda)^{1/2}\left[(b/\lambda) + k_c^{1/2}\right]^{1/2}$

β ratio of cladding yield stress to core stress, $\sigma_{cl}/\sigma_{core}$; also, loading ratio for plate with varying axial load, Maximum load/Minimum load

$\bar{\beta} = \pi(b/\lambda)^{1/2}\left[-(b/\lambda) + k_c^{1/2}\right]^{1/2}$

γ shear strain

ϵ normal strain; also, ratio of rotational rigidity of plate edge stiffener to rotational rigidity of plate

η plasticity-reduction factor

$\bar{\eta}$ cladding reduction factor

η_T total-reduction factor, $\eta\bar{\eta}$

λ buckle half wave length, in.

ν inelastic Poisson's ratio; $\nu = \nu_p - \left(\nu_p - \nu_e\right)\left(E_s/E\right)$ for orthotropic solids

ν_e	elastic Poisson's ratio
ν_p	plastic Poisson's ratio
σ	normal stress, psi
$\bar{\sigma} = (1 - f)\sigma_c + f\sigma_{cl}$.	
σ_i	stress intensity, $\left(\sigma_x^2 + \sigma_y^2 - \sigma_x\sigma_y + 3\tau^2\right)^{1/2}$, psi
$\sigma_{0.7}, \sigma_{0.85}$	stress at secant modulus, 0.7E and 0.85E, respectively, psi
τ	shear stress, psi
φ	angle of diagonal support to plate width, radians or deg

Subscripts:

A,B	values at station A and station B; see fig. 30
av	average
b	bending
c	compression
cl	cladding proportional limit
cr	critical or buckling
e	elastic
p	plastic
pl	proportional limit
r	in traverse rib of compressed plate
s	shear
s_∞	shear on infinitely long plate
x,y	directions of loading
+	loadings producing tension
-	loadings producing compression

edge conditions:

C	clamped
F	free
SS	simply supported (hinged)

In sketches accompanying figures, supported edges with elastic rotational restraint are shown shaded. Unshaded loaded edges are simply supported. Unshaded unloaded edges are free.

BASIC PRINCIPLES

General Remarks

The theoretical buckling stress of a flat structural element is the stress at which an exchange of stable equilibrium configurations occurs between the straight and the slightly bent form. It marks the region in which continued application of load results in accelerated growth of deflections perpendicular to the plane of the plate. Its importance lies in the fact that buckling initiates the physical processes which lead to eventual failure of the plate.

The mathematical solution of particular buckling problems requires that equilibrium and boundary conditions be satisfied. This can be accomplished by integration of the equilibrium partial differential equation of the flat plate or by use of mathematical methods which may not completely satisfy the boundary or equilibrium conditions. The former solutions are exact whereas the methods based generally on energy integrals are approximate although usually very accurate. The need for approximate methods arises from the fact that exact solutions can be found for only a limited number of buckling problems of practical importance.

In this section, a brief outline of the methods of analysis of buckling problems is presented. For extensive discussions of the various methods of analysis and their application to a wide variety of problems, reference to the books of Timoshenko, Sokolnikoff, and Bleich (refs. 2 to 4) is suggested.

Equilibrium Differential Equation

The general form of the differential equation describing the slightly bent equilibrium configuration of an initially flat plate was derived by Stowell in the following form (ref. 5):

$$C_1 \frac{\partial^4 w}{\partial x^4} - C_2 \frac{\partial^4 w}{\partial x^3 \partial y} + 2C_3 \frac{\partial^4 w}{\partial x^2 \partial y^2} - C_4 \frac{\partial^4 w}{\partial x\, \partial y^3} +$$

$$C_5 \frac{\partial^4 w}{\partial y^4} = - \frac{t}{D}\left(\sigma_x \frac{\partial^2 w}{\partial x^2} + 2\tau \frac{\partial^2 w}{\partial x\, \partial y} + \sigma_y \frac{\partial^2 w}{\partial y^2}\right) \qquad (2)$$

in which the constants are defined as:

$$\left.\begin{aligned} C_1 &= 1 - (3/4)\left(\sigma_x/\sigma_i\right)^2\left[1 - \left(E_t/E_s\right)\right] \\ C_2 &= \left(3\sigma_x\tau/\sigma_i^2\right)\left[1 - \left(E_t/E_s\right)\right] \\ C_3 &= 1 - (3/4)\left(\frac{\sigma_x\sigma_y + 2\tau^2}{\sigma_i^2}\right)\left[1 - \left(E_t/E_s\right)\right] \\ C_4 &= \left(3\sigma_y\tau/\sigma_i^2\right)\left[1 - \left(E_t/E_s\right)\right] \\ C_5 &= 1 - (3/4)\left(\sigma_y/\sigma_i\right)^2\left[1 - \left(E_t/E_s\right)\right] \end{aligned}\right\} \qquad (3)$$

These definitions of the constants are based on the assumption that no elastic unloading occurs during the buckling process. Furthermore, a value of Poisson's ratio equal to 1/2 was assumed for both the elastic and inelastic ranges.

In the elastic range, $E_t/E_s = 1$, and, therefore, for all loadings $C_1 = C_3 = C_5 = 1$ and $C_2 = C_4 = 0$, and equation (2) reduces to the familiar equilibrium equation for the elastic case:

$$\nabla^4 w = \frac{\partial^4 w}{\partial x^4} + 2\frac{\partial^4 w}{\partial x^2 \partial y^2} + \frac{\partial^4 w}{\partial y^4}$$

$$= - \frac{t}{D}\left(\sigma_x \frac{\partial^2 w}{\partial x^2} + 2\tau \frac{\partial^2 w}{\partial x\, \partial y} + \sigma_y \frac{\partial^2 w}{\partial y^2}\right) \qquad (4)$$

It should be noted that the value of D is not the same in the inelastic range as in the elastic range because of the change of Poisson's ratio with stress. For the fully plastic plate, $\nu = 1/2$, which yields a bending rigidity of $D' = Et^3/9$, whereas the elastic value is $D = Et^3/12\left(1 - \nu_e^2\right)$.

The solution of individual buckling problems can be most readily handled by selection of appropriate solutions of equation (2), insertion of proper boundary conditions, and minimization to obtain the buckling stress. In this connection, the buckling stresses for simply supported plate columns, compressed flanges, and plates are considered in some detail in the section entitled "Boundary Conditions" to illustrate the differences in buckling behavior of these structural elements.

Energy Integrals

Since exact solutions to equations (2) and (4) can be found for only a limited number of buckling problems of practical importance, approximate solutions generally utilizing energy integrals have found wide application.

The potential energy of the plate and its loading system is represented by the difference of two integrals. The first integral of equation (5) represents the increase in strain energy due to bending and twisting of the plate during the buckling process, whereas the second integral represents energy associated with membrane stresses resulting from lateral deflection. If the plate edges are fixed during buckling, the latter represents the membrane energy. If the edges experience a relative shift, the second integral represents the work of the external loading system.

The general energy integral for plates with simply supported edges was derived by Stowell (ref. 5) for the inelastic case:

$$\Delta W = \frac{D}{2}\iint\left\{C_1\left(\frac{\partial^2 w}{\partial x^2}\right)^2 - C_2\frac{\partial^2 w}{\partial x^2}\frac{\partial^2 w}{\partial x\,\partial y} + C_3\left[\left(\frac{\partial^2 w}{\partial x\,\partial y}\right)^2 + \frac{\partial^2 w}{\partial x^2}\frac{\partial^2 w}{\partial y^2}\right] - C_4\frac{\partial^2 w}{\partial x\,\partial y}\frac{\partial^2 w}{\partial y^2} + C_5\left(\frac{\partial^2 w}{\partial y^2}\right)^2\right\}dx\,dy - \frac{t}{2}\iint\left[\sigma_x\left(\frac{\partial w}{\partial x}\right)^2 + 2\tau\frac{\partial w}{\partial x}\frac{\partial w}{\partial y} + \sigma_y\left(\frac{\partial w}{\partial y}\right)^2\right]dx\,dy \qquad (5)$$

The coefficients C_1 [illegible] are defined by equations (3). It is to be noted that equation (2) is the Euler equation that results from minimization of the energy integral, equation (5). If there are elastic restraints of magnitude ϵ along the edges of the plate, then the strain energy in these restraints is added to equation (5). These terms have the form

$$\frac{\epsilon}{2}\frac{D}{b}\int\left(\frac{\partial w}{\partial y}\right)^2_{y=y_o} dx$$

where y_o is the edge coordinate.

For the elastic case, equation (5) can be simplified to

$$\Delta W = \frac{D}{2}\iint\left\{\left(\frac{\partial^2 w}{\partial x^2}+\frac{\partial^2 w}{\partial y^2}\right)^2 - 2(1-\nu_e)\left[\frac{\partial^2 w}{\partial x^2}\frac{\partial^2 w}{\partial y^2}-\left(\frac{\partial^2 w}{\partial x\,\partial y}\right)^2\right]\right\}dx\,dy -$$

$$\frac{t}{2}\iint\left[\sigma_x\left(\frac{\partial w}{\partial x}\right)^2+2\tau\frac{\partial w}{\partial x}\frac{\partial w}{\partial y}+\sigma_y\left(\frac{\partial w}{\partial y}\right)^2\right]dx\,dy \qquad (6)$$

Solutions

In principle, of all the deflection functions satisfying the geometric boundary conditions of the problem, the potential energy ΔW will be zero for that function which also satisfies the equilibrium differential equation. This function would be an exact solution of the problem. Since exact solutions can be found in only a limited number of cases, the energy integrals are of great usefulness in finding approximate solutions which satisfy the geometric boundary conditions exactly and the differential equation approximately. Thus, of the several functions satisfying the geometric boundary conditions but not necessarily the differential equation, the function for which the energy integral is a minimum constitutes the best approximate solution of the differential equation.

Probably the best known energy method for determining the buckling stress of thin plates is the Rayleigh-Ritz procedure. The method consists of the following steps:

(1) The deflection surface of the buckled plate is expressed in expanded form as the sum of an infinite set of functions having undetermined coefficients. In general, each term of the expansion must satisfy the geometrical boundary conditions of the problem.

(2) The potential energy difference of the load-plate system is computed for this deflection surface by use of equation (5) and is then minimized with respect to the undetermined coefficients.

(3) This minimizing procedure leads to a set of linear homogeneous equations in the undetermined coefficients. These equations have non-vanishing solutions only if the determinant of their coefficient vanishes. The vanishing of this stability determinant provides the equation that may be solved for the buckling stress.

When the set of functions used is a complete set capable of representing the deflection, slope, and curvature of any possible plate deformation, the solution obtained is, in principle, exact. Since, however, the exact stability determinant is usually infinite, a finite determinant yielding approximate results is used instead.

The buckling stresses obtained by the approximate method are always higher than the exact solution although they may be very accurate. This is a result of the fact that the deflection function approximates the true buckle shape and therefore the potential energy resulting from use of the approximating function is greater than zero. If the deflection function is the true one, then an exact solution to the differential equation is obtained.

If a deflection function is chosen which satisfies the geometrical boundary conditions approximately, it is possible to obtain buckling stresses which approach the exact solution from the lower side. This can be accomplished by a revision of the Rayleigh-Ritz procedure known as the Lagrangian multiplier method.

The Lagrangian multiplier method follows the general procedure outlined for the Rayleigh-Ritz method with but one significant change. The restriction in step (1) that the boundary conditions be satisfied by every term of the expansion is discarded and is replaced by the condition, that the expansion as a whole satisfies the boundary conditions. This condition is mathematically satisfied in step (2), during the minimization process, by the use of Lagrangian multipliers.

The advantage of the Lagrangian multiplier method lies in the fact that, with the rejection of the necessity of the fulfillment of boundary conditions term by term, the choice of an expansion is much less restricted. For example, in the clamped-plate compression problem, a simple Fourier expansion may be used instead of the complicated functions usually assumed in the Rayleigh-Ritz analyses of this problem. Furthermore, the orthogonality properties of the simple Fourier expansion lead to energy expressions of a simplicity that is instrumental in permitting accurate computations.

This method and its application to specific problems is described by Budiansky and Hu (ref. 6). They have treated the Lagrangian multiplier method in a manner in which it is possible to obtain approximate solutions for both upper and lower bounds. As determinants of higher order are used to obtain better approximations, both the upper and lower bounds approach the true buckling stress. Thus, the Lagrangian multiplier method may be used to obtain results within any desired degree of accuracy.

In addition to the above procedures which are based on energy integrals, other methods of obtaining approximate solutions of buckling problems have been used which involve the equilibrium differential equation. Functions which satisfy the geometrical boundary conditions exactly are used to satisfy the governing differential equation approximately by processes that lead to integration of these functions. Galerkin's method, finite-difference equations, relaxation techniques, and iteration are some of the numerical methods that can be used.

BOUNDARY CONDITIONS

The nature of the buckle pattern in a plate depends not only upon the type of applied loading but also upon the manner in which the edges are supported. This is illustrated in figure 1 in which the same axial compressive loading is seen to generate three types of buckle patterns on a long rectangular plate with different geometrical boundary conditions. The single wave is representative of column behavior, the twisted wave is representative of flange behavior, and the multiple-buckle pattern is representative of plate behavior.

To indicate the manner in which the geometric boundary conditions mathematically influence the buckling behavior and also to demonstrate the solution of the equilibrium differential equation (eq. (4)) for some particular cases, the plates shown in figure 1 are analyzed. Boundary conditions which characterize simply supported wide columns, flanges, and plates are considered.

Mathematical Analysis

The equilibrium differential equation for elastic buckling of a uniaxially compressed plate can be obtained from equation (4) in the form

$$\frac{\partial^4 w}{\partial x^4} + 2\frac{\partial^4 w}{\partial x^2 \partial y^2} + \frac{\partial^4 w}{\partial y^4} + \frac{\sigma t}{D}\frac{\partial^2 w}{\partial x^2} = 0 \qquad (7)$$

It is assumed that the loaded edges of the plate are simply supported and therefore an appropriate solution of equation (7) is

$$w = \left(c_1 \cosh \frac{\bar{\alpha}y}{b} + c_2 \sinh \frac{\bar{\alpha}y}{b} + c_3 \cos \frac{\bar{\beta}y}{b} + c_4 \sin \frac{\bar{\beta}y}{b}\right)\cos \frac{\pi x}{\lambda} \qquad (8)$$

where

$$\bar{\alpha} = \pi\left(\frac{b}{\lambda}\right)^{1/2}\left[\frac{b}{\lambda} + \left(k_c\right)^{1/2}\right]^{1/2} \qquad (9)$$

$$\bar{\beta} = \pi\left(\frac{b}{\lambda}\right)^{1/2}\left[-\frac{b}{\lambda} + \left(k_c\right)^{1/2}\right]^{1/2} \qquad (10)$$

$$k_c = \frac{12\left(1 - \nu_e^2\right)\sigma_{cr}}{\pi^2 E}\left(\frac{b}{t}\right)^2 \qquad (11)$$

The coefficients c_1 to c_4 are to be determined by the geometrical boundary conditions along the unloaded edges of the plate.

For the wide column, the unloaded edges located at $y = \pm b/2$ are free, and consequently the edge moments and reduced shears must be zero. Therefore,

$$\left(\frac{\partial^2 w}{\partial y^2} + \nu_e \frac{\partial^2 w}{\partial x^2}\right)_{y=\pm b/2} = 0$$

$$\left[\frac{\partial^3 w}{\partial y^3} + 2\left(1 - \nu_e\right)\frac{\partial^3 w}{\partial x^2 \partial y}\right]_{y=\pm b/2} = 0 \qquad (12)$$

For the flange, the unloaded edge at $y = 0$ is assumed to be simply supported and that at $y = b$ is free:

$$\left.\begin{aligned} (w)_{y=0} &= 0 \\ \left(\frac{\partial^2 w}{\partial y^2} + \nu_e \frac{\partial^2 w}{\partial x^2}\right)_{y=0,b} &= 0 \\ \left[\frac{\partial^3 w}{\partial y^3} + 2\left(1 - \nu_e\right)\frac{\partial^3 w}{\partial x^2 \partial y}\right]_{y=b} &= 0 \end{aligned}\right\} \tag{13}$$

The plate is assumed to be simply supported along the unloaded edges located at $y = \pm b/2$:

$$\left.\begin{aligned} (w)_{y=\pm b/2} &= 0 \\ \left(\frac{\partial^2 w}{\partial y^2} + \nu_e \frac{\partial^2 w}{\partial x^2}\right)_{y=\pm b/2} &= 0 \end{aligned}\right\} \tag{14}$$

Incorporation of these boundary conditions into the solution given by equation (8) leads to the following implicit expressions for k_c.

For the column,

$$\bar{p}^2\bar{\beta} \tan(\bar{\beta}/2) + \bar{q}^2\bar{\alpha} \tanh(\bar{\alpha}/2) = 0 \tag{15}$$

for the flange,

$$\bar{p}^2\bar{\beta} \sinh \bar{\alpha} \cos \bar{\beta} - \bar{q}^2\bar{\alpha} \cosh \bar{\alpha} \sin \bar{\beta} = 0 \tag{16}$$

and for the plate

$$\left[\bar{\alpha} \tanh(\bar{\alpha}/2) + \bar{\beta} \tan(\bar{\beta}/2)\right]^{-1} = 0 \tag{17}$$

where

$$\bar{p} = \bar{\alpha}^2 - \nu_e(\pi b/\lambda)^2$$

$$\bar{q} = \bar{\beta}^2 + \nu_e(\pi b/\lambda)^2$$

The buckling coefficient for wide columns and flanges is shown as a function of ν_e and a/b in figure 2. The solutions for wide columns were given by Houbolt and Stowell by use of the differential equation for simply supported loaded edges and the energy method for clamped loaded edges (ref. 7).

The buckling coefficient for a simply supported flange was derived by Lundquist and Stowell (ref. 8) in the form

$$k_c = (6/\pi^2)\left\{(1 - \nu_e) + \left[(\pi b/\lambda)^2/6\right]\right\} \tag{18}$$

When the unloaded edge is clamped,

$$k_c = 0.83 - 0.93\nu_e + 1.34(\lambda/\pi b)^2 + 0.10(\pi b/\lambda)^2 \tag{19}$$

For the simply supported plate

$$k_c = \left[(\lambda/b) + (b/\lambda)\right]^2 \tag{20}$$

Anticlastic Curvature

As may be seen from the solutions in the preceding section, the buckling coefficient for the simply supported plate depends upon only b/λ and is independent of Poisson's ratio, while the coefficients for the wide column and flange are functions of both ν_e and b/λ. This situation is not limited to the case of simple support alone but pertains to any degree of rotational restraint along the unloaded edges of a plate. The influence of ν_e upon k_c is traceable to the reduced-shear terms at the free edges of flanges and columns. Boundary conditions such as simple support do not impose the requirement of zero reduced shear along the unloaded edges, which eliminates the ν_e influence from the relationship for k_c.

The value of the compressive buckling coefficient for an element containing a free unloaded edge depends upon the degree of anticlastic curvature developed. For a very narrow element such as a beam, complete

anticlastic curvature occurs and the bending rigidity is simply EI. For a relatively wide strip, the anticlastic curvature is suppressed so that the cross section remains relatively flat except for a highly localized curling at the free edges where the stress distribution rearranges itself to satisfy the geometrical boundary conditions. The restraint of anticlastic curvature results in an increase in bending stiffness. For a very wide element, the bending stiffness approaches $EI/(1 - \nu^2)$; this limiting condition is known as cylindrical bending.

Plate columns and flanges may often be relatively narrow, in which case the bending stiffness lies between the limiting values discussed. This effect can be accounted for by use of figure 2.

STRESS-STRAIN RELATIONS IN YIELD REGION

Three-Parameter Description of Stress-Strain Curves

Stress-strain curves are of fundamental importance in the computation of inelastic buckling stresses. The number of design charts required for the many materials available and the various allowable stresses for these materials at normal and elevated temperatures can be tremendously reduced by use of a nondimensional mathematical description of stress-strain relations.

Ramberg and Osgood (ref. 9) have proposed a three-parameter representation of stress-strain relations in the yield region which has found wide application. Their equation specifies the stress-strain curve by the use of three parameters: The modulus of elasticity E, the secant yield stress $\sigma_{0.7}$ corresponding to the intersection of the stress-strain curve and a secant of 0.7E, and the shape parameter n which describes the curvature of the knee of the stress-strain curve. The shape parameter is a function of $\sigma_{0.7}$ and $\sigma_{0.85}$, the latter stress corresponding to a secant of 0.85E as shown in figure 3(a). The shape parameter n is presented in figure 3(b) as a function of the ratio $\sigma_{0.7}/\sigma_{0.85}$.

The three-parameter method is based on the experimental observation that for many materials a simple power law describes the relation between the plastic and elastic components of strain. By use of this fact, the following nondimensional equation can be derived:

$$\frac{E\epsilon}{\sigma_{0.7}} = \frac{\sigma}{\sigma_{0.7}} + \frac{3}{7}\left(\frac{\sigma}{\sigma_{0.7}}\right)^n \tag{21}$$

The quantities $E\epsilon/\sigma_{0.7}$ and $\sigma/\sigma_{0.7}$ are nondimensional and consequently the nondimensional stress-strain curves shown in figure 4 can be plotted. Therefore, the stress-strain curves of many materials may be found with the aid of figure 4 providing E, n, and $\sigma_{0.7}$ are known for the specific materials.

Inelastic Moduli

For inelastic-buckling problems, the modulus ratios E_s/E, E_t/E, and E_t/E_s appear. These ratios can be computed in nondimensional form by use of equation (21). Since $E_s = \sigma/\epsilon$, it follows directly from equation (21) that

$$E/E_s = 1 + (3/7)\left(\sigma/\sigma_{0.7}\right)^{n-1} \tag{22}$$

Since $E_t = d\sigma/d\epsilon$, differentiation of equation (21) leads to the expression

$$E/E_t = 1 + (3/7)n\left(\sigma/\sigma_{0.7}\right)^{n-1} \tag{23}$$

From equations (22) and (23) it follows that

$$E_t/E_s = \left(E/E_s\right)\Big/\left(E/E_t\right)$$

$$= \frac{1 + (3/7)\left(\sigma/\sigma_{0.7}\right)^{n-1}}{1 + (3/7)n\left(\sigma/\sigma_{0.7}\right)^{n-1}} \tag{24}$$

These quantities are used in subsequent sections concerned with inelastic buckling.

Inelastic Poisson's Ratio

Poissen's ratio for engineering materials usually has a value in the elastic region of between 1/4 and 1/3 and, on the assumption of a plastically incompressible isotropic solid, assumes a value of 1/2 in the plastic region. The transition from the elastic to the plastic value is most pronounced in the yield region of the stress-strain curve. Since

Poisson's ratio appears in the buckling-stress equation, this transition is of some importance in inelastic-buckling problems.

Gerard and Wildhorn, among others, have studied this problem on several aluminum alloys and have shown that Poisson's ratio is seriously affected by anisotropy of the material (ref. 10). For materials which can be considered to be orthotropic (e.g., having the same properties along the y- and z-axes if loaded along the x-axis) the following relation describes the transition in the yield region:

$$\nu = \nu_p - \left(E_s/E\right)\left(\nu_p - \nu_e\right) \tag{25}$$

In this relation, ν_p is the fully plastic value of Poisson's ratio. For isotropic materials $\nu_p = 1/2$, whereas for orthotropic materials ν_p is generally different from a value of 1/2.

It is evident from the buckling stress expression that two materials which differ only in their values of Poisson's ratio should have different buckling stresses. As a rule, however, the value of ν_e is virtually constant for a material whose properties may change as a result of heat treatment, details of composition, or amount of cold-work.

The usual range of ν_e for most technically important structural materials is between 0.25 and 0.35. There are exceptions, however. One of the most extreme materials is beryllium, for which Udy, Shaw, and Boulger report a value of 0.02 (ref. 11).

In the inelastic range, presumably because of anisotropy, numerical values of ν have been found which are considerably in excess of the theoretical upper limit of 0.5, which is derived on the assumption of incompressibility of an isotropic material. For example, Gerard and Wildhorn obtained values of ν as large as 0.70 for several high-strength aluminum alloys (ref. 10), while Goodman and Russell reported a value of 0.77 for commercially pure titanium sheet and 0.62 for FS-1h magnesium alloy (ref. 12). Stang, Greenspan, and Newman also obtained data at variance with the theoretical value of 0.5 for plastic strains (ref. 13). These three reports cover a large variety of alloys, deformed by various total strains in both bar and sheet stock, and should be consulted for more complete data.

PLASTICITY-REDUCTION FACTORS

Inelastic-Buckling-Stress Equation

The elastic buckling stress of a flat rectangular plate can be expressed in the form

$$\sigma_{cr_e} = \frac{k\pi^2 E}{12\left(1 - \nu_e^2\right)}\left(\frac{t}{b}\right)^2 \tag{26}$$

When the buckling stress exceeds the proportional limit of the plate material, the terms in equation (26) which are influenced are k, E, and ν. The buckling coefficient k depends upon the type of loading, the buckle wave length as affected by the geometrical features of boundary conditions and aspect ratio, the stress level, and Poisson's ratio in the case of plates with free edges. The elastic modulus E is altered by the reduction in bending stiffness associated with inelastic behavior. Poisson's ratio in the yield region exhibits a gradual transition from the elastic value ν_e to a value of 1/2 for a plastically incompressible isotropic material.

For simplicity of calculation all effects of exceeding the proportional limit are generally incorporated in a single coefficient referred to as the plasticity-reduction factor η. By definition

$$\eta = \sigma_{cr_p}/\sigma_{cr_e} \tag{27}$$

Substituting equation (27) into equation (26),

$$\sigma_{cr} = \eta \frac{k\pi^2 E}{12\left(1 - \nu_e^2\right)}\left(\frac{t}{b}\right)^2 \tag{28}$$

Since $\eta = 1$ in the elastic range, equation (28) is perfectly general and it is not necessary to distinguish between elastic and plastic buckling. The values of k and ν_e are always the elastic values since the coefficient η contains all changes in those terms resulting from inelastic behavior.

Comparison of Theories and Experimental Data

The theoretical and experimental determinations of the values of η appropriate to various types of loadings and boundary conditions have resulted in extensive literature. The assumptions underlying the various theories differ with respect to plasticity laws, stress-strain relations, and buckling models used. In order to avoid possible confusion in discussing the various theories, it appears desirable to resort to the expedient of comparing theories with test data first.

Rather precise experimental data exist for plastic buckling of columns, simply supported flanges and plates under compressive loads, and elastically supported plates under shear loads. For practical aluminum-alloy columns under compression, it is a well-known fact that the experimental failing stress is closely approximated by the Euler formula with the tangent modulus substituted for the elastic modulus.

In figure 5, test data for buckling of simply supported flanges under compression are shown in comparison with the theoretical values as derived by Stowell (ref. 14) according to the method of Gerard (ref. 15). Excellent agreement is obtained.

In figure 6, test data of Pride and Heimerl (ref. 16) and Peters (ref. 17) for plastic buckling of simply supported plates under compression are shown in comparison with the theories of Bijlaard (ref. 18), Handelman and Prager (ref. 19), Ilyushin (ref. 20), and Stowell (ref. 5), and the method of Gerard (ref. 15). Poor agreement is obtained between the test data and the flow theory of Handelman and Prager, whereas relatively good agreement is obtained for the deformation theories of the others with Stowell's theory in best agreement.

In figure 7, test data for plastic buckling of elastically supported plates under shear are shown in comparison with the theories of Bijlaard (ref. 18), Gerard (ref. 21), and Stowell (ref. 5). It can be observed that the method of Gerard, which is based on the maximum-shear plasticity law to transform an axial stress-strain curve into a shear stress-strain curve, is in good agreement with test data on aluminum alloys.

On the basis of the agreement with test data, the values of η recommended for use with equation (28) appear in the appendix. Also, nondimensional buckling charts derived through the use of these reduction factors appear in figures 8, 9, and 10 for axially compressed flanges and plates and for shear-loaded plates.

Assumptions of Inelastic-Buckling Theories

The state of knowledge up to 1936 concerning inelastic buckling of plates and shells has been summarized by Timoshenko (ref. 2). The main

efforts reported therein were concerned with attempts to modify the various bending-moment terms of the equilibrium differential equations by the use of suitable plasticity coefficients determined from experimental data on columns. Although such semiempirical efforts met with a reasonable degree of success, the theoretical determination of plasticity-reduction factors for flat plates has been achieved within recent years as the result of the development of a satisfactory inelastic-buckling theory. Because such developments are recent and because the various theories have not been, as yet, adequately treated in text books, the following discussion concerning the assumptions and results of the various theories is presented in some detail.

Mathematical theories of plasticity are phenomenological in nature since such theories generally proceed from the experimentally determined stress-strain relations for simple uniaxial loadings. In the elastic range, stress and strain are linearly related by the elastic modulus. At strains beyond the proportional limit, a finite stress-strain relation can be used in the form

$$\sigma = E_s \epsilon \tag{29}$$

or an incremental relation can be used

$$d\sigma = E_t \, d\epsilon \tag{30}$$

In either relation the secant modulus E_s or the tangent modulus E_t varies with stress and applies as long as the loading continues to increase. Unloading usually occurs along an elastic line parallel to the initial elastic portion of the stress-strain curve.

In the buckling process, for example, the stress state is considerably more complex than simple uniaxial loading. Therefore, formulation of suitable stress-strain laws for three-dimensional stress states beyond the proportional limit forms one of the basic assumptions of the various plasticity theories. Based on generalizations of equation (29) which involve finite relations, deformation types of stress-strain laws have been advanced. Similar generalizations of equation (30) involving incremental relations are referred to as flow-type theories. In both theories, unloading occurs elastically.

The use of the various plasticity theories is greatly facilitated by the introduction of rotationally invariant functions to define the three-dimensional stress and strain states; such functions are termed stress and strain intensities. The assumption that the stress intensity is a uniquely defined, single-valued function of the strain intensity

for a given material when the stress intensity increases (loading) and is elastic when it decreases (unloading) is a second of the fundamental hypotheses of plasticity theory.

The definitions of the stress and strain intensities theoretically can be chosen from a family of rotationally invariant functions. Two such functions referred to as the maximum-shear law and octahedral-shear law have been found to be of considerable usefulness for correlating stress data on ductile materials. Thus, both of these laws have been assumed to apply in various solutions for inelastic buckling.

In order to obtain solutions to various plasticity problems, additional assumptions are generally employed. These ordinarily include the assumption that the principal axes of stress and strain coincide and the assumption of plastic isotropy. Furthermore, the variation of Poisson's ratio from the elastic value to the value of 0.5 for a plastically incompressible, isotropic solid is most pronounced in the yield region. Some solutions account for the instantaneous value of Poisson's ratio whereas others assume a value of 0.5 for both the elastic and plastic region. The latter assumption serves to simplify the analysis considerably. Corrections for the use of the fully plastic value of Poisson's ratio can generally be incorporated in the final results.

All the foregoing assumptions form the basis for solution of plasticity problems in general. For the specific problem of inelastic buckling, it is necessary to make an additional assumption concerning the stress distribution at the instant of buckling.

From the standpoint of classical stability theory, the buckling load is the load at which an exchange of stable equilibrium configurations occurs between the straight form and the bent form. Since the load remains constant during this exchange, a strain reversal must occur on the convex side and, therefore, the buckling model leading to the reduced-modulus concept for columns is correct theoretically.

Practical plates and columns invariably contain initial imperfections of some sort, and, therefore, axial loading and bending proceed simultaneously. In this case, the bent form is the only stable configuration. Since in the presence of relatively large axial compressive stresses the bending stresses are small, no strain reversal occurs and the incremental bending stresses in the inelastic range are given by equation (30).

Since failing loads obtained from tests on aluminum-alloy columns are closely approximated by the Euler buckling equation with the tangent modulus substituted for the elastic modulus, certain of the inelastic-buckling theories assume the no-strain-reversal, or tangent-modulus, model as the basic buckling process and then proceed to solutions by use of equilibrium equations based on classical stability concepts.

Inelastic-Buckling Theories

Different investigators have used various ones of those assumptions discussed above. In order to indicate the major assumptions underlying each of the theories, a summary is presented in table 1.

Historically, Bijlaard appears to have been the first to arrive at satisfactory theoretical solutions for inelastic-buckling theories (ref. 18). His work is the most comprehensive of all those considered in that he considers both incremental and deformation theories and concludes that the deformation type is correct since it leads to lower inelastic buckling loads than are obtained from incremental theories. His work was first published in 1937. This paper and later publications include solutions to many important inelastic-buckling problems. However, this work appears to have remained unknown to most of the later investigators.

Ilyushin briefly referred to Bijlaard's work and then proceeded to derive the basic differential equation for inelastic buckling of flat plates according to the strain-reversal model (ref. 20). The derivation of this equation is rather elegant and was used by Stowell, who, however, used the no-strain-reversal model (ref. 5). The differential equation obtained by Bijlaard reduces to that derived by Stowell by setting $\nu = 1/2$ in the former. Handelman and Prager, during this time, obtained solutions to several inelastic-buckling problems by use of incremental theory (ref. 19). Test data, such as shown in figure 6, indicate that the results of incremental theories, regardless of the buckling model, are definitely unconservative, whereas deformation-type theories are in relatively good agreement.

All the foregoing theories were based on the use of the octahedral-shear law. However, test data on the inelastic buckling of aluminum-alloy plates in shear indicated that the results of the above theories were unconservative. Gerard used the maximum-shear law in place of the octahedral-shear law to transform axial stress-strain curves to shear stress and found good agreement with the aluminum-alloy-plate shear-buckling data (ref. 21).

To summarize, then, the assumptions which lead to the best agreement between theory and test data on inelastic buckling of aluminum-alloy flat plates under compression and shear loadings include deformation-type stress-strain laws, stress and strain intensities defined by the octahedral-shear law, and the no-strain-reversal model of inelastic buckling. Although there may be theoretical objections to deformation theories as a class and the use of a no-strain-reversal model in conjunction with classical stability concepts, test data do suggest the use of results obtained from a theory based on these assumptions in engineering applications. The choice of laws to transform axial stress-strain data to shear stress-strain data

depends upon the degree of correlation obtained between each of these laws with polyaxial test data for individual materials.

Factors Used in Computations

As already indicated, the inelastic-buckling stress may be computed by use of plasticity-reduction factors appropriate to the boundary and loading conditions. The factors incorporate all effects of exceeding the proportional limit upon k, E, and ν. For convenience in preparing design charts for inelastic buckling, the critical elastic strain can be used:

$$\epsilon_{cr} = \frac{k\pi^2}{12\left(1 - \nu_e^2\right)}\left(\frac{t}{b}\right)^2 \tag{31}$$

From equations (28) and (31)

$$\sigma_{cr} = \eta E \epsilon_{cr} \tag{32}$$

The recommended values of η are given in table 2. For compressive loads, the values of η derived by Stowell for infinitely long plates except in the case of plate columns (see refs. 5 and 22) have been corrected to account for the instantaneous value of Poisson's ratio according to a method suggested by Stowell and Pride (ref. 23). Thus,

$$\eta = \eta_s \frac{\left(1 - \nu_e^2\right)}{\left(1 - \nu^2\right)} \tag{33}$$

where η_s is the original value given by Stowell. Equation (33) is the form of the plasticity-reduction factors that appears in table 2 and has been used to construct the nondimensional buckling charts of figures 8, 9, and 10.

For long simply supported plates under combined axial compression and bending Bijlaard found theoretically, by a finite-difference approach (ref. 24), that

$$\eta = \left(\frac{1 - \nu_e^2}{1 - \nu^2}\right)\left[\frac{\alpha}{2}\left(E_s/E\right) + \left(1 - \frac{\alpha}{2}\right)\eta_c\right] \tag{34}$$

where α is found from equation (36) and $\left[\left(1 - \nu_e^2\right)/\left(1 - \nu^2\right)\right]\eta_c$ is the plasticity-reduction factor for axial compression. Equation (34) reduces to this value for axial load alone, since $\alpha = 0$ for this case. For pure bending $\alpha = 2$ and equation (34) is equal to the plasticity-reduction factor for a hinged flange.

To determine the instantaneous value of Poisson's ratio, equation (25) can be used. For the nondimensional buckling charts the theoretical fully plastic value of 0.5 was assumed for Poisson's ratio, as was assumed by Stowell in his determinations of the plasticity-reduction factors. Stowell and Pride reported on computations made using equation (34) instead of $\nu = 0.5$ and showed that there was little difference between the two curves for flanges and simply supported plates (ref. 23). Bijlaard took exception to this report (ref. 25); however, the differences were slight, as was pointed out by Stowell and Pride, and it can be assumed for practical purposes that the plasticity-reduction factors shown in the appendix are satisfactory for general design and analysis.

Construction of Nondimensional Buckling Charts

The nondimensional buckling-stress charts of figures 8, 9, and 10 were constructed from the basic nondimensional stress-strain curves of figure 4 and the plasticity-reduction factors shown in the appendix, incorporating the method of critical strains as depicted through equations (31) and (32). Since there is little difference among the numerical values of the buckling stresses that would be obtained for the plasticity-reduction factors applicable to a long clamped flange and to a long plate with any amount of edge rotational restraint, these cases were grouped into one employing the reduction factor for the simply supported plate, which is the average of the three factors.

CLADDING REDUCTION FACTORS

Basic Principles

The presence of cladding on the faces of plates may have an appreciable effect on the buckling stress since the cladding material, which usually has lower mechanical strength than the plate core, is located at the extreme fibers of the plate cross section (fig. 11) where the bending strains during buckling attain their highest values.

Buchert determined buckling-stress-reduction factors for clad plates which include plasticity effects as well as reduction due to cladding (ref. 26). However, it is possible to determine a reduction factor for

cladding alone that may be multiplied by the inelastic buckling stress to yield a final buckling stress for the clad plate that agrees quite closely with the test data. The cladding reduction factors may then be used with the existing inelastic-buckling curves of figures 8, 9, and 10.

The form of buckling equation commonly used for determining the buckling stress of a bare flat plate with any type of loading and boundary supports is given as equation (28). For clad plates this expression is used to find a nominal buckling stress, where the thickness is that of the total plate and the material properties are those of the core. The actual buckling stress of a clad plate then may be found by applying a simple numerical multiplier $\bar{\eta}$ to this stress. This multiplier, termed the cladding reduction factor because it reduces the ratio of the nominal core stress to the buckling stress of the clad plate, is a function of the relative core and cladding stress levels and the respective moduli of the core and cladding materials. The clad-plate buckling stress can be found from

$$\bar{\sigma}_{cr} = \bar{\eta}\sigma_{cr} \tag{35}$$

If the nominal buckling stress exceeds the proportional limit of the core material, then the nominal buckling stress for the clad plate may be found by using the appropriate value of η, the plasticity-reduction factor of the core material. Values of η may be obtained from the clad-plate stress-strain curve shown in figure 12, the derivation of which is discussed below.

It should be noted that the plasticity-reduction factor depends upon the stress level and consequently requires an estimate of the final buckling stress of the plate before equation (28) can be used to find σ_{cr}. The cladding reduction factor has been found to be of such a nature, however, that little error is involved in first finding the nominal buckling stress and then multiplying it directly by the cladding reduction factor to find the actual buckling stress of the clad plate. The product $\eta\bar{\eta}$ is η_T, which was determined by Buchert.

Table 3 contains a listing of the various cladding reduction factors determined in subsequent portions of this section. In the table, all plates are long and simply supported. In all cases for which the cladding proportional-limit stress σ_{cl} exceeds the nominal buckling stress σ_{cr} the cladding reduction factor is equal to unity. The quantity β is defined as $\beta = \sigma_{cl}/\sigma_{cr}$, and f is the ratio of the total cladding thickness to the clad-plate total thickness.

Derivation of Core Stress-Strain Curve

The core stress-strain curve may be derived from a stress-strain curve for the entire clad plate as shown in figure 12. Using the notation of figure 11, in which a section of a clad plate is shown, the total axial load acting on the section is determinable from

$$N_x = t\bar{\sigma} = t(1 - f)\sigma_{core} + tf\sigma_{cl} \tag{36}$$

Dividing this expression by $t\sigma_{core}$ yields

$$\bar{\sigma}/\sigma_{core} = 1 - f + \beta f \tag{37}$$

where $\beta = \sigma_{cl}/\sigma_{core}$.

Thus, the core stress-strain curve can be constructed by plotting the core stress determined from equation (37) at each value of strain for which the corresponding clad-plate stress was found. (See fig. 12.) The initial slope of the core curve, which is the same as the initial slope of the clad-plate curve, is the elastic modulus to be used in the nominal-buckling-stress equation. Since the buckling stress refers to the core material, σ_{core} was replaced by its counterpart σ_{cr} in the succeeding derivations.

Typical values of f for alclad plate appear in table 4 for several aluminum alloys. Buchert showed a value of $\sigma_{cl} = 10{,}000$ psi for 1100-H14 alloy (ref. 26). However, the cladding stress will vary with the cladding material, of which different types are used on different alloy cores.

Comparison of Theory and Experiment

The total-reduction factor, defined as the product of the plasticity- and cladding-reduction factors, has been plotted in figure 13 as a function of stress for both the test data and the theory in the case of axially compressed plates. Two materials are represented, each with a different percentage of cladding thickness. Furthermore, the first (2024-T84 sheet) is a simply supported plate whereas the second (2024-T3 sheet) is a long column. Plasticity-reduction factors for these two cases were obtained from table 2. It is instructive to notice the close correlation for the column case, for which the tangent modulus is the applicable plasticity-reduction modulus. This follows the prediction of the simplified theory,

which stipulates that the cladding reduction factor is independent of stress level when the nominal core stress exceeds the cladding proportional limit. Thus, the theory and test data agree in the sharp drop in the total-reduction factor at the cladding proportional limit.

Derivations of Simplified Cladding Reduction Factors

Buchert derived expressions for the total-reduction factor for flat simply supported rectangular plates subjected to several types of loadings. In the following sections are presented derivations of simplified cladding reduction factors that yield buckling stresses at all stress levels merely by multiplying the nominal stress (elastic or inelastic) by the cladding reduction factor at that stress. This is done by separating the cladding effect from the total-reduction factor by using the relationship $\bar{\eta} = \eta_T/\eta$.

Case 1. Long simply supported plates in compression.- Buchert derived the expression for η_T at $\sigma_{cr} > \sigma_{pl}$ (of the core) (ref. 26):

$$\eta_T = \frac{E_s/E}{2(1 + 3f)}\left(\left[1 + \left(3f\bar{E}_s/E_s\right)\right] + \left\{\left[1 + \left(3f\bar{E}_s/E_s\right)\right]\left[(1/4) + (3/4)\left(E_t/E_s\right) + W\right]\right\}^{1/2}\right) \tag{38}$$

where

$$W = \left(3f\bar{E}_s/E_s\right)\left[(1/4) + (3/4)\left(\bar{E}_t/\bar{E}_s\right)\right]$$

For a bare plate $f = 0$ and $\eta_T = \eta$, which give

$$\eta = \left(E_s/2E\right)\left\{1 + \left[(1/4) + (3/4)\left(E_t/E_s\right)\right]^{1/2}\right\} \tag{39}$$

(cf. table 2). Then

$$\bar{\eta} = \frac{1}{1 + 3f}\left(\frac{\left[1 + \left(3f\bar{E}_s/E_s\right)\right] + \left\{\left[1 + \left(3f\bar{E}_s/E_s\right)\right]\left[(1/4) + (3/4)\left(E_t/E_s\right) + W\right]\right\}^{1/2}}{1 + \left[(1/4) + (3/4)\left(E_t/E_s\right)\right]^{1/2}}\right) \tag{40}$$

(a) When $\sigma_{cr} < \sigma_{cl}$, $E_s = E_t = \bar{E}_s = \bar{E}_t = E$, and therefore $\bar{\eta} = 1$.

(b) When $\sigma_{cl} < \sigma_{cr} < \sigma_{pl}$, $E_s = E_t = E$, and for the cladding stress-strain curve of figure 12 $\bar{E}_t = 0$. Then with $\frac{\bar{E}_s}{E} = \frac{\sigma_{cl}/\epsilon}{\sigma_{cr}/\epsilon} = \frac{\sigma_{cl}}{\sigma_{cr}} = \beta$,

$$\bar{\eta} = \frac{1}{2(1 + 3f)}\left\{(1 + 3\beta f) + \frac{1}{2}\left[(1 + 3\beta f)(4 + 3\beta f)\right]^{1/2}\right\} \tag{41}$$

which may be written

$$\bar{\eta} = \frac{1 + 3\beta f}{1 + 3f}\left(\frac{1}{2}\right)\left(1 + \frac{1}{2}\left\{4 - \left[9\beta f/(1 + 3\beta f)\right]\right\}^{1/2}\right)$$

If it is assumed that $9\beta f/(1 + 3\beta f) << 4$, the following simple expression is obtained for the cladding reduction factor:

$$\bar{\eta} = \frac{1 + 3\beta f}{1 + 3f} \tag{42}$$

(c) For large stresses, $\beta \rightarrow 0$ and therefore

$$\bar{\eta} = \frac{1}{1 + 3f} \tag{43}$$

Equations (42) and (43) appear in figure 13 in the form of $\eta_T = \eta\bar{\eta}$, where they may be seen to agree closely with the total-reduction factor and the test data.

Case 2. Plate columns.- The derivations of $\bar{\eta}$ for short and long plate columns follow the form used in case 1 for the supported plate without any simplifying assumptions. The results are shown in table 3. The column curve is plotted in figure 13 in the form $\eta_T = \eta\bar{\eta}$, where it is seen to agree closely with the data and with Buchert's theory.

Case 3. Long simply supported plates in shear.- Buchert (ref. 26) shows that η_T for shear on a long simply supported plate is

$$\eta_T = \frac{C_{5\tau}\left(E_s/E\right)}{4\sqrt{2}(1 + 3f)}\left\{3\alpha^2 + \left(C_{3\tau}/C_{5\tau}\right) + \left[\alpha^4 + 2\alpha^2\left(C_{3\tau}/C_{5\tau}\right) + 1\right]^{1/2}\right\} \tag{44}$$

where the nodal-line slope of the shear buckles is obtained from the implicit equation

$$\left[\alpha^4 + 2\alpha^2\left(C_{3\tau}/C_{5\tau}\right) + 1\right]^{1/2} = (1 - \alpha^4)\Big/\left[3\alpha^2 - \left(C_{3\tau}/C_{5\tau}\right)\right]$$

and

$$C_{3\tau} = (1/2)\left\{1 + \left(E_t/E_s\right) + 3\beta f\left[1 + \left(\bar{E}_t/\bar{E}_s\right)\right]\right\}$$

$$C_{5\tau} = 1 + 3\beta f$$

The minimum-energy state occurs for unclad elastic plates when $\alpha \rightarrow 1/\sqrt{2}$, and there is little reason to expect a significantly different value for clad plates. Consequently, this value of α is assumed in the following development:

$$\eta_T = \frac{C_{5\tau}\left(E_s/E\right)}{4(1 + 3f)}\left[(3/2) + \left(C_{3\tau}/C_{5\tau}\right) + \frac{3/4}{(3/2) - \left(C_{3\tau}/C_{5\tau}\right)}\right] \tag{45}$$

(a) When $\sigma_{cr} < \sigma_{cl}$, $\eta = \bar{\eta} = \eta_T = 1$.

(b) The plasticity-reduction factor for $\sigma_{cr} > \sigma_{cl}$ is derivable from the total-reduction factor in the form

$$\eta = \left(E_s/8E\right)\left[4 + \left(E_t/E_s\right) + \frac{3}{2 - \left(E_t/E_s\right)}\right] \tag{46}$$

from which, using $\bar{\eta} = \eta_T/\eta$,

$$\bar{\eta} = \frac{Y}{1 + 3f}\left\{\frac{4 + \left(E_t/YE_s\right) + 3\Big/\left[2 - \left(E_t/YE_s\right)\right]}{4 + \left(E_t/E_s\right) + 3\Big/\left[2 - \left(E_t/E_s\right)\right]}\right\} \tag{47}$$

where $Y = 1 + 3\beta f$.

The expression in braces deviates about 2 percent from unity for $f = 0.10$ and for $\beta \rightarrow 0.2$, which will be in the neighborhood of the proportional limit for typical structural aluminum alloys. Consequently, it will not introduce an appreciable error to consider it equal to unity, in which case equation (42) for the compressed simply supported plate holds true.

(c) For large stresses, $\beta \rightarrow 0$, and therefore $\bar{\eta} = \dfrac{1}{1 + 3f}$.

BUCKLING OF FLAT RECTANGULAR PLATES UNDER COMPRESSIVE LOADS

In the preceding sections the mathematical and physical background for the flat-plate buckling problem has been presented. It was shown that basic equation (1) can be used for the solution of buckling problems pertaining to flat rectangular plates under various types of loadings in the elastic and inelastic ranges by suitable choice of reduction factors and buckling coefficients. Considerations that influence the determination of k have been analyzed in the sections entitled "Basic Principles" and "Boundary Conditions." The plasticity-reduction and cladding reduction factors were discussed in the sections "Plasticity-Reduction Factors" and "Cladding Reduction Factors." In this section, and in those to follow, the buckling coefficient k will be discussed and its numerical values for various loading and boundary conditions will be presented.

Historical Background

Bryan investigated the buckling of a simply supported flat rectangular plate under axial loading in the elastic range using the energy method (ref. 27). He obtained the explicit form for k_c for this type of loading and support:

$$k_c = \left[(a/nb) + (nb/a)\right]^2 \tag{48}$$

Timoshenko treated numerous additional cases of loading and boundary conditions utilizing both the energy approach and the solution of the differential equation (ref. 2). Hill constructed a chart of k_c covering the complete range of possible boundary conditions for axial loadings: simply supported, clamped or free edges on one side, and simply supported or clamped edges on the other, with the loaded edges either clamped or simply supported (ref. 28).

Lundquist and Stowell presented the first unified treatment of the compressive-buckling problem in their analyses, by both the differential-equation and energy methods, of the cases of supported plates and flanges with simply supported loaded edges and with varying degrees of elastic rotational restraint along the supported unloaded edges (refs. 8 and 29).

Stein and Libove, in considering combined longitudinal and transverse axial loads, covered the effects of clamping along the unloaded edges of rectangular plates (ref. 30).

Numerical Values of Compressive-Buckling Coefficients for Plates

Figure 14 is a summary chart depicting the variation of k_c as a function of a/b for various limiting conditions of edge support and rotational restraint on a rectangular flat plate. It is apparent that for values of a/b greater than four the effect of rotational restraint along the loaded edges becomes negligible and that the clamped plate would buckle at virtually the same compressive load as a plate with simply supported loaded edges.

Supported Plate, Edges Elastically Restrained Against Rotation

The behavior of compressed plates with various amounts of elastic rotational restraint along the unloaded edges can be understood by examining the relation between buckling coefficient and buckle wave length. For plates supported along both unloaded edges the curves appear in figure 15 for rotational restraint from full clamping ($\epsilon = \infty$) to hinged supports ($\epsilon = 0$). From this figure, which is taken from the report by Lundquist and Stowell (ref. 29), it is possible to see the manner in which the buckle wave length decreases as rotational restraint increases, and the value of λ/b for a minimum value of k_c can be seen to increase from 2/3 for clamped edges to 1.00 for hinged edges. The lower portions of these curves and the portions to the left of the minimum k_c line form the first arms of the curves of k_c as a function

of a/b, as in figure 16. For completeness, several lines denoting the transitions from 1 to 2, 2 to 3, . . . n to n + 1 buckles have been included in figure 15. The intersections of these lines with the curves of k_c against λ/b correspond to the cusps on the curves of figure 16.

Plates With Unequal Edge Rotational Restraint

Figure 15 can also be used when there are unequal rotational restraints along the unloaded edges of a plate. This can be done by determining the k_c value for the ϵ on each unloaded edge. The effective value for use in equation (1) can then be found from

$$\bar{k}_c = \left(k_{c_1} k_{c_2}\right)^{1/2} \tag{49}$$

The accuracy of this method has been demonstrated by Lundquist and Stowell who compared results so obtained with the values obtained by solving directly with the equations used by them for the general case of rotational restraint (ref. 29).

The elastic restraints are mathematically equivalent to a series of unconnected torsional springs. Since this does not necessarily conform to the behavior of the usual edge member or stiffener of a flat panel, it is necessary to evaluate the effective single spring stiffness of the actual stiffener in order to use either figure 15 or figure 16. However, it is not necessary to determine this stiffness to a high degree of accuracy since the influence of ϵ upon k_c embraces a large range of stiffness ratios, as is shown in figure 17 for infinitely long plates. When the stiffener rotational rigidity has been found, ϵ may be computed by forming the ratio of this rigidity to the rotational rigidity of the plate.

From test data Gerard was able to construct a chart of k_c for long plates as a function of b/t for strong and weak stiffeners (ref. 31 and fig. 18). Above $b/t = 200$ it is seen that most stiffeners will effectively clamp the plate edge.

Supported Flanges With Elastic Rotational Restraint

The relationships among k_c, λ/b, and ϵ are depicted for flanges in figure 19. It should be noted that these curves were constructed for a Poisson's ratio value of 0.3, which also applies to the curves of k_c as a function of a/b in figure 20. The determination of k_c for other values of ν is discussed in the section entitled "Boundary Conditions."

The transition lines for 1 to 2, 2 to 3, . . . n to n + 1 buckles are shown in figure 19. However, it should be noted that the minimum line does not intersect the curve for a hinged flange ($\epsilon = 0$). For this case there is only one buckle which extends the full length of the flange.

As in the case of the plate, the theoretical restraint action on the unloaded supported edge of the flange is assumed to be a series of disconnected torsional springs, and it is necessary in this case also to determine the effective restraint for the edge stiffener in order to use the curves of figures 19 and 20. However, as in the case of supported plates, it is not necessary to determine ϵ too accurately, as figure 17 shows, since k_c is relatively insensitive to large variations in ϵ.

Effect of Lateral Restraint on Buckling

In the usual buckling-stress computations the plate analyzed is assumed to be unrestrained against distortion in its plane under the external loads applied. However, for longitudinal compressive loads on a rectangular plate, the edges parallel to the loads would tend to move apart as a result of the Poisson's ratio expansion. If this motion should be restrained to any extent, forces would be developed transverse to the applied load which would influence the longitudinal stress that the plate might withstand before it would buckle. If the interaction concept is employed, it is apparent that the transverse compression would lower the permissible longitudinal stress by an amount that could be found from interaction curves utilizing stress ratios.

If the plate edges are restrained by rigid stiffeners held in place by transverse ribs each with a section area A_r, the balance of transverse forces requires that

$$\sigma_r A_r = \sigma_y a t \tag{50}$$

The directions of σ_x, σ_y, and σ_r are shown in figure 21. The equivalence of transverse strain requires that

$$\left(\nu\sigma_x/E\right) - \left(\sigma_y/E\right) = \sigma_r/E \tag{51}$$

assuming that the ribs and plate are of the same material. From equations (50) and (51), the transverse stress becomes

$$\sigma_y/\sigma_x = \nu \Big/ \left[1 + \left(at/A_r\right)\right] \tag{52}$$

From this point it is a simple matter to determine the reduced longitudinal-buckling stress. This may be expressed in terms of the new value of the buckling coefficient k_c as shown in figure 21, which is a modification of curves presented by Argyris and Dunne (ref. 32).

BUCKLING OF FLAT RECTANGULAR PLATES UNDER SHEAR LOADS

Historical Background

Southwell and Skan computed the critical shear load for a flat rectangular plate with simply supported edges and with fixed edges by means of the buckling differential equation (ref. 33). Timoshenko investigated shear buckling also (ref. 2); however, he used the energy method and obtained a critical loading 6.5 percent higher than the exact result of Southwell and Skan.

Stowell determined shear-buckling coefficients for infinitely long supported plates with the edges elastically restrained against rotation (ref. 34). He utilized the differential equation for an exact solution and the energy integrals for plotting purposes. Stowell presented his results in the manner of Southwell and Skan, who plotted the buckling coefficient as a function of λ/b for long plates. This is the same procedure used by Lundquist and Stowell for compressive loading on plates of any length (refs. 8 and 29).

Symmetric and Antisymmetric Modes

The solutions obtained by Southwell and Skan (ref. 33) and by Timoshenko (ref. 2) pertained to a buckle form termed the symmetric mode because of the symmetry of the mode shape with respect to a diagonal across the plate at the node-line slope. Stein and Neff examined the antisymmetric buckle mode for simply supported plates and found that it has a lower buckling stress, within a small range of a/b values, than does the symmetric mode (ref. 35). Stein and Neff also repeated Timoshenko's calculations for greater precision and obtained an estimated error of 1 percent.

Budiansky and Connor investigated the short clamped plate for both symmetric and antisymmetric buckle modes using the Lagrangian multiplier method (ref. 36). Except for a small range of a/b values, the symmetric mode was shown to yield the lower buckling stress.

Numerical Values of Shear-Buckling Coefficient

The plot of k_s as a function of a/b appears in figure 22. It may be seen from the curves how the symmetric and antisymmetric modes alternate with one another as a/b increases. For long plates the value of k_s may be found from figure 23(a), in which k_{s_∞} appears as a function of ϵ.

Effect of Plate Length on Buckling Coefficient

When k_s is plotted as a function of a/b for infinite and zero values of ϵ (clamped and hinged edges) as shown in figure 23(b), it may be seen that there is little difference between the two curves. This suggests a rapid method of computing the shear-buckling coefficient for any value of ϵ. The coefficient for the specified ϵ is obtained from the curve of k_{s_∞} as a function of ϵ (fig. 23(a)), which is a replot of the minimum k_s line ($n = \infty$) of figure 24. Also, the ratio k_s/k_{s_∞} is found from figure 23(b). Then k_s for the specified a/b and ϵ may be found by computing the product of these two numbers. Estimation of the correct value of k_s/k_{s_∞} will be relatively free from error because of the proximity of the two limiting curves in figure 23(b).

BUCKLING OF FLAT RECTANGULAR PLATES UNDER BENDING LOADS

Historical Background

Timoshenko investigated the buckling stresses for flat rectangular plates under combined longitudinal and bending loads using energy integrals and obtained values for k_b that agree well with later calculations of higher precision (ref. 2). Schuette and McCulloch analyzed long plates under pure bending with supported edges and elastic rotational restraint (ref. 37). Johnson and Noel also investigated the buckling of plates under longitudinal axial load and bending (ref. 38), and Noel analyzed plates for longitudinal bending plus axial load combined with transverse axial load (ref. 39).

Numerical Values of Bending-Buckling Coefficient

The relations between buckle wave length and buckling coefficient for various values of rotational restraint appear in figure 25 together with the wave-length transition lines. The curves of k_b as a function of a/b are shown in figure 26. It is of interest to note that the

value of k_b for infinite plates is roughly six times as great as the value for the supported plate k_c for all values of rotational restraint.

BUCKLING OF FLAT RECTANGULAR PLATES UNDER COMBINED LOADS

General Background

Flat rectangular plates frequently are subjected to combinations of elementary loadings. It has been common practice to consider elementary loadings in pairs and to determine an interaction curve or curves for the combination. However, two recent papers treat triple combinations of the elementary loads, so that an interaction surface in stress ratios is generated, and by taking appropriate sections (e.g., letting one of the stress ratios equal zero) it is possible to reproduce the interaction curves that were derived previously in the literature.

Interaction curves for the combination of bending, shear, and transverse compression on long plates were developed by Johnson and Buchert (ref. 40), and Noel constructed the two-dimensional sections of the surface for longitudinal bending, longitudinal compression, and transverse compression (ref. 39). The backgrounds for the various combinations of loadings are discussed in the following paragraphs. Interaction charts are shown in figures 27 and 28, in which sections of the triple stress-ratio surfaces appear.

A summary of the loading conditions discussed in the following paragraphs appears in table 5. Interaction equations which exist for a few cases are included in the table.

Biaxial Compression

Timoshenko derived a relation between the longitudinal and transverse edge stresses acting on a rectangular plate at buckling (ref. 2). This relation was evaluated for the lowest possible combination of stresses by means of a chart that must be drawn for each a/b value under consideration. As one limiting case of plate proportion and loading, Timoshenko demonstrated that a square plate loaded by equal biaxial stresses has a buckling coefficient of 2, or half of that for a uniaxially loaded square plate.

Libove and Stein evaluated buckling under biaxial loadings by the energy method for rectangular plates supported in several different manners and presented the results in charts of k_x as functions of a/b for various values of k_y, where

$$\left.\begin{aligned}\sigma_x &= k_x\left(\frac{\pi^2 D}{b^2 t}\right)\\ \sigma_y &= k_y\left(\frac{\pi^2 D}{b^2 t}\right)\end{aligned}\right\} \tag{53}$$

and σ_x and σ_y are the two stresses acting on the plate at buckling (ref. 30).

No simple interaction expressions exist for the stress ratios in the general case for the loadings and supports investigated by Libove and Stein. However, for square panels, or for long panels that buckle in square waves, it can be shown, from Timoshenko's results, that

$$R_x + R_y = 1 \tag{54}$$

Noel considered more complicated loading conditions and presented data from which interaction curves may be constructed for biaxial loadings for any value of a/b (ref. 39). Noel's curves appear in figure 28.

Shear and Normal Stress

By application of the energy method, Stowell and Schwartz examined the conditions under which buckling will occur on a long, flat, rectangular panel with edges elastically restrained against rotation under the simultaneous action of shear and normal stresses (ref. 41). They derived the interaction relationship between the stress ratios in the form

$$R_c + R_s^2 = 1 \tag{55}$$

They also derived an expression for the stress combination at buckling through use of the differential equation and tested the interaction equation for several values of restraint coefficient ϵ. The agreement with the interaction equation was found to be excellent, as a consequence of which the interaction equation written above may be applied to this loading case for all values of restraint coefficient and may be used when the axial load is either compression or tension, provided the restraint coefficients are the same on both edges and the panel is infinitely long.

The problem of determining critical loading combinations for shear and transverse normal stress was solved by Batdorf and Houbolt by both the energy method and the differential equation (ref. 42). The significant result of this work is the demonstration that roughly half of the critical shear stress may be applied to a transversely compressed panel without lowering its permissible compressive-buckling stress.

This work was done on infinitely long panels with the long edges supported and elastically restrained against rotation. The restraint coefficient was found to exert an appreciable (although not very large) effect upon the critical loading combination. The results for this type of loading, consequently, do not lend themselves to the writing of a simple explicit interaction equation between the stress ratios. The curves were plotted by Batdorf and Houbolt for both compressive and tensile transverse normal loadings in combination with shear over the entire range of restraint coefficients.

The two preceding loading conditions were reexamined for simply supported plates of finite a/b by Batdorf and Stein with the use of the energy equations (ref. 43). They showed that the parabolic interaction expression of Stowell and Schwartz (eq. (55)) agrees with the interaction curves for finite values of a/b for shear plus longitudinal compression (or tension) (ref. 41). However, the curve derived for infinitely long panels under shear and transverse loading requires modification for finite values of a/b. For a square panel the parabola agrees with the modified curve, while the simple-edge-support case of Batdorf and Houbolt (ref. 42) may be used for $a/b = 4$. The transition region from the modified curves to those for $a/b = \infty$ lies between these two values of a/b.

The large shear stress that may be superimposed upon the critical compressive stress without lowering the permissible compressive stress for infinitely long panels is not possible for square plates. In fact, it appears to be possible for infinitely long plates only.

Bending and Normal Stress

Timoshenko determined the critical combination of bending and normal stresses acting on simply supported flat rectangular plates using the energy method (ref. 2). He determined the buckling coefficient as a function of α for several ratios of moment loading to axial loading for panels with various values of a/b.

Johnson and Noel broadened the scope of the problem by including elastic rotational restraint along the unloaded compression edge (ref. 38). Their results were plotted as k_b versus λ/b for all values of restraint

coefficient. One chart is required for each of the loading ratios (longitudinal loading to moment loading), of which four values were chosen. The loading ratio is defined by

$$\left.\begin{aligned} \alpha &= \frac{12M}{Pb + 6M} \\ \frac{Pb}{M} &= \frac{6(2 - \alpha)}{\alpha} \end{aligned}\right\} \tag{56}$$

where P is the longitudinal load, M is the bending moment, and b is the panel width. They also plot k_b as a function of a/b for the cases of simple support and clamping of the unloaded compression edge of the panel. In addition, the effect of fixity of the unloaded tension edge is depicted for various values of α in a plot of k_b versus a/b in which the hinged and fixed cases are drawn on the same graph. It is apparent that edge fixity does not become important until α falls below 7/4, which corresponds approximately to a Pb/M of 1 or more.

Grossman examined bending in combination with transverse compression using the energy method (ref. 44). He found that for infinite a/b the bending stress ratio can be 0.9 at the same time that the transverse compressive stress ratio is 1. He also provides a graph of the stress ratios for several values of a/b; however, apparently only the infinitely long plate is capable of withstanding bending stresses without buckling while the transverse stress is at its critical value. This is similar to the result found by Batdorf and Stein for shear and transverse compression (ref. 45).

Noel provides interaction curves for simply supported rectangular plates loaded in longitudinal bending, longitudinal compression, and transverse compression (ref. 39). For the limiting case of no transverse loading they agree with the results of Johnson and Noel (ref. 38), and when the longitudinal compression vanishes they agree with those of Grossman (ref. 44). Consequently, their charts can be used for both of these loading combinations. The curves appear in figure 28.

The data of Johnson and Noel and of Noel were obtained from equations solved for infinite values of a/b and were applied to finite values of a/b by use of the identity

$$\lambda/b = a/mb \tag{57}$$

This procedure may be questioned for small aspect ratios; however, it may be justified by comparison with the work of Timoshenko (longitudinal compression and bending) and with the work of Grossman (transverse compression and bending), with which the results of Johnson and Noel and of Noel show good agreement.

Bending and Shear Stress

Timoshenko reports the result of analyzing a rectangular flat plate to determine the critical combination of bending and shear stresses (ref. 2). He used the energy method and plotted the buckling coefficient of the panel as a function of the shear stress ratio. The coefficient, when divided by that for the bending load alone, becomes the bending stress ratio, and the set of curves provided by Timoshenko for various values of a/b becomes an interaction chart, from which it may be seen that the interaction equation is a unit circle:

$$R_s^2 + R_b^2 = 1 \tag{58}$$

The range of a/b for which Timoshenko plotted the curves is from 0.5 to 1.0. However, the curves loop back on themselves as a/b increases, thus indicating that larger values of a/b would yield curves falling within the plot. The maximum variation of stress ratios about the values obtainable from the circular interaction equation is 7 percent, with the equation values the lowest (and hence the most conservative) of all.

Bending, Shear, and Transverse Compression

Johnson and Buchert utilized the Lagrangian multiplier method to determine the critical combinations of bending, shear, and transverse compressive loads on rectangular flat plates of infinite a/b (ref. 40). The results appear as interaction surfaces in the three stress ratios R_b, R_s, and R_c. The two types of support for the plate are simple support along both long edges and simple support along the tension (due to bending) edge with clamping along the compression (due to bending) edge.

Sections of the interaction surfaces taken perpendicular to any of the three stress-ratio axes yield plane stress-ratio curves that agree with the results obtained directly for these cases in previous publications. This is true only of the simply supported plate, of course, since nothing has appeared in the literature for shear plus bending of plates with the compression edge clamped. The interesting result of a shear stress ratio equal to 1.2, with R_b equal to 0.5, is revealed (fig. 27(b)), as well as the combination of $R_c = 0.94$, $R_b = 0.50$, and $R_s = 0.43$.

Longitudinal Bending, Longitudinal Compression, and Transverse Compression

The work of Noel (ref. 39) on the problem of longitudinal bending, longitudinal compression, and transverse compression has been discussed in the section on combined bending and normal stress. The pertinent interaction curves appear in figure 28.

Combined Inelastic Stresses

Stowell utilized the concept of an equivalent-stress intensity for combined stresses applied in constant ratio during loading in the inelastic range (ref. 45). He examined the problem of determining the critical combination of shear and longitudinal compression in elastically supported flat rectangular plates by using the energy method to determine the buckling stresses. From these results, stress ratios were plotted directly from the theoretical results and were also corrected for the changes in effective modulus. From this, Stowell concluded that with little error the following stress-ratio equation is applicable:

$$R_c \frac{(E_s)_{pc}}{(E_s)_{\sigma_i}} + \left[R_s \frac{(E_s)_{ps}}{(E_s)_{\sigma_i}} \right]^2 = 1 \qquad (59)$$

In equation (59), $(E_s)_{pc}$ is the secant modulus at $\sigma = \sigma_{cr}$ for pure compression, $(E_s)_{ps}$ is the corresponding secant modulus for pure shear, and $(E_s)_{\sigma_i}$ is the secant modulus for the effective stress of the combined loading at buckling; $(E_s)_{\sigma_i} = \left[3\left(\sigma_x^2 + 3\tau^2\right) \Big/ \left(3\epsilon_x^2 + \gamma^2\right) \right]^{1/2}$. The similarity of this expression to that for the elastic case is apparent; in fact, in the elastic range the expression reduces to the equation for elastic loads.

A recent investigation of Peters on long square tubes loaded in torsion and compression (ref. 17) indicates that a stress-ratio equation of the form

$$R_c^2 + R_s^2 = 1 \qquad (60)$$

agrees slightly better with the test data (fig. 29) than does the modified parabola of Stowell (ref. 45). Actually, the data yield slightly higher stress-ratio combinations than do either of interaction equations (59) or (60), with the discrepancy increasing with decreasing stress levels. For stresses wholly in the elastic range the data are as much as 100 percent higher (that is, R_s is 0.4 instead of 0.2 for R_c equal to 1). The data also agree closely with a theoretical curve obtained by Budiansky, Stein, and Gilbert for long square tubes loaded elastically in torsion and compression (ref. 46).

EFFECT OF PRESSURE ON BUCKLING OF RECTANGULAR FLAT PLATES

Range of Published Results

The effect of normal pressure on the longitudinal compressive-buckling stress of a rectangular flat plate has been investigated for both simply supported and clamped edges. Levy, Goldenberg, and Zibritosky (ref. 47) analyzed the simply supported plate using the large-deflection differential equations of Von Kármán. The plate length was four times the width, which places it in the long-plate category. The data reveal a rise in longitudinal compressive-buckling stress for this configuration which increases with pressure. However, this rise may be realizable only in a plate of such proportions and loading because of the significant difference in wave forms of the long plate under compressive and pressure loadings. It may be intuitively evident that when there is little difference between these wave forms, such as for a short plate under combined longitudinal compression and normal pressure, there may be a reduction in the compressive-buckling stress of the plate. No data are available in this case, however.

Longitudinally Compressed Long Simply Supported Plates

High normal pressure was found to increase the compressive-buckling stress considerably for the long simply supported plate tested by Levy, Goldenberg, and Zibritosky (ref. 47). For example, when the pressure applied to a plate with length four times the width reached $24.03Et^4/b^4$, the buckling stress was 3.1 times that for zero normal pressure on the plate. Levy, Goldenberg, and Zibritosky also showed that more than one equilibrium configuration of the plate was possible when normal pressure was applied, with the configuration at any instant depending upon the previous loading history. The plate could be either buckled or unbuckled under various specific combinations of axial load and normal pressure.

Longitudinally Compressed Long Clamped Plates

Woolley, Corrick, and Levy analyzed a longitudinally compressed long clamped plate (ref. 48). For this case the effect of pressure was not so pronounced as for simply supported edges. The maximum buckling load for a pressure of $37.55Et^4/b^4$ was found to be 1.3 times that for no normal pressure. Also, for clamped plates the buckle pattern was found to be unique for any particular combination of pressure and axial loading.

SPECIAL CASES

Use of Elastic-Buckling-Stress Expression

It has been shown that the elastic-buckling stress for any flat rectangular plate of constant thickness can be computed using equation (26) for various loading and boundary conditions. There are also flat plates of interest to aeronautical engineers that are neither rectangular nor of constant thickness. By suitable choice of the buckling coefficient and definition of the plate thickness and proportions it is possible to utilize equation (26) to compute the buckling stresses for these plates also.

Axially Compressed Plate With Variable Loading and Thickness

Pines and Gerard investigated the proportions of a simply supported flat rectangular plate under varying axial loading to determine an efficient thickness variation for minimum weight (ref. 49). The plate rigidity was assumed to be proportional to the axial load in order to satisfy equation (26) at any spanwise station. The load variation along the plate was assumed to be produced by shear stresses small enough to have negligible influence upon the buckling characteristics of the plate. Furthermore, the airloading on a typical wing develops a cover axial loading that closely follows an exponential variation that decays from the root outboard. This will dictate maximum axial loading on the cover at the root, which is depicted as station A in figure 30, in which a sketch of the tapered plate is shown together with the loading and plate thickness variations that follow as a result of the assumptions made by Pines and Gerard.

Results presented in the form of the buckling coefficient as a function of a/b for various values of the logarithm of the loading ratio (Maximum loading/Minimum loading) reveal little increase of buckling coefficient until the loading ratio begins to exceed e (the base of natural logarithms) (fig. 30).

In cases in which β is large, the buckling-coefficient chart reveals that the number of buckles in a panel of predetermined a/b may exceed the number of buckles for $\beta = 1$.

Axially Compressed Plate With Variable Loading and Constant Thickness

The problem of determining the buckling stress of an axially compressed flat rectangular plate was investigated by Libove, Ferdman, and Reusch for a simply supported plate with constant thickness and a linear axial load gradient (ref. 50). They plotted the effective buckling-stress coefficient as a function of the loading ratio for various values of a/b. For the sake of uniformity of presentation, their curves have been replotted here in the form of $k_{c_{av}}$ as a function of a/b for various values of the loading ratio, including negative values (tension at one edge) as large as -3. These curves appear in figure 31.

The buckling coefficient $k_{c_{av}}$ applies to the average axial loading on the plate, which is equal to $(\sigma_A + \sigma_B)/2$ with σ_A assumed to be the larger of the two end loads. The average plate load is $(\sigma_A/2)\left[1 + (1/\beta)\right]$. This permits rapid comparison with the buckling stress of a plate with constant axial load, which is the curve for $\beta = 1$ in figure 31.

Long plates will buckle at the end at which the maximum load is applied, for which k_c is equal to 4.

Parallelogram Panels in Compression

Anderson investigated compressive buckling of a flat sheet subdivided into panels by nondeflecting supports that form a parallelogram gridwork under the sheet (ref. 51). One set of supports (all equally spaced) runs longitudinally, and the other runs at an angle φ to the normal, or transverse, direction. The longitudinal spacing of the diagonal supports is a, and the transverse spacing of the longitudinal supports is b. Buckling coefficients were plotted as functions of a/b for both longitudinal compression and transverse compression for various values of the angle φ (figs. 32(a) and 32(b)). In addition, interaction curves were provided for combinations of these two loadings in the form of buckling-coefficient combinations for various values of φ (fig. 32(c)).

For large values of a/b the buckling-coefficient curves approach the curves for simply supported rectangular plates under compression. The largest φ for which Anderson provides curves is 60°. For longitudinal loading the angularity of the supports does not appear to influence k until φ exceeds 15°. For small values of a/b the influence becomes pronounced at values of a/b in the region of unity, with the buckling coefficient reaching a value of over 20 for φ equal to 60°.

The transverse-buckling coefficient is not so severely affected by φ, since k increases from 4 to 5 as φ increases from zero to 30°. For φ equal to 60°, k is 9 at $a/b = 1$.

Parallelogram Plates

Wittrick determined the buckling stress of a parallelogram plate with clamped edges under the action of uniform compression in one direction (ref. 52). His work differs from the work of Anderson (ref. 51) in that specified rotational boundary conditions are applied to the plate in this case. Both Wittrick and Anderson employed the energy approach in oblique coordinates to obtain solutions. Results are presented in the form of curves of the buckling coefficient k_c as a function of a/b. Wittrick presented data for edge angles of 0° (rectangular plate), 30°, and 45° as shown in figure 33(a), in which the plate geometry is depicted.

Guest (ref. 53) and Guest and Silberstein (ref. 54) analyzed simply supported parallelogram plates under longitudinal compression and, for a rhombic plate of 30° edge angle, determined that $k_c = 5.60$. Wittrick also analyzed clamped parallelogram plates in shear and obtained the results shown in figure 33(b) (ref. 55). Hasegawa analyzed buckling of clamped rhombic plates in shear (ref. 56), for which buckling coefficients appear in the table below. The general plate geometry of figure 33(b) applies to this case.

θ, deg . .	0	15	20	30	35
k_s	14.7	21.0	26.6	40.0	51.0

Triangular Plates

The buckling of triangular plates under various loads and edge supports was investigated by Woinowsky-Krieger (ref. 57), Klitchieff (ref. 58), Wittrick (refs. 59 to 61), and Cox and Klein (ref. 62). Woinowsky-Krieger computed the buckling stress of a simply supported equilateral triangular

plate under uniform compression and found k_c to equal 5 when the base of the triangle is taken equal to b in equation (26). Klitchieff investigated the buckling of right-angle isosceles triangular plates with pure shear on the orthogonal sides applied so as to produce compression along the altitude upon the hypotenuse. Wittrick evaluated the buckling coefficient for shear applied so as to produce either compression or tension along the altitude and also included the effects of normal stresses applied to the equal legs of the triangle. Cox and Klein analyzed buckling in isosceles triangles of any vertex angle for normal stress alone and for shear alone.

The buckling coefficients presented in this section are to be used in conjunction with equation (26). The geometry of a triangular plate is shown in figure 34. The data of Cox and Klein appear in figure 34(a) for uniform compression and in figure 34(b) for shear along the equal legs. Both simply supported and clamped edges were considered. The results of Cox and Klein agree with the data of Wittrick for right-angle isosceles triangular plates, which appear in table 6. The shear buckling coefficients k_{s_+} and k_{s_-} refer to pure shear loadings which produce tension and compression, respectively, along the altitude upon the hypotenuse of the triangle.

For shear and normal stress on a right-angle isosceles plate the interaction equation

$$\left(\frac{2\tau}{\tau_{cr_+} + \tau_{cr_-}} + u\right)^2 + \frac{\sigma}{\sigma_{cr}}(1 - u^2) = 1 \tag{61}$$

applies, in which $u = \left(k_{s_+} - k_{s_-}\right)\Big/\left(k_{s_+} + k_{s_-}\right)$.

Research Division, College of Engineering,
New York University,
New York, N. Y., October 29, 1954.

APPENDIX A

APPLICATION SECTION

Introduction

Procedures for the computation of the elastic and plastic buckling stresses of flat plates based on general plate-buckling equation (1) are summarized in this section. The factors appearing in this equation are briefly discussed and charts are presented from which numerical values of these factors may be obtained.

The elementary loadings such as compression, shear, and bending frequently are considered in preliminary design by using the buckling coefficients for the limiting cases (infinite values of a/b, clamping or hinging of the plate edges, and so forth). For convenience table 7 has been compiled containing the values of the buckling coefficients that pertain to some of these limiting cases, while figure 14 displays the curves for k_c as a function of a/b for different combinations of limiting edge conditions.

Physical Properties of Materials

The buckling stress of a flat plate is determined when the loading, plate geometry, and material are specified. The loading dictates the particular chart to be used to find the buckling coefficient k, and the plate a/b and edge restraint locate the numerical value of k to be found from that chart. For an unclad plate ($\bar{\eta} = 1$) which buckles elastically ($\eta = 1$), σ_{cr} can be found directly from equation (1) if E is known. The effects of cladding and plasticity depend upon the type of loading and the stress level and therefore require a more detailed knowledge of the stress-strain characteristics of the material.

The three-parameter description of stress-strain data can be used as a convenient generalized approach in buckling problems. With this method figure 3 can be employed to find the shape factor n. Since E, $\sigma_{0.7}$, and n can be readily determined (see table 8 for average values of n), nondimensional curves are available from figure 4. It is to be noted that, in many cases, plastic-buckling charts have been prepared from which the plastic-buckling stress may be determined if one knows E, $\sigma_{0.7}$, and n.

Table 9 contains the old and new designations for wrought aluminum alloys. The new designations are used throughout this report and the table is included for use with the various references. Characteristics of the cladding used on several structural aluminum alloys are shown in table 4.

Poisson's ratio beyond the proportional limit can be calculated using $\nu_{pl} = 0.5$ in the expression

$$\nu = \nu_{pl} - \left(\nu_{pl} - \nu_e\right)\left(E_s/E\right) \tag{A1}$$

Frequently buckling stresses are computed using the equation

$$\sigma_{cr} = \bar{\eta}\eta KE(t/b)^2 \tag{A2}$$

where $K = k\pi^2/12(1 - \nu^2)$. The expression K/k can be found as a function of ν in figure 35.

Compressive Buckling

Plates.- For plates, k_c appears in figure 16 in terms of a/b and ϵ and in figure 15 in terms of λ/b and ϵ. For an infinitely long plate, k_c may be found from figure 17 in terms of ϵ alone. When ϵ is not the same for both unloaded edges, the geometric mean of the k_c values for each edge may be used (eq. (49)).

The plasticity-reduction factor for a long plate with simply supported edges is

$$\eta = \left[\left(E_s/E\right)\left(1 - \nu_e^2\right)\Big/\left(1 - \nu^2\right)\right]\left\{0.500 + 0.250\left[1 + \left(3E_t/E_s\right)\right]\right\}^{1/2} \tag{A3}$$

while for a long clamped plate

$$\eta = \left[\left(E_s/E\right)\left(1 - \nu_e^2\right)\Big/\left(1 - \nu^2\right)\right]\left\{0.352 + 0.324\left[1 + \left(3E_t/E_s\right)\right]\right\}^{1/2} \tag{A4}$$

Inelastic plate-buckling stresses may be calculated using the nondimensional chart of figure 9.

The cladding reduction factor for $\sigma_{cl} < \sigma_{cr} < \sigma_{pl}$ is approximately given by equation (42):

$$\bar{\eta} = \frac{1 + 3\beta f}{1 + 3f} \tag{42}$$

For $\sigma_{cr} > \sigma_{pl}$, as an adequate approximation, equation (40) holds true:

$$\bar{\eta} = \frac{1}{1 + 3f}\left(\frac{\left\{\left[1 + \left(3f\bar{E}_s/E_s\right)\right] + \left\{\left[1 + \left(3f\bar{E}_s/E_s\right)\right]\left[(1/4) + (3/4)\left(E_t/E_s\right) + \nu\right]\right\}^{1/2}}{1 + \left[(1/4) + (3/4)\left(E_t/E_s\right)\right]^{1/2}}\right) \tag{43}$$

The effect of lateral restraint in reducing k_c may be determined from figure 21 for values of A_r/at, and the effects of thickness taper and axial load variation may be calculated with the aid of figures 30 and 31.

The gain in buckling stress with obliquity of the loaded edges is shown in figure 33(a) for clamped parallelogram plates, while figure 32 depicts buckling coefficients for large sheets divided into parallelogram panels by nondeflecting supports. For data on triangular plates, figure 34(a) may be used to find k_c.

The variation in k_c with b/t for stiffened plates with torsionally weak or strong edge stiffeners appears in figure 18. Because of the sparse data available, no recommendation can be made concerning the effect of normal pressure upon buckling.

Flanges.- For flanges, k_c may be found in figure 20 as a function of a/b and ϵ and in figure 19 as a function of λ/b and ϵ for $\nu = 0.3$. For an infinitely long flange, figure 17 contains k_c as a function of ϵ alone. The effect of varying ν appears in figure 2.

The plasticity-reduction factor for a long hinged flange is

$$\eta = \left(E_s/E\right)\left(1 - \nu_e^2\right)\Big/\left(1 - \nu^2\right) \tag{A5}$$

For a long clamped flange,

$$\eta = \left[\left(E_s/E\right)\left(1 - \nu_e^2\right)\Big/\left(1 - \nu^2\right)\right]\left\{0.330 + 0.335\left[1 + \left(3E_t/E_s\right)\right]\right\}^{1/2} \tag{A6}$$

For the former case the nonlinensional buckling chart of figure 8 may be used, while that of figure 9 may be used for the latter case with little error.

For flange cladding reduction factors when $\sigma_{cr} > \sigma_{pl}$, it may be permissible to use equation (40). Although this factor was not computed in the section entitled "Cladding Reduction Factors," it appears to be reasonable by comparison with the factors for plates and columns.

Plate columns.- For plate columns, the buckling stress may be determined using figure 2(a).

For a short plate column ($L/b < 1$) the plasticity-reduction factor is

$$\eta = \left[\left(E_s/4E\right)\left(1 - \nu_e^2\right)\Big/\left(1 - \nu^2\right)\right]\left[1 + \left(3E_t/E_s\right)\right] \tag{A7}$$

For a square plate column ($L/b = 1$),

$$\eta = \left[\left(E_s/E\right)\left(1 - \nu_e^2\right)\Big/\left(1 - \nu^2\right)\right]\left[0.114 + \left(0.886E_t/E_s\right)\right] \tag{A8}$$

For a long plate column ($L/b > 1$), the plasticity-reduction factor is

$$\eta = \left(E_t/E\right)\left(1 - \nu_e^2\right)\Big/\left(1 - \nu^2\right) \tag{A9}$$

The cladding reduction factor for short plate columns in which $\sigma_{cl} < \sigma_{cr} < \sigma_{pl}$ is

$$\bar{\eta} = \left[1 + \left(3\bar{\epsilon}/4\right)\right]\Big/\left(1 + 3\bar{\epsilon}\right) \tag{A10}$$

and when $\sigma_{cr} > \sigma_{pl}$ equation (4C) holds true which is also applicable to long plate columns at all stress levels above σ_{cl}.

Shear Buckling

The shear-buckling-stress coefficient as a function of a/b is shown in figure 22 for clamped and hinged plate edges. For long plates,

which buckle in the symmetric mode, figure 24 may be used to find k_s as a function of λ/b and ϵ. For plates of finite length the procedure of the section entitled "Buckling of Flat Rectangular Plates Under Shear Loads" may be used in conjunction with figures 22 and 23.

The plasticity-reduction factor for long plates in shear is given by equation (A5). Inelastic shear-buckling stresses may be calculated with the aid of the nondimensional chart of figure 10.

The cladding reduction factor for $\sigma_{cl} < \sigma_{cr} < \sigma_{pl}$ is given by equation (42), and for $\sigma_{cr} > \sigma_{pl}$ equation (40) holds true.

For clamped oblique plates figure 32(b) may be used to find k_s when the plate edge angle is 45°. For triangular-plate shear-buckling coefficients figure 34(b) may be used. In addition, the section entitled "Special Cases" should be consulted.

Bending Buckling

The bending-buckling coefficient appears in figure 26 as a function of a/b and ϵ and in figure 25 as a function of λ/b. The plasticity-reduction factor for a simply supported plate is the same as for a hinged flange. Little error should be expected in using elastically restrained flange plasticity-reduction factors for elastically restrained plates in bending. For these cases the plastic-buckling chart of figure 9 may be used to find σ_{cr}, which is the maximum compressive stress on the plate section. In order to find the corresponding moment it is necessary to integrate the stress distribution, for which purpose the curves of figure 9 may be used.

Combined Loading

Interaction equations for various combinations of compression, shear, and bending appear in table 5. These expressions are presented in graphical form in figures 27 and 28 for elastic buckling. For longitudinal compression and shear on a long rectangular plate, with both applied stresses in the inelastic range, equation (60) holds true:

$$R_c^2 + R_s^2 = 1 \tag{60}$$

The plasticity-reduction factor for a simply supported plate in combined compression and axial load varies between that for a hinged flange and that for a simply supported plate under axial compression, depending

upon the ratio of bending stress to axial stress. The value of η for this case is shown in equation (34):

$$\eta = \left(\frac{1 - \nu_e^2}{1 - \nu^2}\right)\left[\frac{\alpha}{2}\left(E_s/E\right) + \left(1 - \frac{\alpha}{2}\right)\eta_e\right] \tag{34}$$

Actually, utilization of the plastic-buckling chart of figure 9 for all cases of combined bending and axial load to find σ_{cr} (after which the plate loading may be found by integrating the cross-section stress distribution) should give conservative results.

On right-angle isosceles triangular plates loaded under shear and compression as shown in the sketches in figures 34(a) and 34(b), equation (61) applies:

$$\left(\frac{2\tau}{\tau_{cr_+} + \tau_{cr_-}} + u\right)^2 + \frac{\sigma}{\sigma_{cr}}(1 - u^2) = 1 \tag{61}$$

Table 6 contains numerical values of k_c and k_s for different types of plate edge supports.

REFERENCES

1. Seehler, E. E., and Newell, J. S.: Progress Report on Methods of Analysis Applicable to Monocoque Aircraft Structures. Tech. Rep. No. 4313, Air Materiel Command, Army Air Forces, Oct. 1947.

2. Timoshenko, S.: Theory of Elastic Stability. First ed., McGraw-Hill Book Co., Inc., 1936.

3. Sokolnikoff, I. S.: Mathematical Theory of Elasticity. First ed., McGraw-Hill Book Co., Inc., 1946.

4. Bleich, Friedrich: Buckling Strength of Metal Structures. First ed., McGraw-Hill Book Co., Inc., 1952.

5. Stowell, Elbridge Z.: A Unified Theory of Plastic Buckling of Columns and Plates. NACA Rep. 898, 1948. (Supersedes NACA TN 1556.)

6. Budiansky, Bernard, and Hu, Pai C.: The Lagrangian Multiplier Method of Finding Upper and Lower Limits to Critical Stresses of Clamped Plates. NACA Rep. 848, 1946.

7. Houbolt, John C., and Stowell, Elbridge Z.: Critical Stress of Plate Columns. NACA TN 2163, 1950.

8. Lundquist, Eugene E., and Stowell, Elbridge Z.: Critical Compressive Stress for Outstanding Flanges. NACA Rep. 734, 1942.

9. Ramberg, Walter, and Osgood, William R.: Description of Stress-Strain Curves by Three Parameters. NACA TN 902, 1943.

10. Gerard, George, and Wildhorn, Sorrel: A Study of Poisson's Ratio in the Yield Region. NACA TN 2561, Jan. 1952.

11. Udy, M. C., Shaw, H. L., and Boulger, F. W.: Properties of Beryllium. Nucleonics, vol. 11, no. 5, May 1953, pp. 52-59.

12. Goodman, Stanley, and Russell, Stanton B.: Poisson's Ratio of Aircraft Sheet Material for Large Strains. Tech. Rep. 53-7, Contract PO 33(038)51-4061, WADC and Nat. Bur. Standards, Feb. 1953.

13. Stang, A. H., Greenspan, M., and Newman, S. B.: Poisson's Ratio of Some Structural Alloys for Large Strains. Res. Paper RP 1742, Jour. Res., Nat. Bur. Standards, vol. 37, no. 4, Oct. 1946, pp. 211-221.

14. Stowell, Elbridge Z.: Compressive Strength of Flanges. NACA Rep. 1029, 1951. (Supersedes NACA TN 2020.)

15. Gerard, G.: Secant Modulus Method for Determining Plate Instability Above the Proportional Limit. Jour. Aero. Sci., vol. 13, no. 1, Jan. 1946, pp. 38-44, 48.

16. Pride, Richard A., and Heimerl, George J.: Plastic Buckling of Simply Supported Compressed Plates. NACA TN 1817, 1949.

17. Peters, Roger W.: Buckling of Long Square Tubes in Combined Compression and Torsion and Comparison With Flat-Plate Buckling Theories. NACA TN 3184, 1954.

18. Bijlaard, P. P.: Theory and Tests on the Plastic Stability of Plates and Shells. Jour. Aero. Sci., vol. 16, no. 9, Sept. 1949, pp. 529-541.

19. Handelman, G. H., and Prager, W.: Plastic Buckling of a Rectangular Plate Under Edge Thrusts. NACA Rep. 946, 1949. (Supersedes NACA TN 1530.)

20. Ilyushin, A. A.: The Theory of Elasto-Plastic Strains and Its Application. Bull. Acad. Sci., URSS, Sec. Tech. Services, June 1948, pp. 769-788.

21. Gerard, G.: Critical Shear Stress of Plates Above the Proportional Limit. Jour. Appl. Mech., vol. 15, no. 1, Mar. 1948, pp. 7-12.

22. Stowell, Elbridge Z.: Critical Shear Stress of an Infinitely Long Plate in the Plastic Region. NACA TN 1681, 1948.

23. Stowell, E. Z., and Pride, R. A.: The Effect of Compressibility of the Material on Plastic Buckling Stresses. Readers' Forum, Jour. Aero. Sci., vol. 18, no. 11, Nov. 1951, p. 773; and Author's Reply, Readers' Forum, Jour. Aero. Sci., vol. 19, no. 7, July 1952, p. 494.

24. Bijlaard, P. P.: Theory of Plastic Buckling of Plates and Application to Simply Supported Plates Subjected to Bending or Eccentric Compression in Their Plane. Reprint No. 55 - A-8, A.S.M.E., Nov. 1955.

25. Bijlaard, P. P.: Taking Account of the Compressibility of the Material in the Plastic Buckling of Plates. Readers' Forum, Jour. Aero. Sci., vol. 19, no. 7, July 1952, pp. 493-494.

26. Buchert, Kenneth P.: Stability of Alclad Plates. NACA TN 1986, 1949.

27. Bryan, G. H.: On the Stability of a Plane Plate Under Thrusts in Its Own Plane, With Applications to the "Buckling" of the Sides of a Ship. Proc. London Math. Soc., vol. 22, Dec. 11, 1890, pp. 54-67.

28. Hill, H. N.: Chart for Critical Compressive Stress of Flat Rectangular Plates. NACA TN 733, 1940.

29. Lundquist, Eugene E., and Stowell, Elbridge, Z.: Critical Compressive Stress for Flat Rectangular Plates Supported Along All Edges and Elastically Restrained Against Rotation Along the Unloaded Edges. NACA Rep. 733, 1942.

30. Libove, Charles, and Stein, Manuel: Charts for Critical Combinations of Longitudinal and Transverse Direct Stress for Flat Rectangular Plates. NACA WR L-224, 1946. (Formerly NACA ARR L6A05.)

31. Gerard, George: Effective Width of Elastically Supported Flat Plates. Jour. Aero. Sci., vol. 13, no. 10, Oct. 1946, pp. 518-524.

32. Argyris, J. H., and Dunne, P. C.: Structural Principles and Data. Handbook of Aero., no. 1, pt. 2, 1952.

33. Southwell, R. V., and Skan, Silvia W.: On the Stability Under Shearing Forces of a Flat Elastic Strip. Proc. Roy. Soc. (London), ser. A, vol. 105, 1924, pp. 582-607.

34. Stowell, Elbridge Z.: Critical Shear Stress of an Infinitely Long Flat Plate With Equal Elastic Restraints Against Rotation Along the Parallel Edges. NACA WR L-476, 1943. (Formerly NACA ARR 3K12.)

35. Stein, Manuel, and Neff, John: Buckling Stresses of Simply Supported Rectangular Flat Plates in Shear. NACA TN 1222, 1947.

36. Budiansky, Bernard, and Connor, Robert W.: Buckling Stresses of Clamped Rectangular Flat Plates in Shear. NACA TN 1559, 1948.

37. Schuette, Evan H., and McCulloch, James C.: Charts for the Minimum-Weight Design of Multiweb Wings in Bending. NACA TN 1323, 1947.

38. Johnson, James E., Jr., and Noel, Robert G.: Critical Bending Stress for Flat Rectangular Plates Supported Along All Edges and Elastically Restrained Against Rotation Along the Unloaded Compression Edge. Jour. Aero. Sci., vol. 20, no. 8, Aug. 1953, pp. 535-540.

39. Noel, Robert G.: Elastic Stability of Simply Supported Flat Rectangular Plates Under Critical Combinations of Longitudinal Bending, Longitudinal Compression, and Lateral Compression. Jour. Aero. Sci., vol. 19, no. 12, Dec. 1952, pp. 829-834.

40. Johnson, Aldie E., Jr., and Buchert, Kenneth P.: Critical Combinations of Bending, Shear, and Transverse Compressive Stresses for Buckling of Infinitely Long Flat Plates. NACA TN 2536, 1951.

41. Stowell, Elbridge Z., and Schwartz, Edward B.: Critical Stress for an Infinitely Long Flat Plate With Elastically Restrained Edges Under Combined Shear and Direct Stress. NACA WR L-340, 1943. (Formerly NACA ARR 3K13.)

42. Batdorf, S. B., and Houbolt, John C.: Critical Combinations of Shear and Transverse Direct Stress for an Infinitely Long Flat Plate With Edges Elastically Restrained Against Rotation. NACA TR 847, 1946.

43. Batdorf, S. B., and Stein, Manuel: Critical Combinations of Shear and Direct Stress for Simply Supported Rectangular Flat Plates. NACA TN 1223, 1947.

44. Grossman, Norman: Elastic Stability of Simply Supported Flat Rectangular Plates Under Critical Combinations of Transverse Compression and Longitudinal Bending. Jour. Aero. Sci., vol. 16, no. 5, May 1949, pp. 272-276.

45. Stowell, Elbridge Z.: Plastic Buckling of a Long Flat Plate Under Combined Shear and Longitudinal Compression. NACA TN 1990, 1949.

46. Budiansky, Bernard, Stein, Manuel, and Gilbert, Arthur C.: Buckling of a Long Square Tube in Torsion and Compression. NACA TN 1751, 1948.

47. Levy, Samuel, Goldenberg, Daniel, and Zibritosky, George: Simply Supported Long Rectangular Plate Under Combined Axial Load and Normal Pressure. NACA TN 949, 1944.

48. Woolley, Ruth M., Corrick, Josephine N., and Levy, Samuel: Clamped Long Rectangular Plate Under Combined Axial Load and Normal Pressure. NACA TN 1047, 1946.

49. Pines, S., and Gerard, G.: Instability Analysis and Design of an Efficiently Tapered Plate Under Compressive Loading. Jour. Aero. Sci., vol. 14, no. 10, Oct. 1947, pp. 594-599.

50. Libove, Charles, Ferdman, Saul, and Reusch, John J.: Elastic Buckling of a Simply Supported Plate Under a Compressive Stress that Varies Linearly in the Direction of Loading. NACA TN 1891, 1949.

51. Anderson, Roger A.: Charts Giving Critical Compressive Stress of Continuous Flat Sheet Divided Into Parallelogram-Shaped Panels. NACA TN 2392, 1951.

52. Wittrick, W. H.: Buckling of Oblique Plates With Clamped Edges Under Uniform Compression. Rep. SM. 182, Aero. Res. Labs., Dept. Supply (Melbourne), Nov. 1951. (Also, Aero. Quart., vol. 4, pt. II, Feb. 1953, pp. 151-163.)

53. Guest, J.: The Compressive Buckling of a Parallelogram Plate Simply Supported Along All Four Edges. Rep. SM. 199, Aero. Res. Labs., Dept. Supply (Melbourne), Sept. 1952.

54. Guest, J., and Silberstein, J. P. O.: A Note on the Buckling of Simply Supported Parallelogram Plates. Structures and Materials Note 204, Aero. Res. Labs., Dept. Supply (Melbourne), May 1953.

55. Wittrick, W. H.: Buckling of Oblique Plates With Clamped Edges Under Uniform Shear. Rep. SM. 210, Aero. Res. Labs., Dept. Supply (Melbourne), June 1953.

56. Hasegawa, M.: On Buckling of a Clamped Rhombic Thin Plate in Shear. Readers' Forum, Jour. Aero. Sci., vol. 21, no. 10, Oct. 1954, p. 720.

57. Woinowsky-Krieger, S.: Über die Biegung von Platten durch Einzellasten mit rechteckiger Aufstandsfäche. Ing.-Archiv, vol. 21, 1953, pp. 331-338.

58. Klitchieff, J. M.: Buckling of a Triangular Plate by Shearing Forces. Quart. Jour. Mech. and Appl. Math., vol. IV, pt. 3, 1951, pp. 257-259.

59. Wittrick, W. H.: Buckling of a Simply Supported Triangular Plate in Combined Compression and Shear. Rep. SM. 197, Aero. Res. Labs., Dept. Supply (Melbourne), July 1952.

60. Wittrick, W. H.: Buckling of a Right-Angled Isosceles Triangular Plate in Combined Compression and Shear (Perpendicular Edges Simply Supported, Hypotenuse Clamped). Rep. SM. 220, Aero. Res. Labs., Dept. Supply (Melbourne), Nov. 1955.

61. Wittrick, W. H.: Buckling of a Right-Angled Isosceles Triangular Plate in Combined Compression and Shear (Perpendicular Edges Clamped, Hypotenuse Simply Supported). Rep. SM. 211, Aero. Res. Labs., Dept. Supply (Melbourne), June 1953.

62. Cox, H. L., and Klein, B.: The Buckling of Isosceles Triangular Plates. Jour. Aero. Sci., vol. 22, no. 5, May 1955, pp. 321-325.

63. Cozzone, F. P., and Melcon, M. A.: Nondimensional Buckling Curves - Their Development and Application. Jour. Aero. Sci., vol. 13, no. 10, Oct. 1946, pp. 511-517.

64. Anon.: Chemical Composition Limits for Aluminum Alloys. Alcoa Data Sheet, Aluminum Co. of Am., Jan. 4, 1955.

TABLE 1.- ASSUMPTIONS OF INELASTIC-BUCKLING THEORIES

Investigator	Stress-strain law	Plasticity law	Buckling model
Bijlaard (ref. 18)	Incremental and deformation types, ν instantaneous	Octahedral shear	No strain reversal
Handelman-Prager (ref. 19)	Incremental type, ν instantaneous	Octahedral shear	Strain reversal
Ilyushin (ref. 20)	Deformation type, $\nu = 0.5$	Octahedral shear	Strain reversal
Stowell (refs. 5 and 34)	Deformation type, $\nu = 0.5$	Octahedral shear	No strain reversal

TABLE 2.- PLASTICITY-REDUCTION FACTORS

$$\left[j = \left(E_s/E\right)\left(1 - \nu_e^2\right)\Big/\left(1 - \nu^2\right)\right]$$

Loading	Structure	η/j
Compression	Long flange, one unloaded edge simply supported	1
	Long flange, one unloaded edge clamped	$0.330 + 0.335\left[1 + \left(3E_t/E_s\right)\right]^{1/2}$
	Long plate, both unloaded edges simply supported	$0.500 + 0.250\left[1 + \left(3E_t/E_s\right)\right]^{1/2}$
	Long plate, both unloaded edges clamped	$0.352 + 0.324\left[1 + \left(3E_t/E_s\right)\right]^{1/2}$
	Short plate loaded as a column ($L/b \ll 1$)	$0.250\left[1 + \left(3E_t/E_s\right)\right]$
	Square plate loaded as a column ($L/b = 1$)	$0.114 + 0.886\left(E_t/E_s\right)$
	Long column ($L/b \gg 1$)	E_t/E_s
Shear	Rectangular plate, all edges elastically restrained	$0.83 + 0.17\left(E_t/E_s\right)$

TABLE 3.- SUMMARY OF SIMPLIFIED CLADDING REDUCTION FACTORS

Loading	$\sigma_{cl} < \bar{\sigma}_{cr} < \sigma_{pl}$	$\bar{\sigma}_{cr} > \sigma_{pl}$
Short plate columns	$\frac{1 + (3\beta f/4)}{1 + 3f}$	$\frac{1}{1 + 3f}$
Long plate columns	$\frac{1}{1 + 3f}$	$\frac{1}{1 + 3f}$
Compression and shear panels	$\frac{1 + 3\beta f}{1 + 3f}$	$\frac{1}{1 + 3f}$

TABLE 4.- CLADDING MATERIAL AND THICKNESS FOR ALCLAD PLATES

[Data taken from reference 64]

Material designation	Cladding material	Total plate thickness, in.	Total cladding thickness, f, in.
Alclad 2014	6053	<0.040 ≥.040	0.20 .10
Alclad 2024	1230	<0.064 ≥.064	0.10 .05
Alclad 7075	7072	All thicknesses	0.08

TABLE 5.- COMBINED LOADING CONDITIONS FOR WHICH INTERACTION CURVES EXIST

Theory	Loading combination	Interaction equation	Figure
Elastic	Biaxial compression	For plates that buckle in square waves, $R_x + R_y = 1$	28
	Longitudinal compression and shear	For long plates, $R_c + R_s^2 = 1$	27
	Longitudinal compression and bending	None	28
	Bending and shear	$R_b^2 + R_s^2 = 1$	27
	Bending, shear, and transverse compression	None	27
	Longitudinal compression and bending and transverse compression	None	28
Inelastic	Longitudinal compression and shear	$R_c^2 + R_s^2 = 1$	29

TABLE 6.- BUCKLING COEFFICIENTS FOR RIGHT-ANGLE ISOSCELES TRIANGULAR PLATES LOADED INDEPENDENTLY IN UNIFORM COMPRESSION, POSITIVE SHEAR, AND NEGATIVE SHEAR

Edge supports (a)	k_c	k_{s_+}	k_{s_-}
All edges simply supported	10.0	62.0	23.2
Sides simply supported, hypotenuse clamped	15.6	70.8	34.0
Sides clamped, hypotenuse simply supported	18.8	80.0	44.0

[a]Hypotenuse = b in figure 34.

TABLE 7.- BUCKLING COEFFICIENTS FOR INFINITELY LONG PLATES UNDER VARIOUS TYPES OF LOADS

Loading	Edge support	Coefficient	
Compression 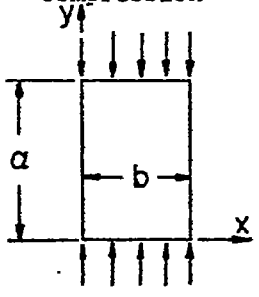	SS on all edges	$k_c = 4.0$	NACA Rep. 733 (ref. 29)
	C on all edges	$k_c = 6.98$	
	SS on $y = 0$, $y = a$, $x = 0$ F on $x = b$	$k_c = 0.43$	NACA Rep. 734 (ref. 8)
	C on $y = 0$, $y = a$, $x = 0$ F on $x = b$	$k_c = 1.28$	
Shear 	SS on all edges	$k_s = 5.35$	NACA TN 1222 (ref. 35)
	C on all edges	$k_s = 8.98$	NACA TN 1223 (ref. 43)
Bending 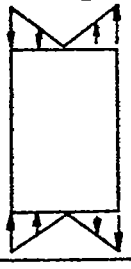	SS on all edges	$k_b = 23.9$	NACA TN 1323 (ref. 37)
	C on all edges	$k_b = 41.8$	

TABLE 8.- VALUES OF SHAPE PARAMETER n FOR SEVERAL ENGINEERING MATERIALS

[Data taken from reference 63]

n	Material
3	One-fourth hard to full hard 18-8 stainless steel, with grain One-fourth hard 18-8 stainless steel, cross grain
5	One-half hard and three-fourths hard 18-8 stainless steel, cross grain
10	Full hard 18-8 stainless steel, cross grain 2024-T and 7075-T aluminum-alloy sheet and extrusion 2024R-T aluminum-alloy sheet
20 to 25	2024-T80, 2024-T81, and 2024-T86 aluminum-alloy sheet 2024-T aluminum-alloy extrusions SAE 4130 steel heat-treated up to 100,000 psi ultimate stress
35 to 50	2014-T aluminum-alloy extrusions SAE 4130 steel heat-treated above 125,000 psi ultimate stress
∞	SAE 1025 (mild) steel

TABLE 9.- DESIGNATIONS FOR WROUGHT ALUMINUM ALLOYS

Old	New
14S, R301	2014
17S	2017
24S	2024
61S	6061
75S	7075

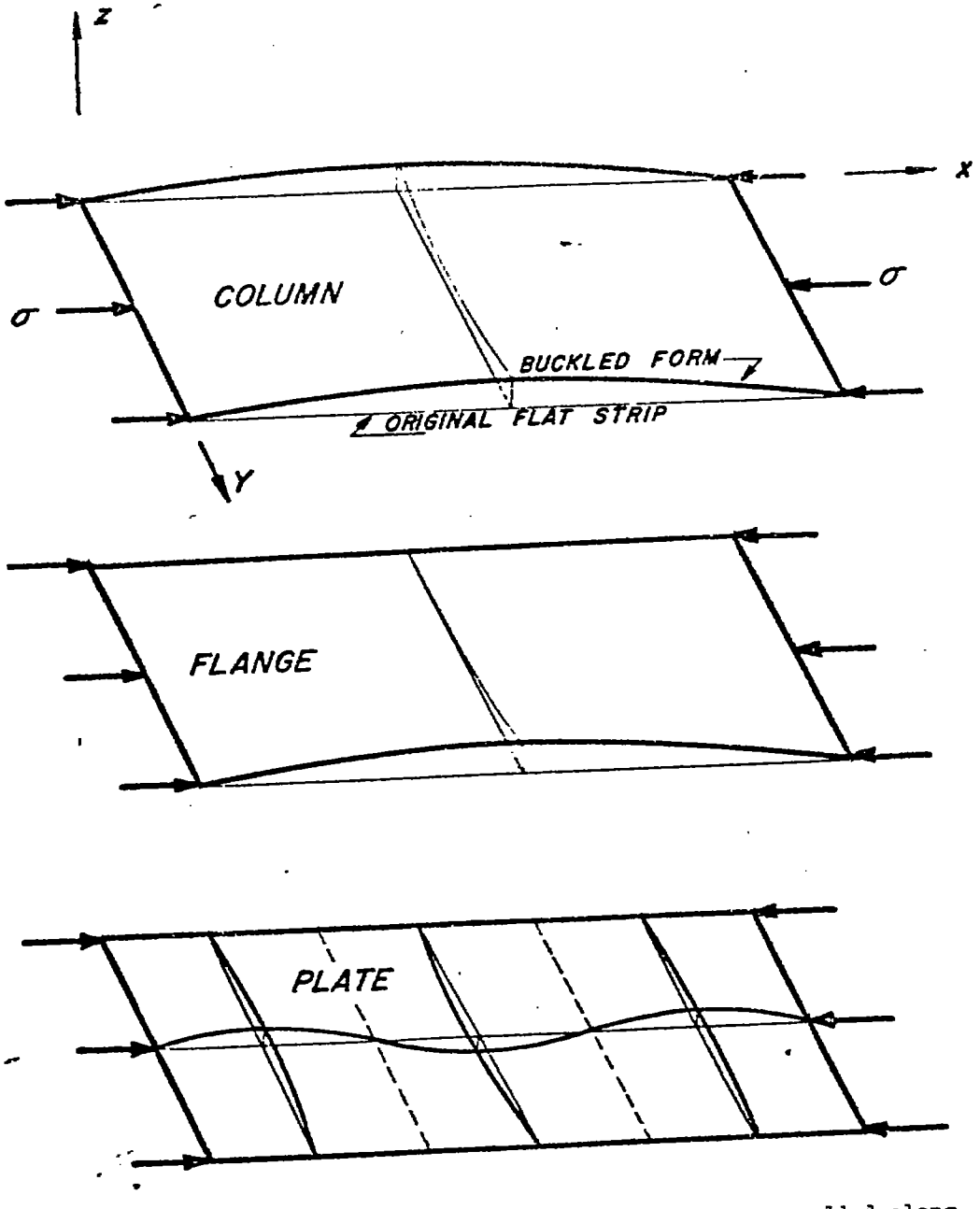

Figure 1.- Transition from column to plate as supports are added along unloaded edges. Note changes in buckle configurations.

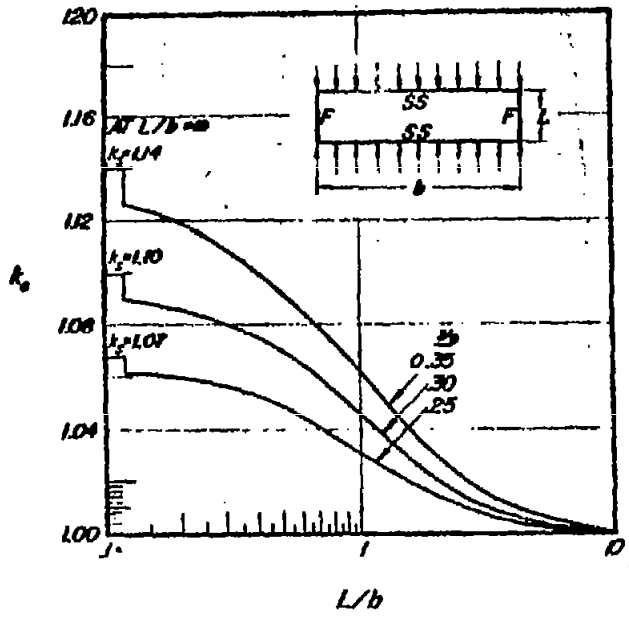

(a) Plate columns with hinged loaded edges.

$\sigma_{cr} = k_c \pi^2 E/(L/\rho)^2$.

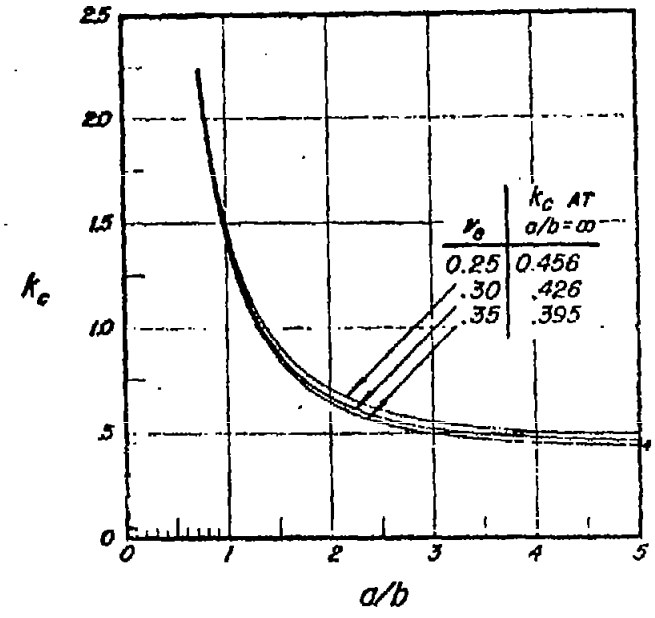

(b) Hinged flanges.

Figure 2.- Compressive-buckling coefficients of plate columns and flanges as functions of Poisson's ratio.

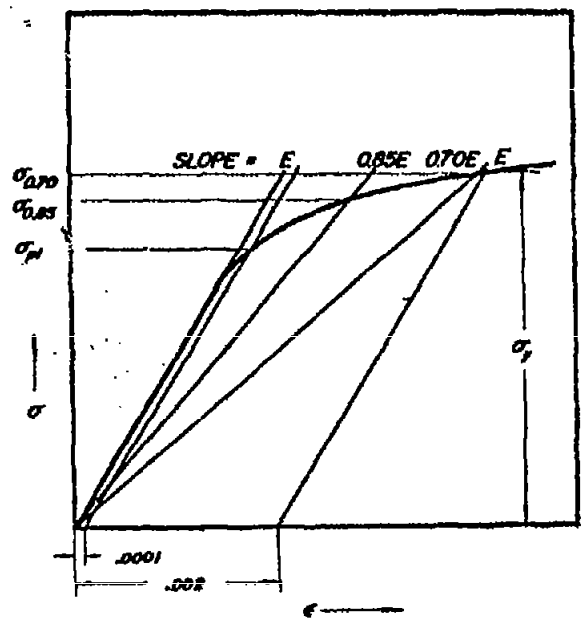

(a) Significant stress quantities on a typical stress-strain curve.

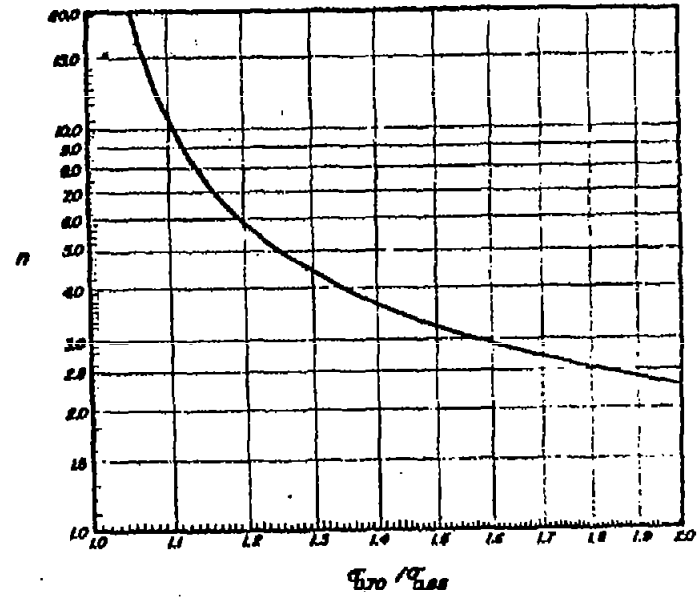

(b) Dependence of shape factor on ratio $\sigma_{0.70}/\sigma_{0.85}$.
$n = 1 + \log_e(17/7)/\log_e\left(\sigma_{0.70}/\sigma_{0.85}\right)$.

Figure 3.- Characteristics of stress-strain curves for structural alloys depicting quantities used in three-parameter method.

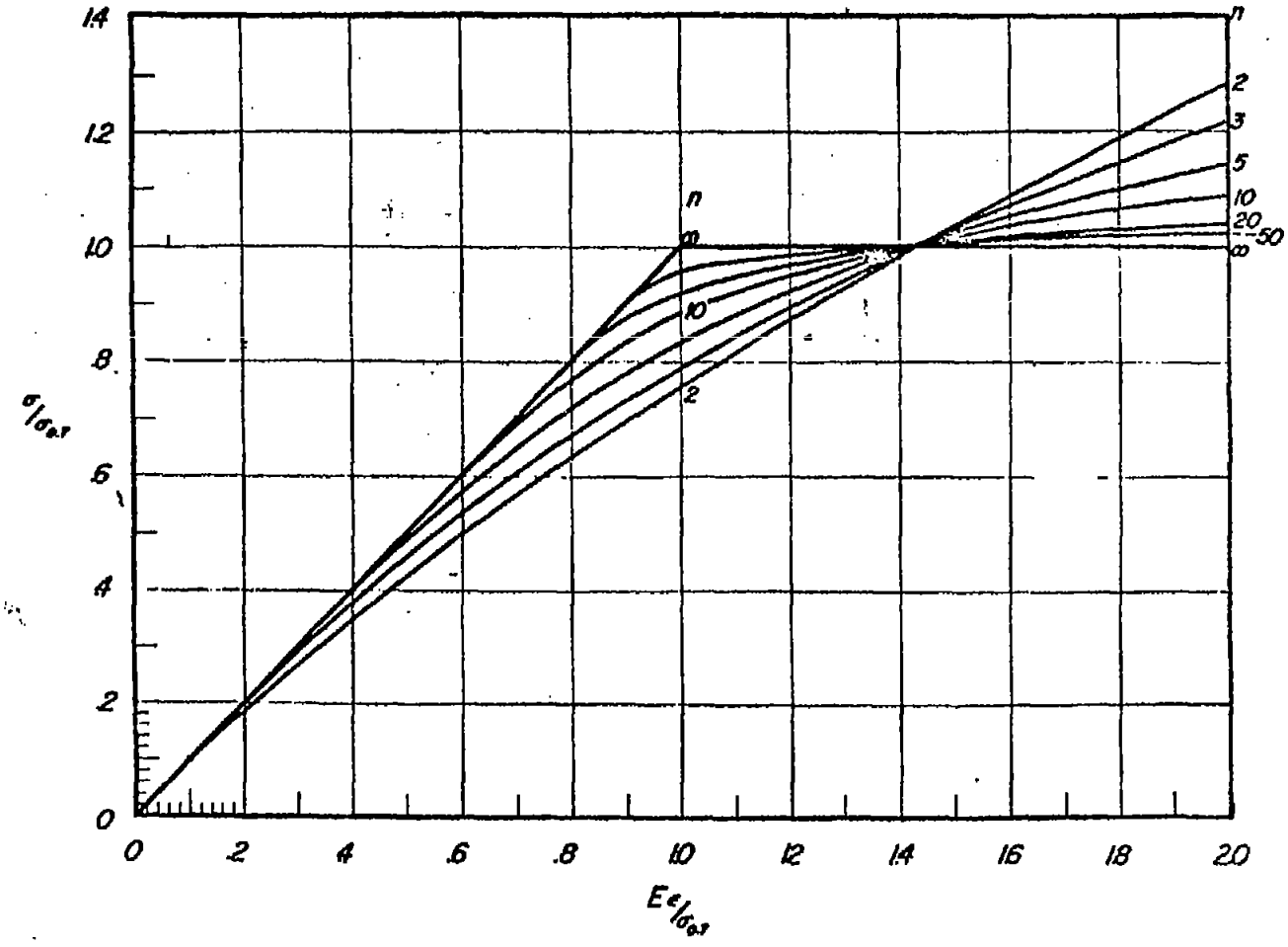

Figure 4.- Nondimensional stress-strain curves for various values of n for three-parameter method.

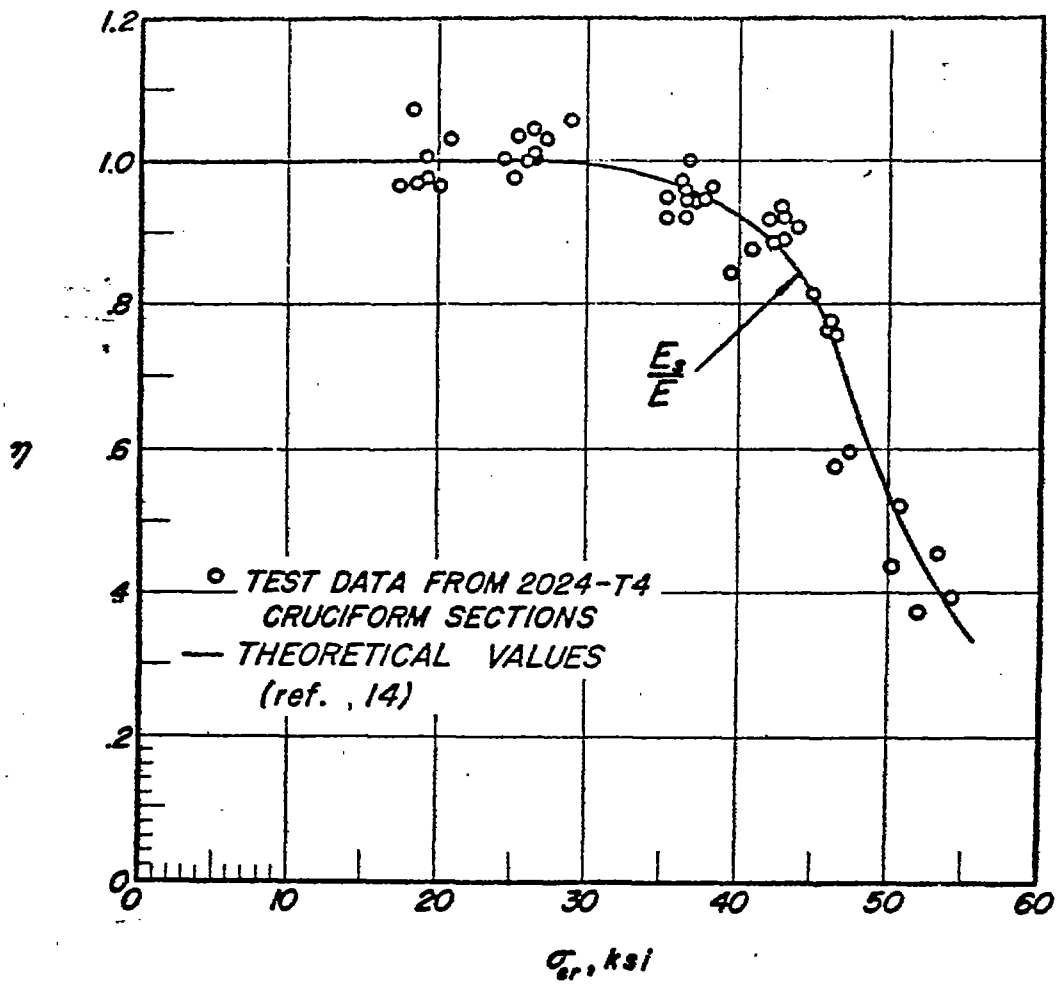

Figure 5.- Comparison of theory and experiment for compressed simply supported flanges.

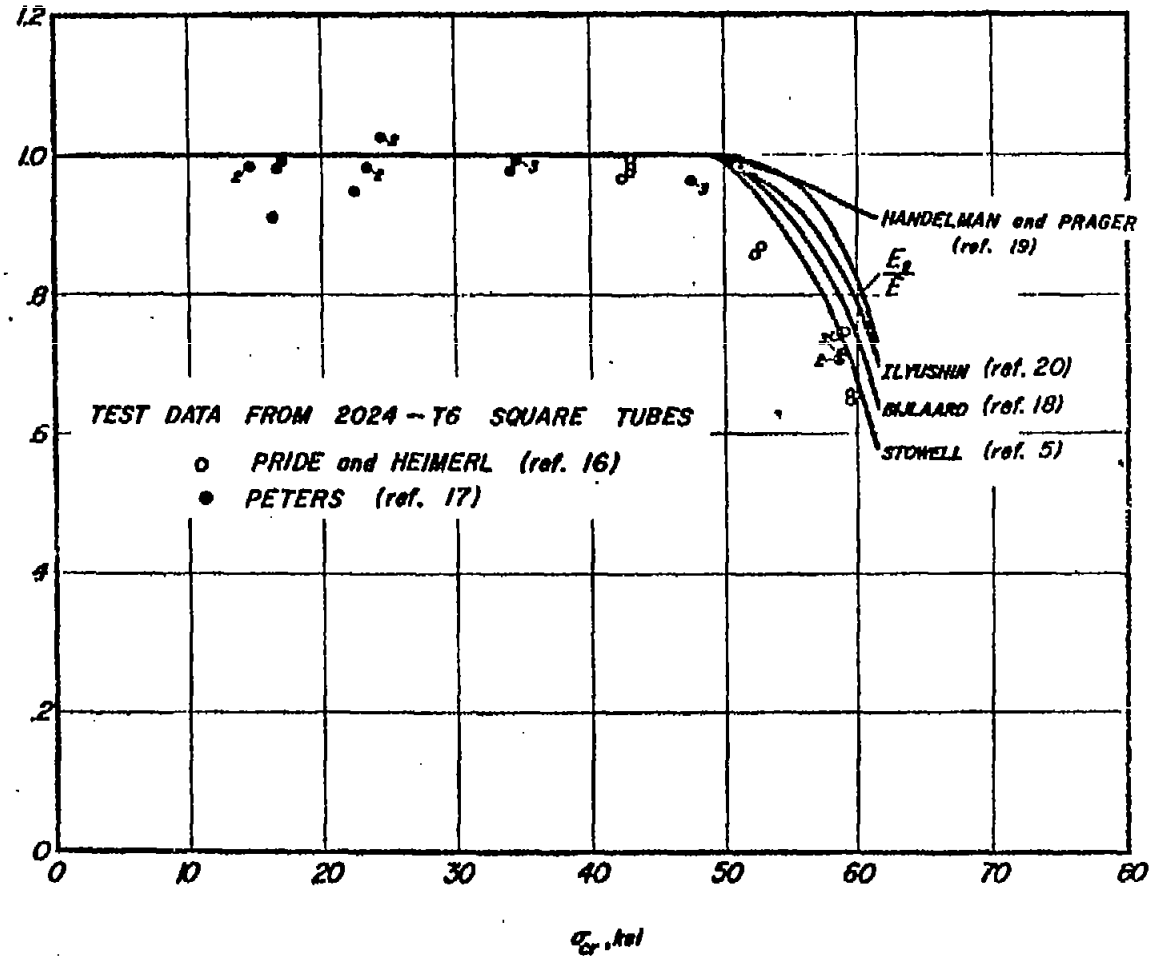

Figure 6.- Comparison of theory and experiment for compressed simply supported plates.

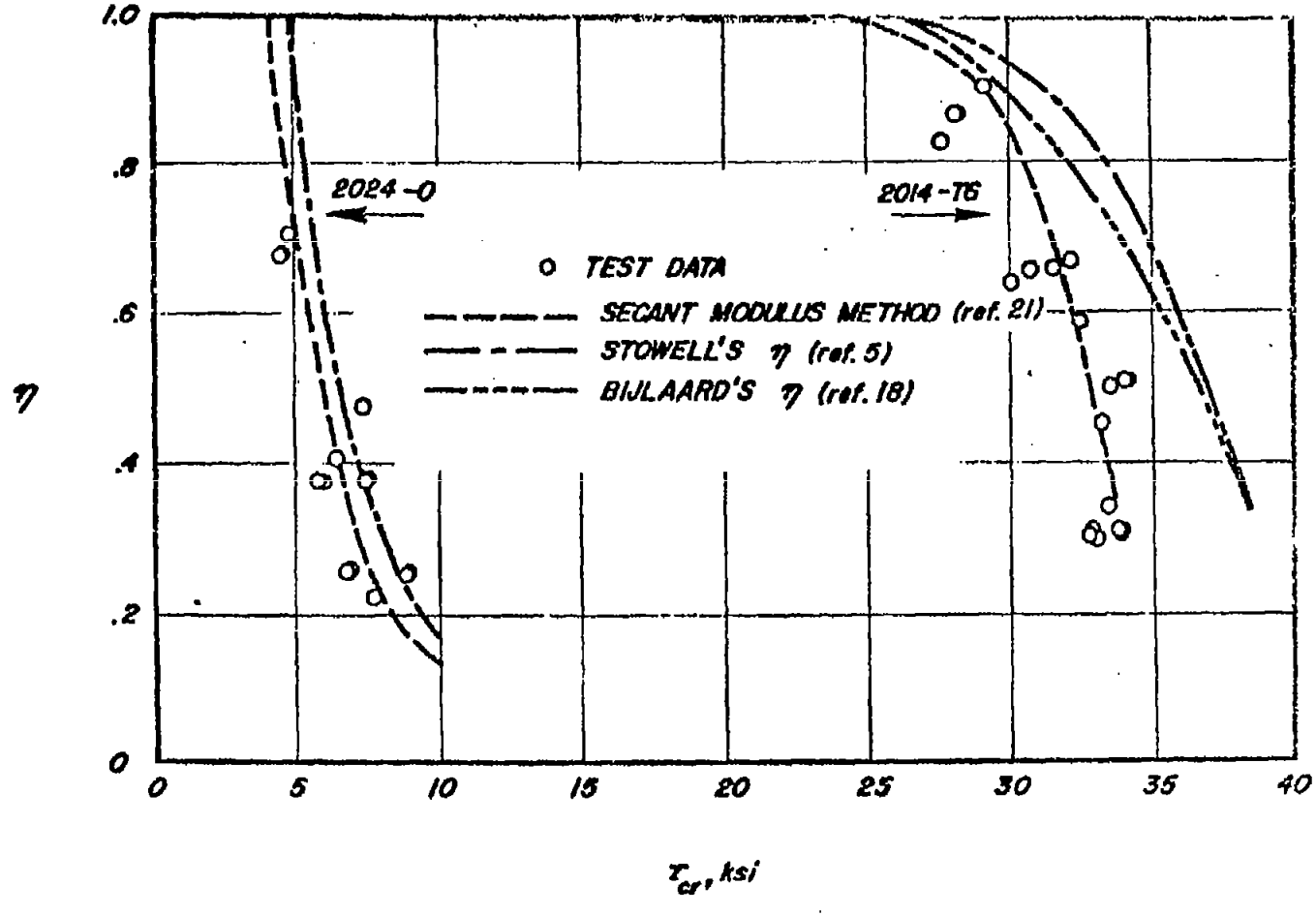

Figure 7.- Comparison of shear buckling theories and test data for plastic buckling of compressed elastically supported plates.

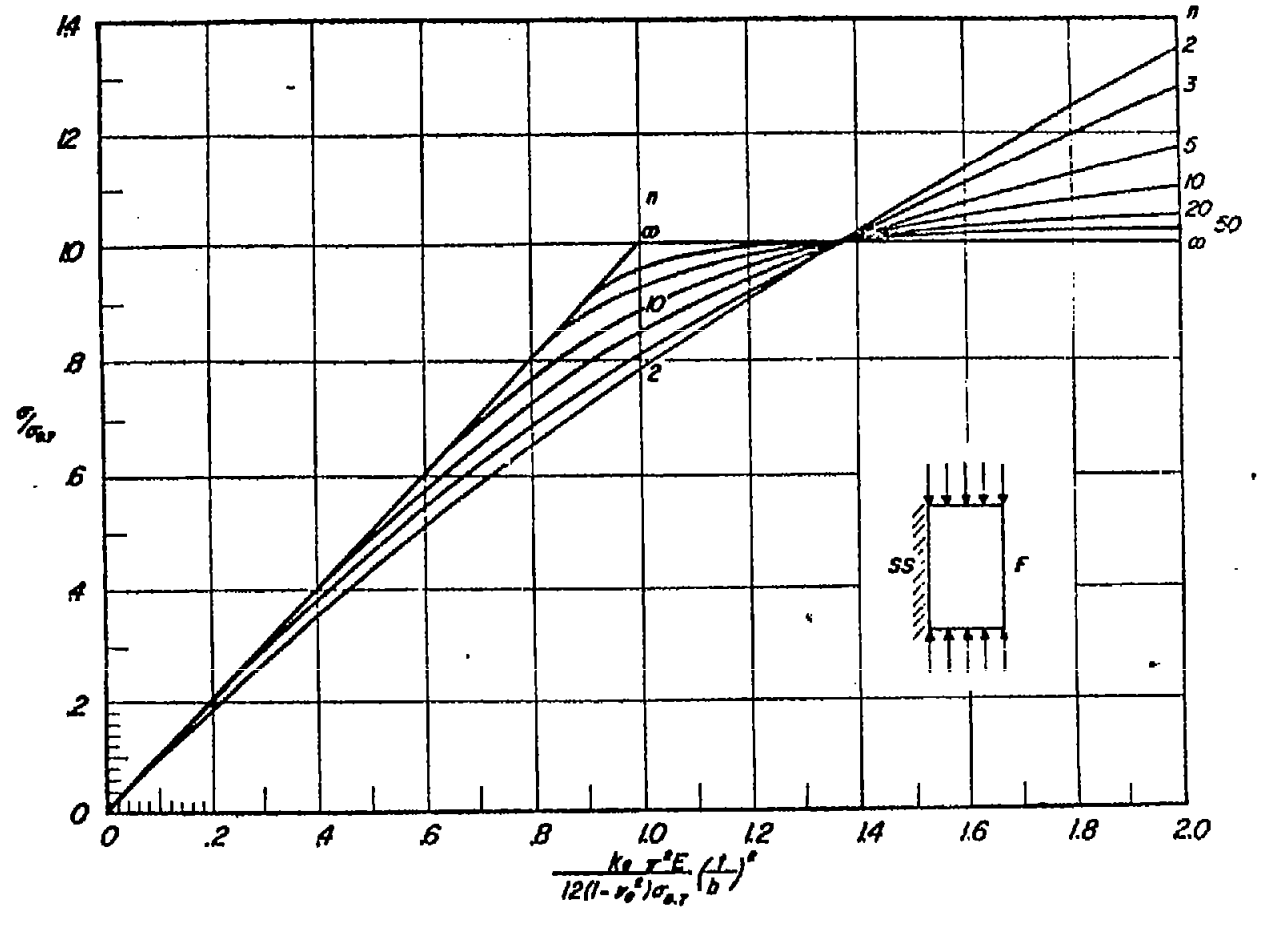

Figure 8.- Chart of nondimensional compressive buckling stress for long hinged flanges. $\eta = \left(E_t/E\right)\left(1 - \nu_e^2\right)\Big/\left(1 - \nu^2\right)$.

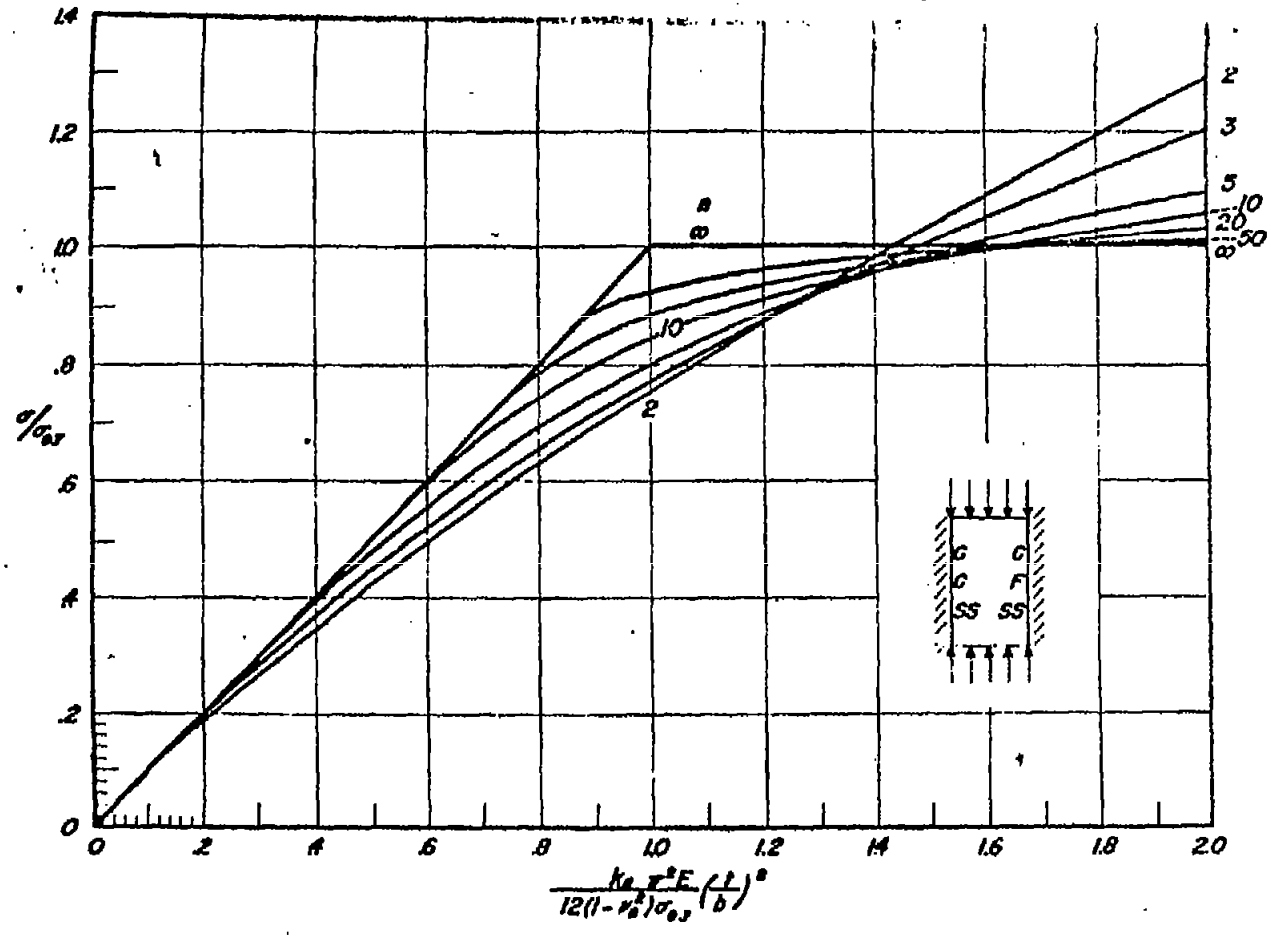

Figure 9.- Chart of nondimensional compressive buckling stress for long clamped flanges and for supported plates with edge rotational restraint.

$$\eta = \left(E_s/2E\right)\left\{1 + 0.5\left[1 + \left(\overline{5}E_t/E_s\right)\right]^{1/2}\right\}\left(1 - \nu_e^2\right)\Big/\left(1 - \nu^2\right).$$

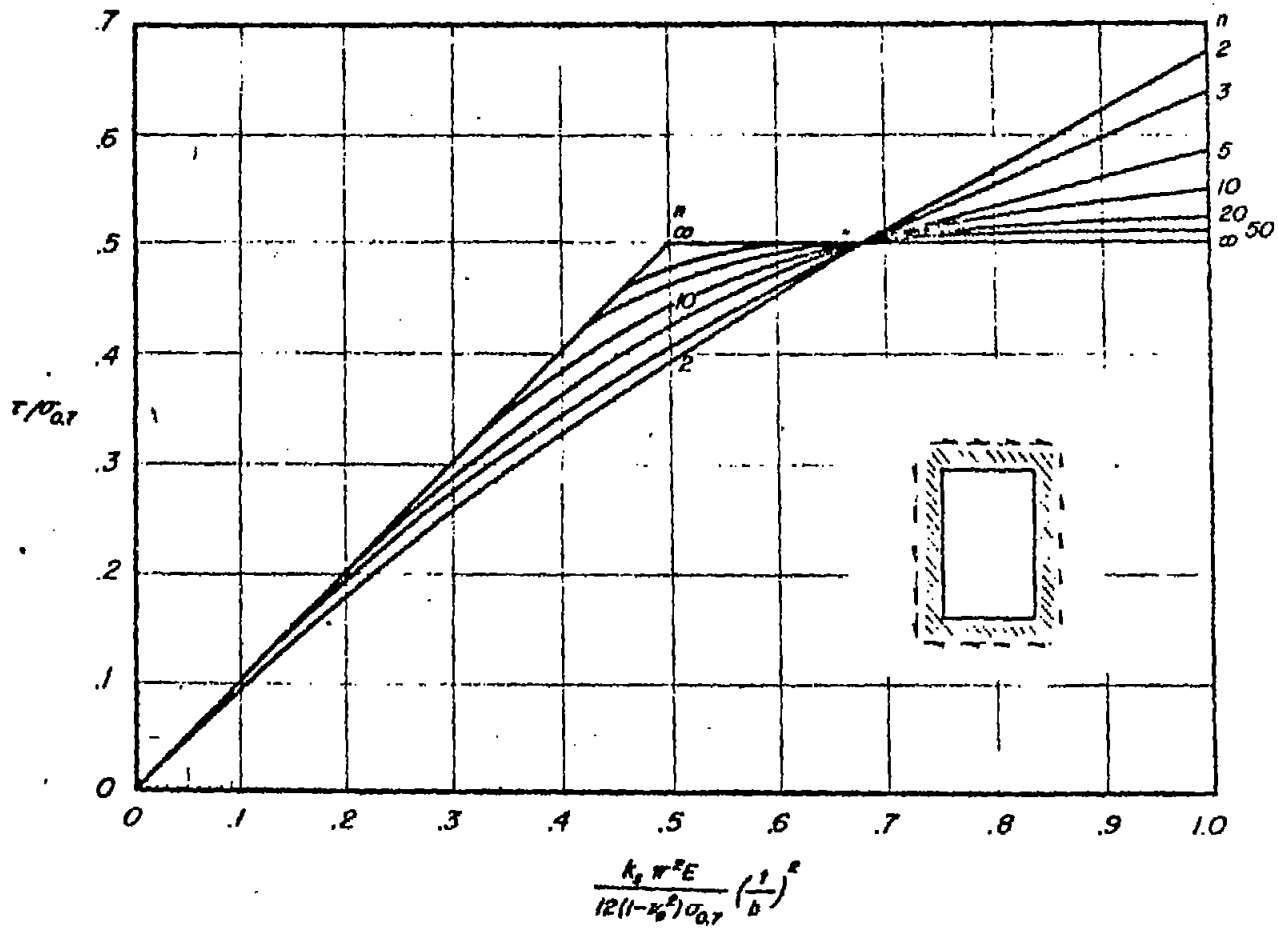

Figure 10.- Chart of nondimensional shear buckling stress for panels with edge rotational restraint. $\eta = \left(E_3/E\right)\left(1 - \nu_c^2\right)\Big/\left(1 - \nu^2\right)$.

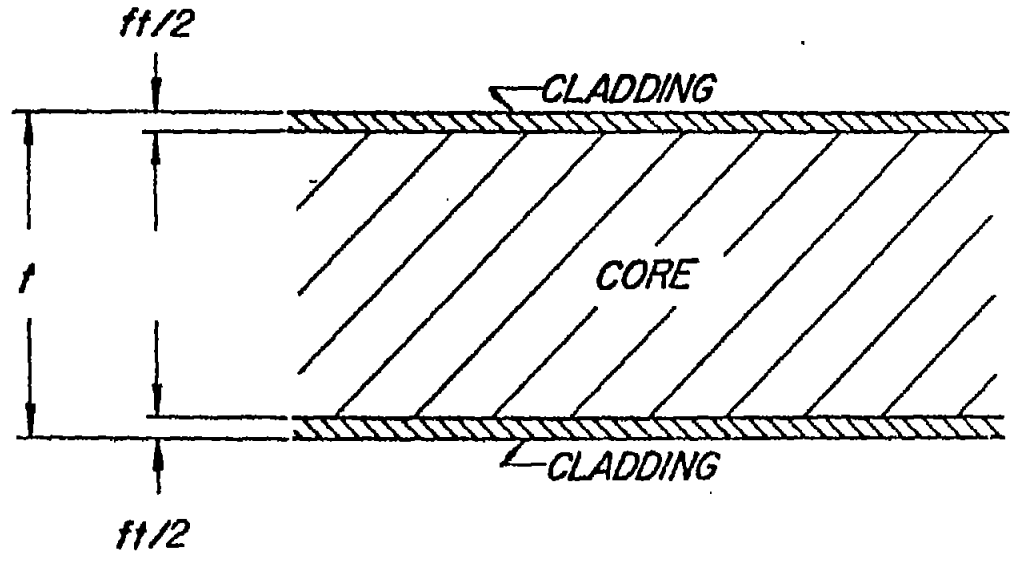

Figure 11.- Cross section of clad plate.

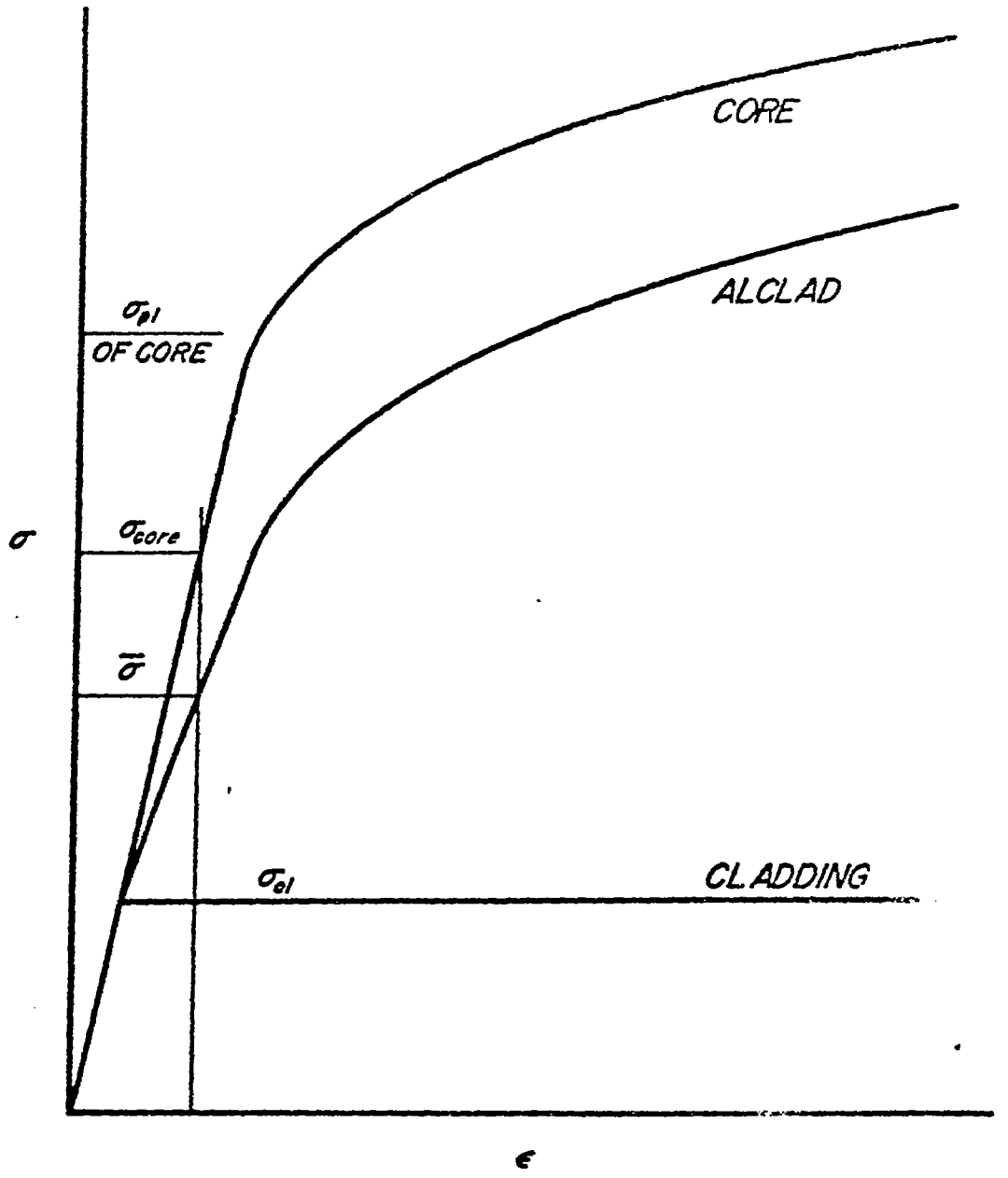

Figure 12.- Stress-strain curves for cladding, core, and alclad combinations. $\bar{\sigma}/\sigma_{core} = 1 - f + \beta f$; $\beta = \sigma_{cl}/\sigma_{core}$.

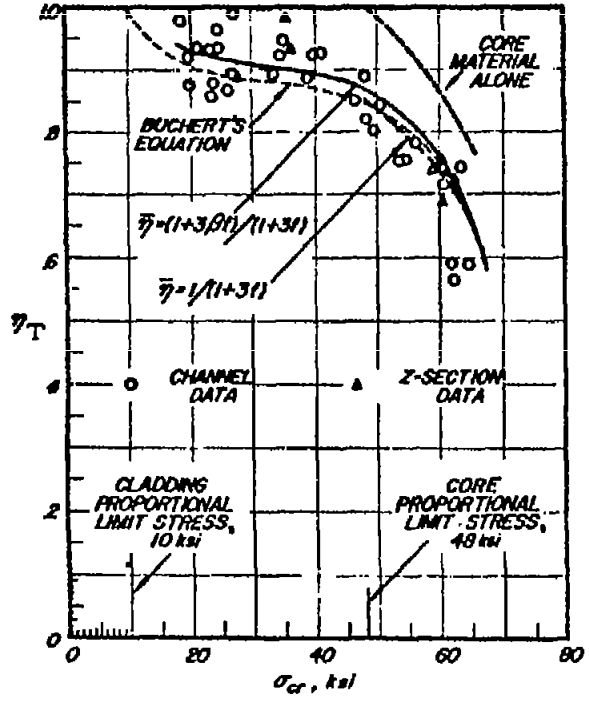

(a) Simply supported 2024-T84 plate with 5 percent cladding. Tests were made on Z- and channel sections.

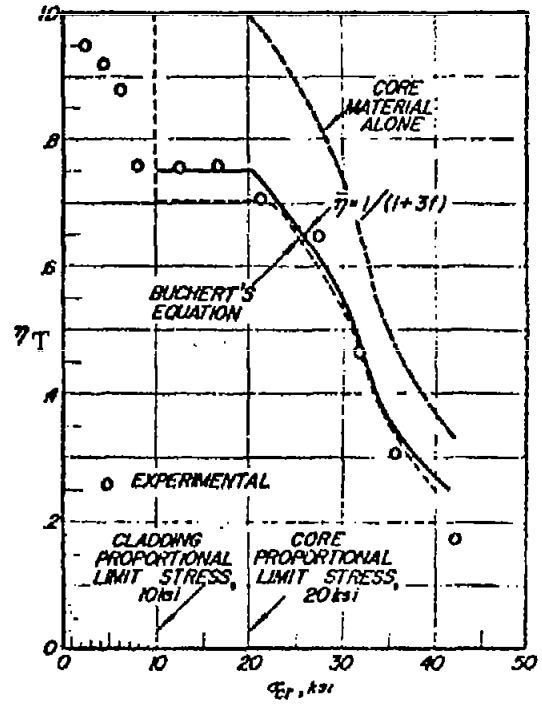

(b) Long 2024-T3 plate columns with 11 percent cladding.

Figure 13.- Comparison of experimental and theoretical cladding reduction factors.

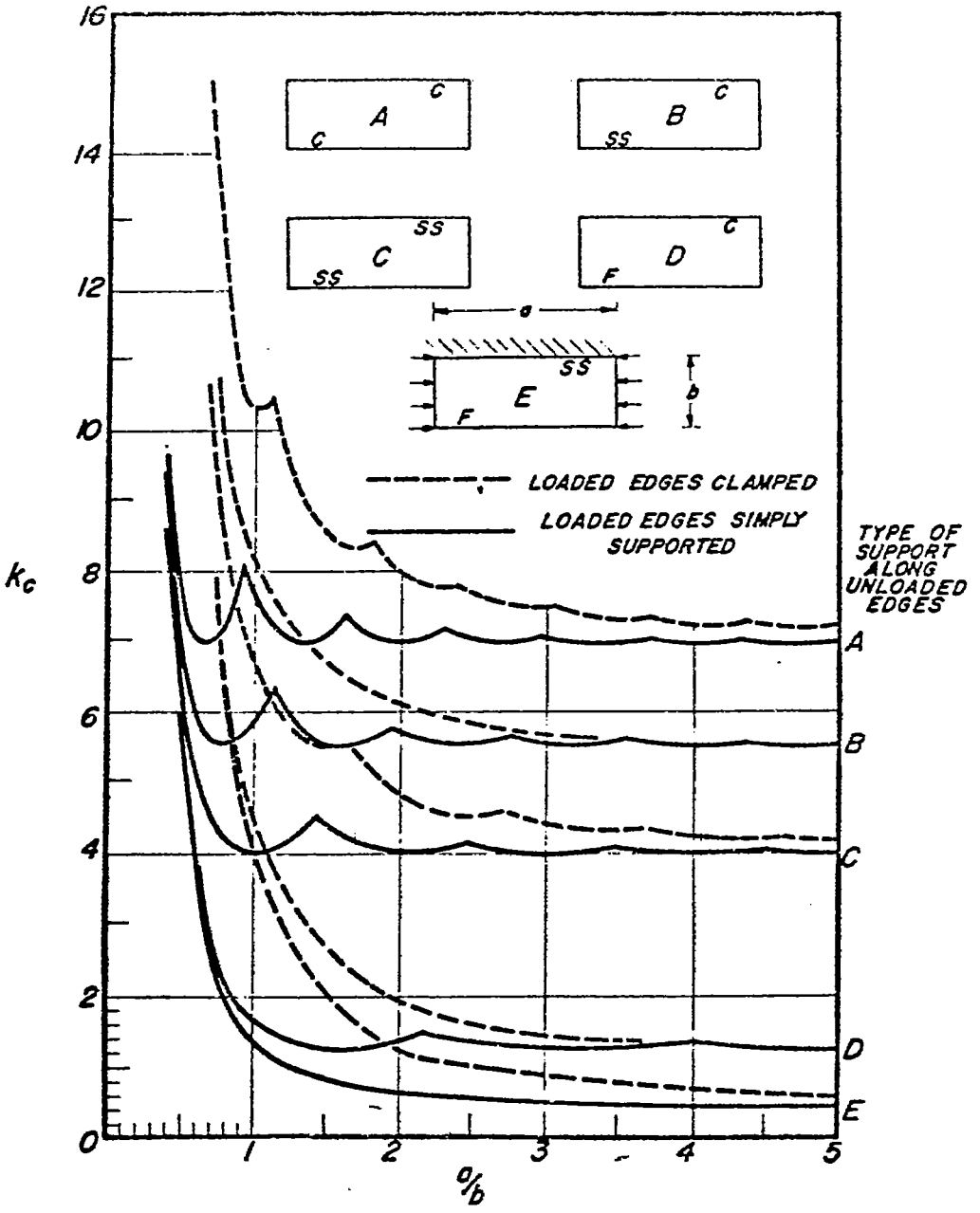

Figure 14.- Compressive-buckling coefficients for flat rectangular plates.

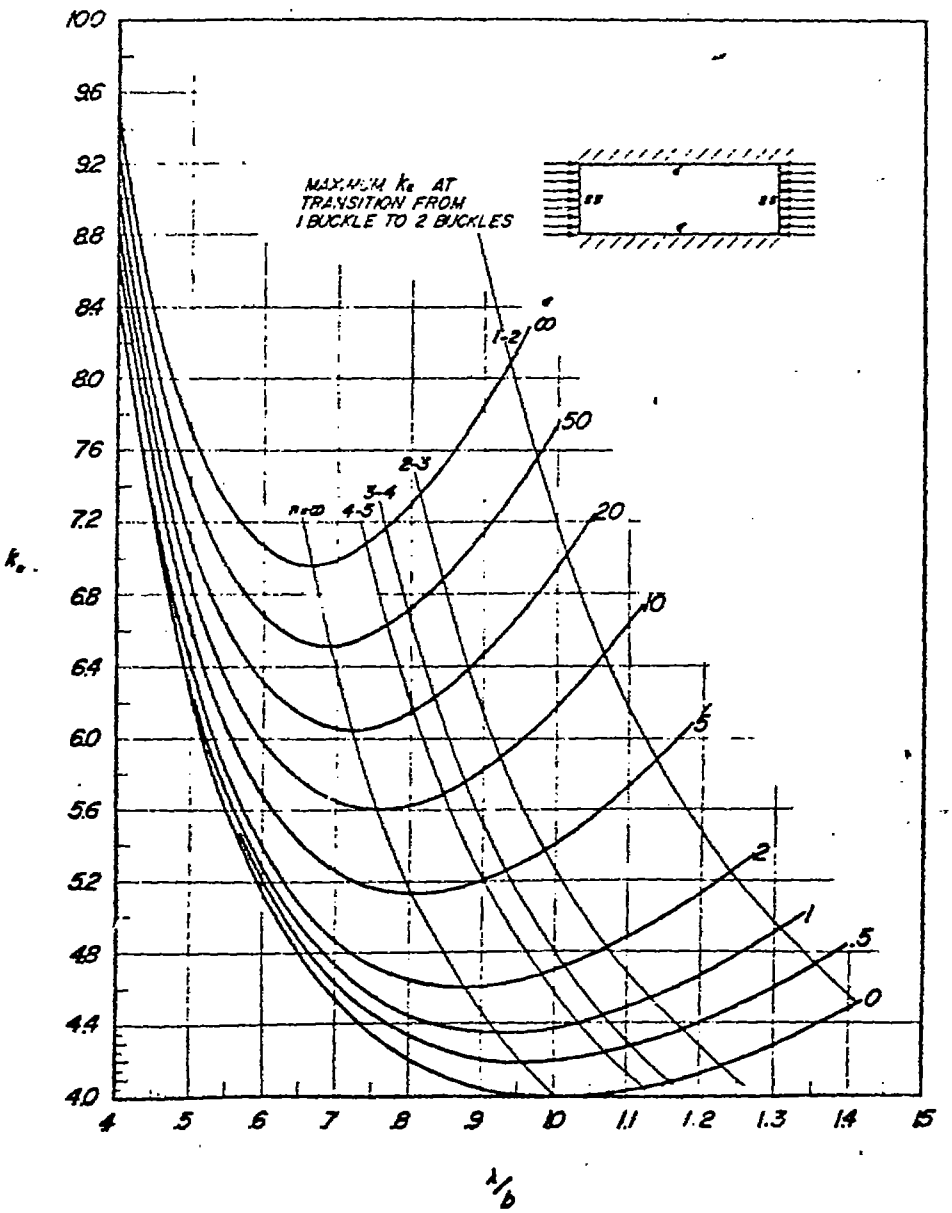

Figure 15.- Compressive-buckling-stress coefficient of plates as a function of λ/b for various amounts of edge rotational restraint. Figure taken from reference 29.

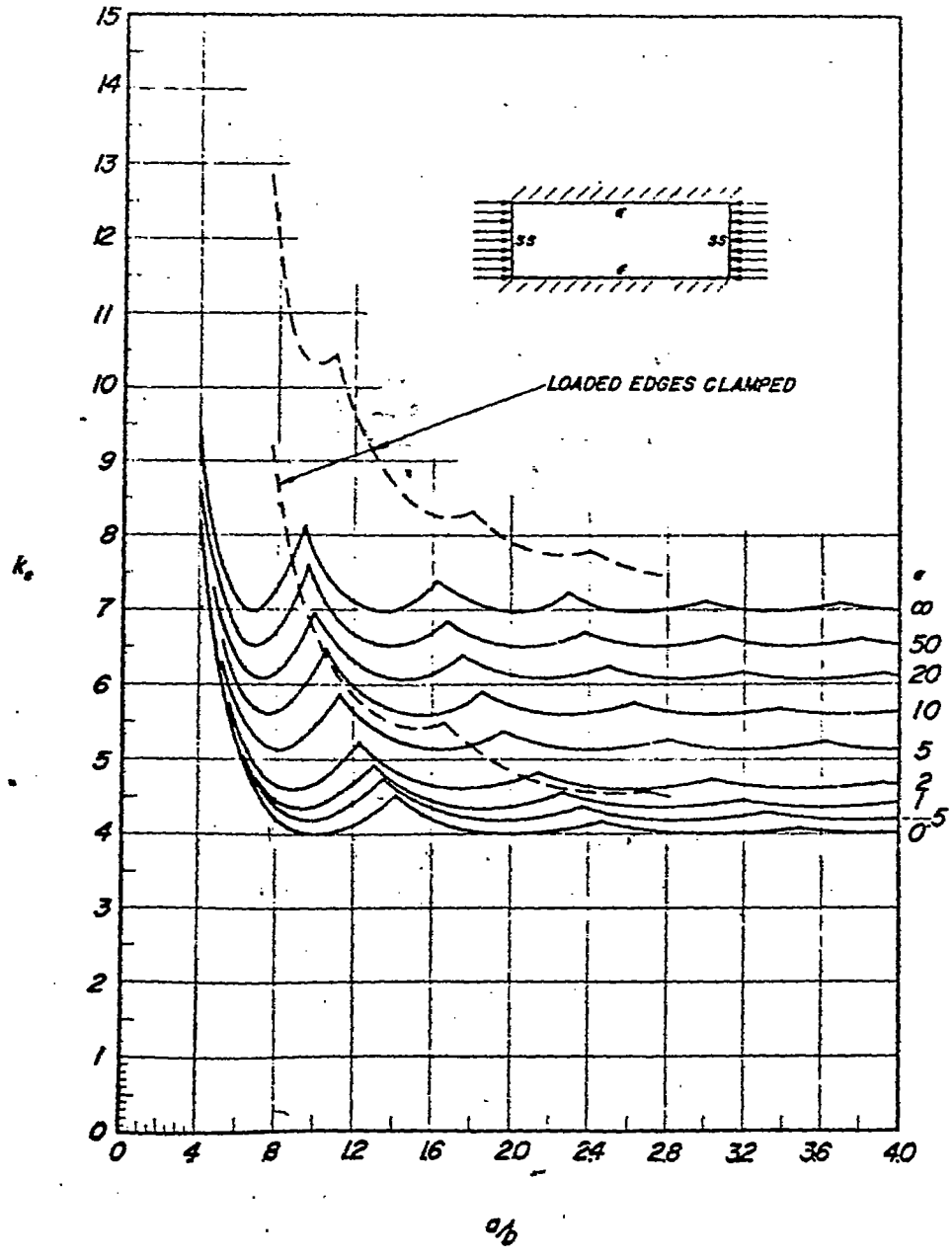

Figure 16.- Compressive-buckling-stress coefficient of plates as a function of a/b for various amounts of edge rotational restraint.

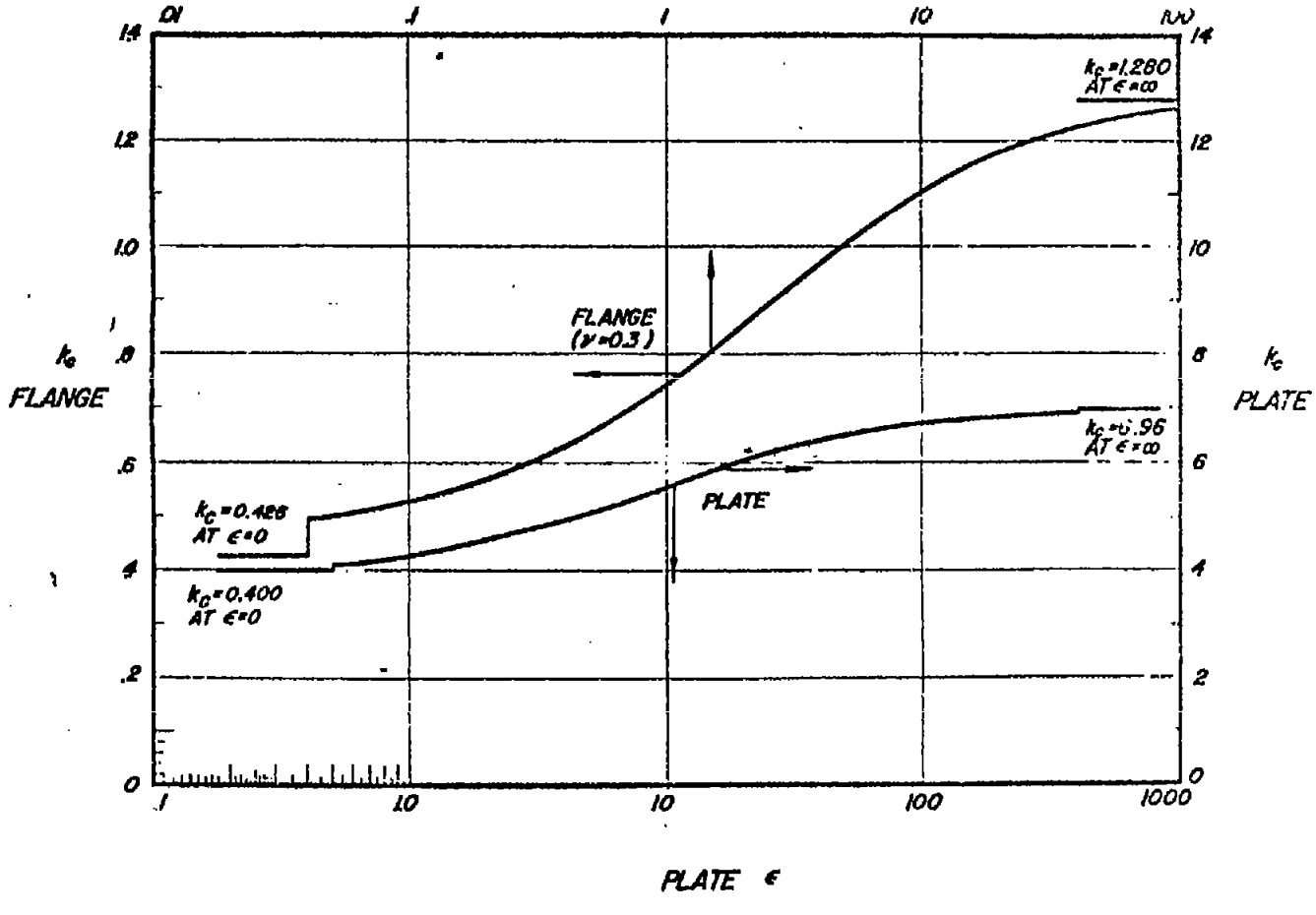

Figure 17.- Compressive-buckling coefficients for infinitely long flanges and plates as functions of edge rotational restraint.

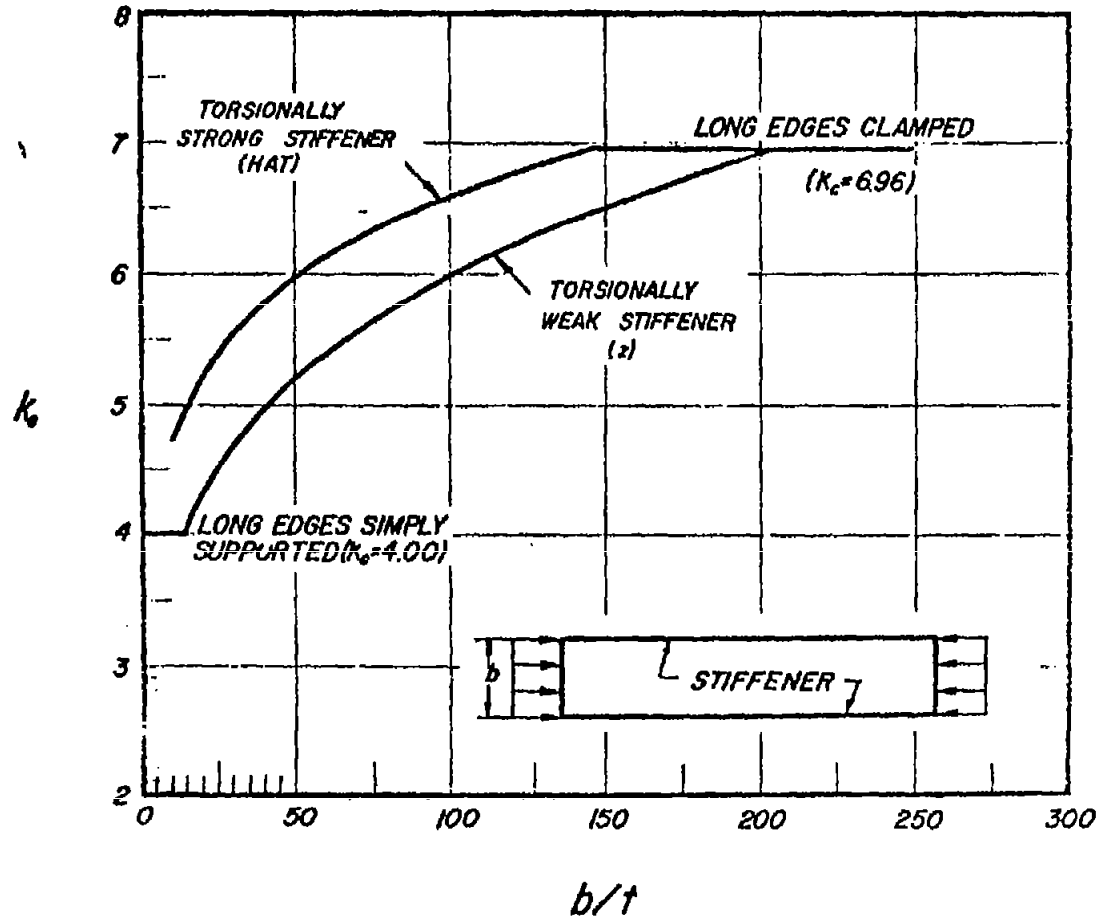

Figure 18.- Compressive-buckling coefficient for long rectangular stiffened panels as a function of b/t and stiffener torsional rigidity. Figure taken from reference 51.

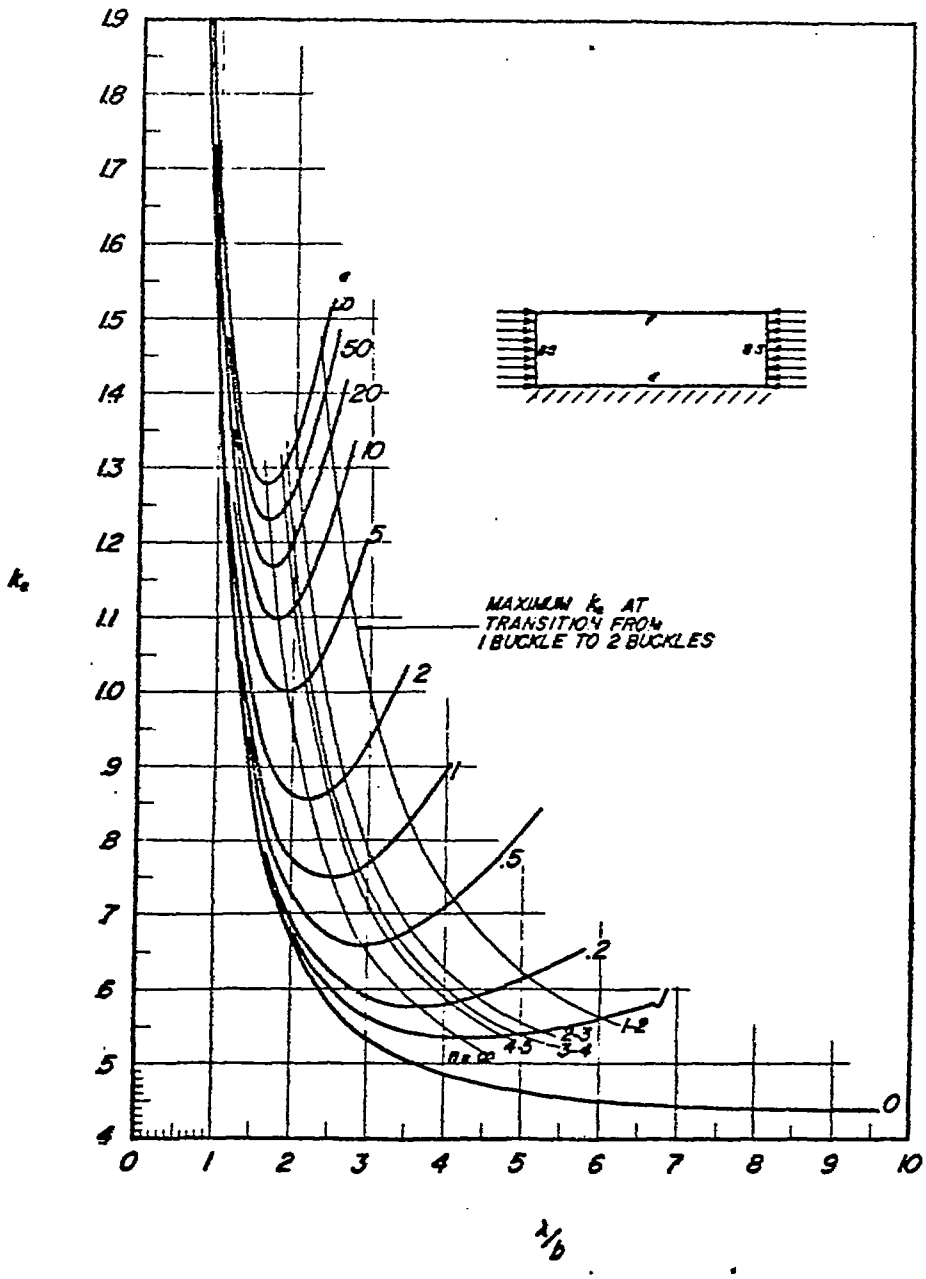

Figure 19.- Compressive-buckling-stress coefficient of flanges as a function of λ/b for various amounts of edge rotational restraint.

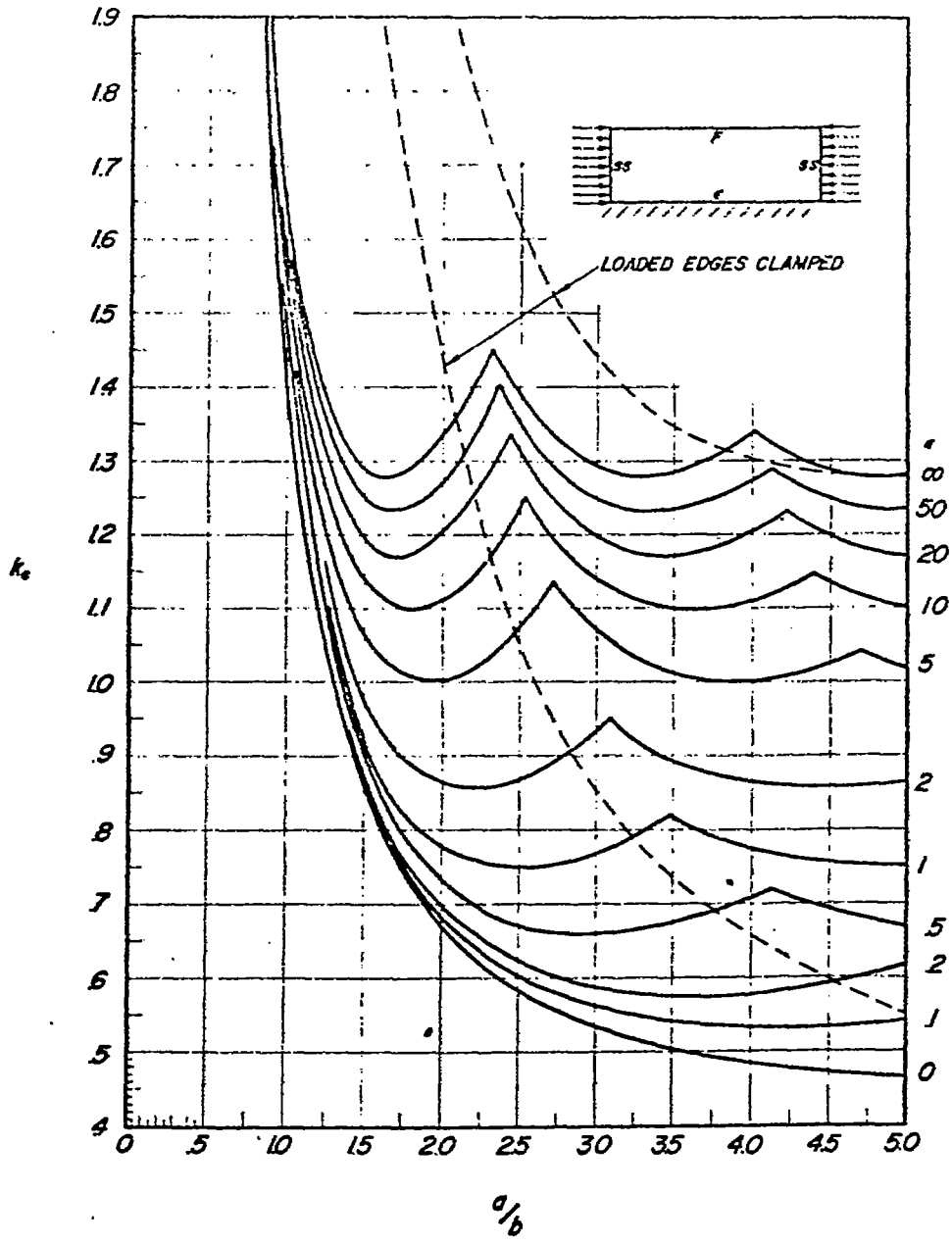

Figure 20.- Compressive-buckling-stress coefficient of flanges as a function of a/b for various amounts of edge rotational restraint.

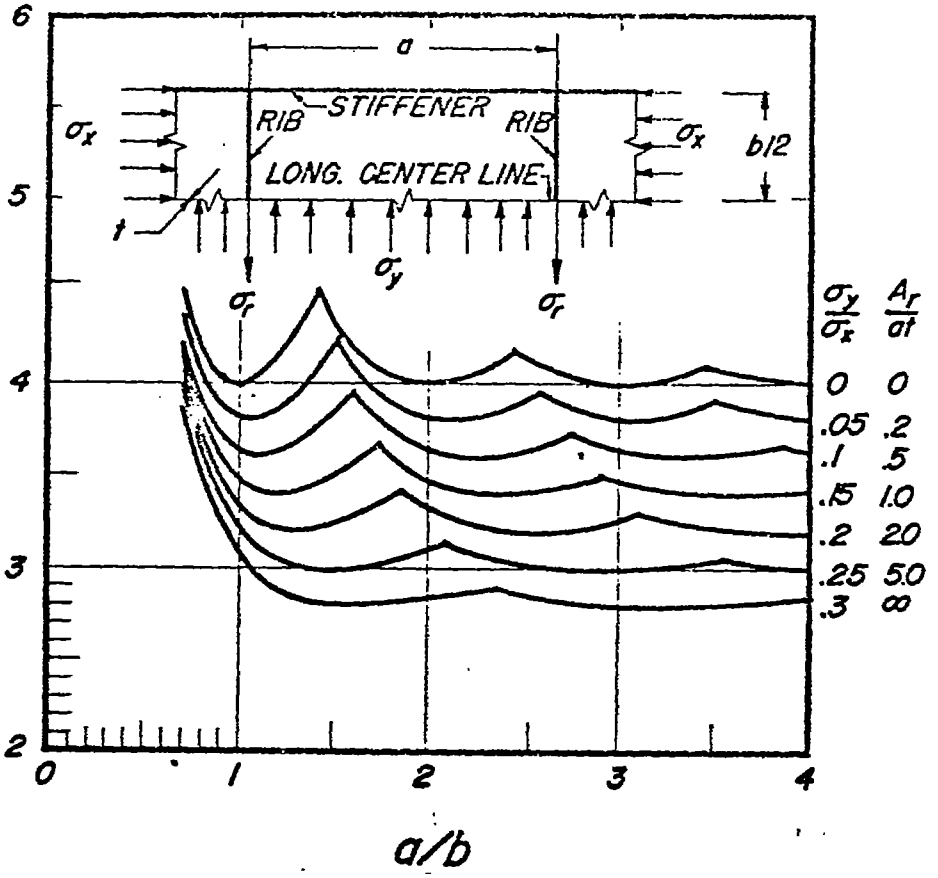

Figure 21.- Compressive-buckling coefficient of flat plates restrained against lateral expansion. Poisson's ratio equals 0.3; $\sigma_y/\sigma_x = \left(\nu A_r/at\right)/\left(1 + A_r/at\right)$.

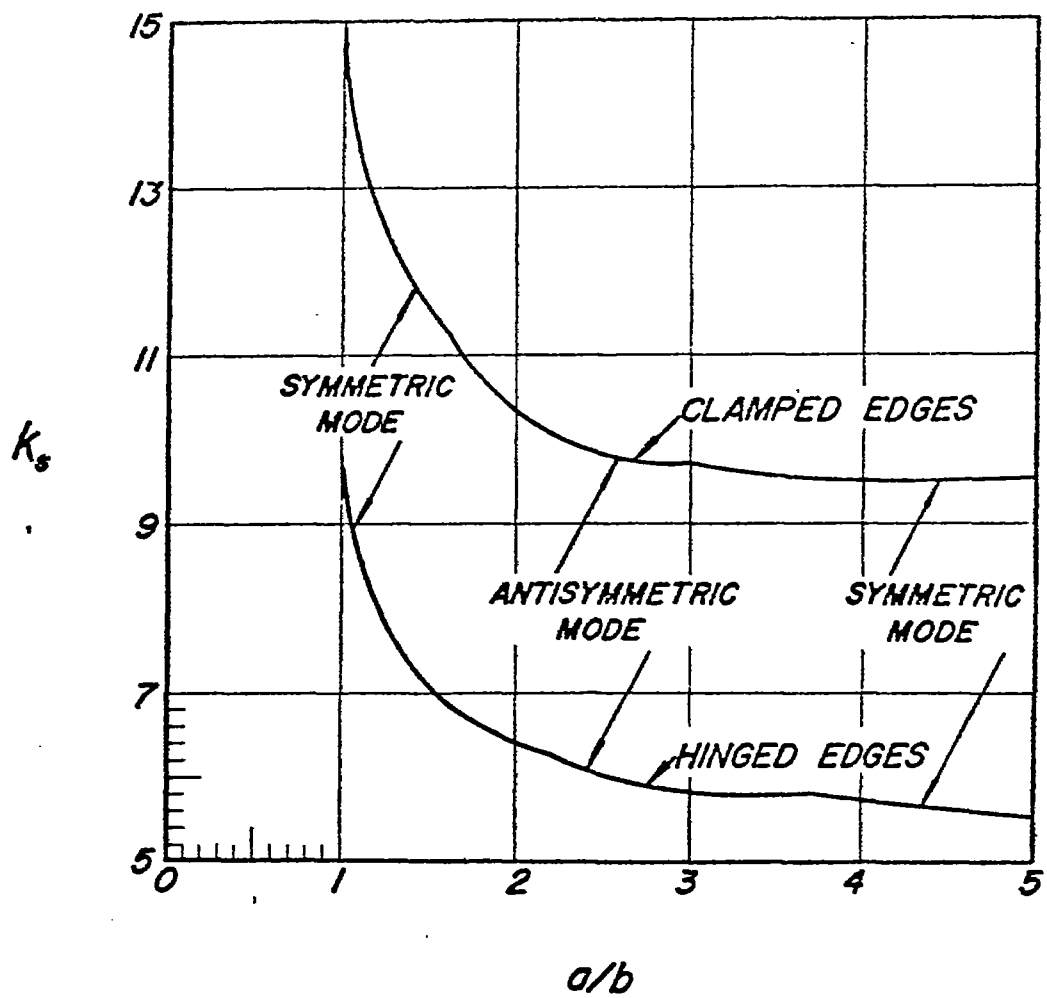

Figure 22.- Shear-buckling-stress coefficient of plates as a function of a/b for clamped and hinged edges.

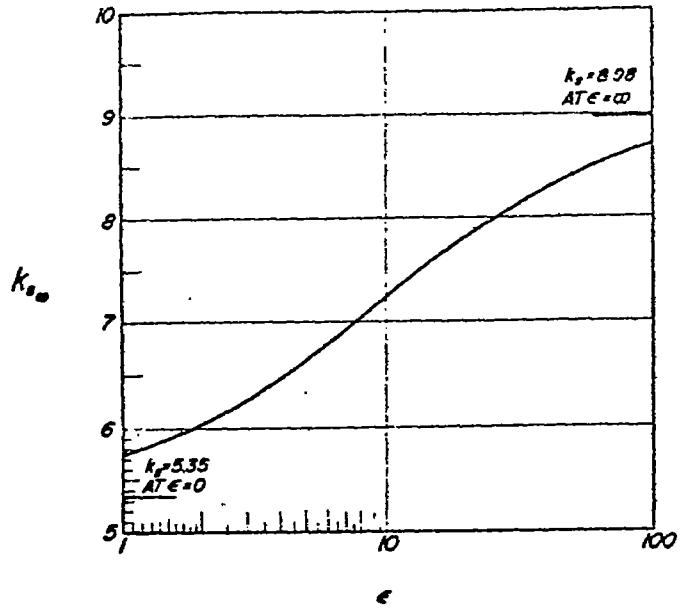

(a) k_{s_∞} as a function of ϵ.

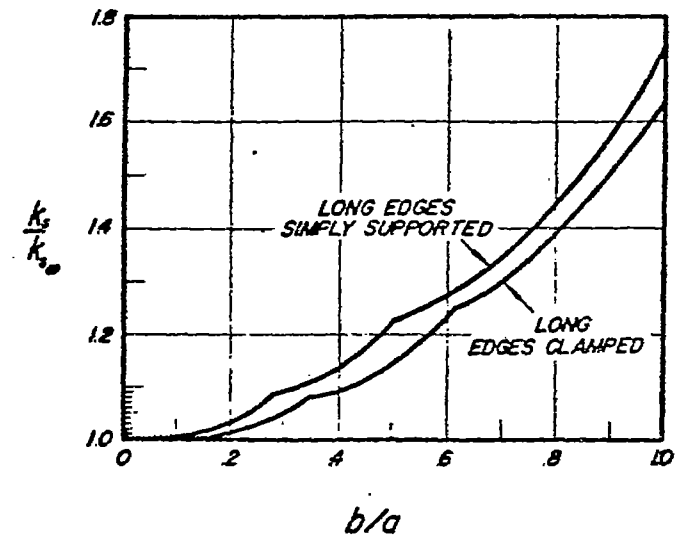

(b) k_s/k_{s_∞} as a function of b/a.

Figure 23.- Curves for estimation of shear-buckling coefficient of plates with various amounts of edge rotational restraint.

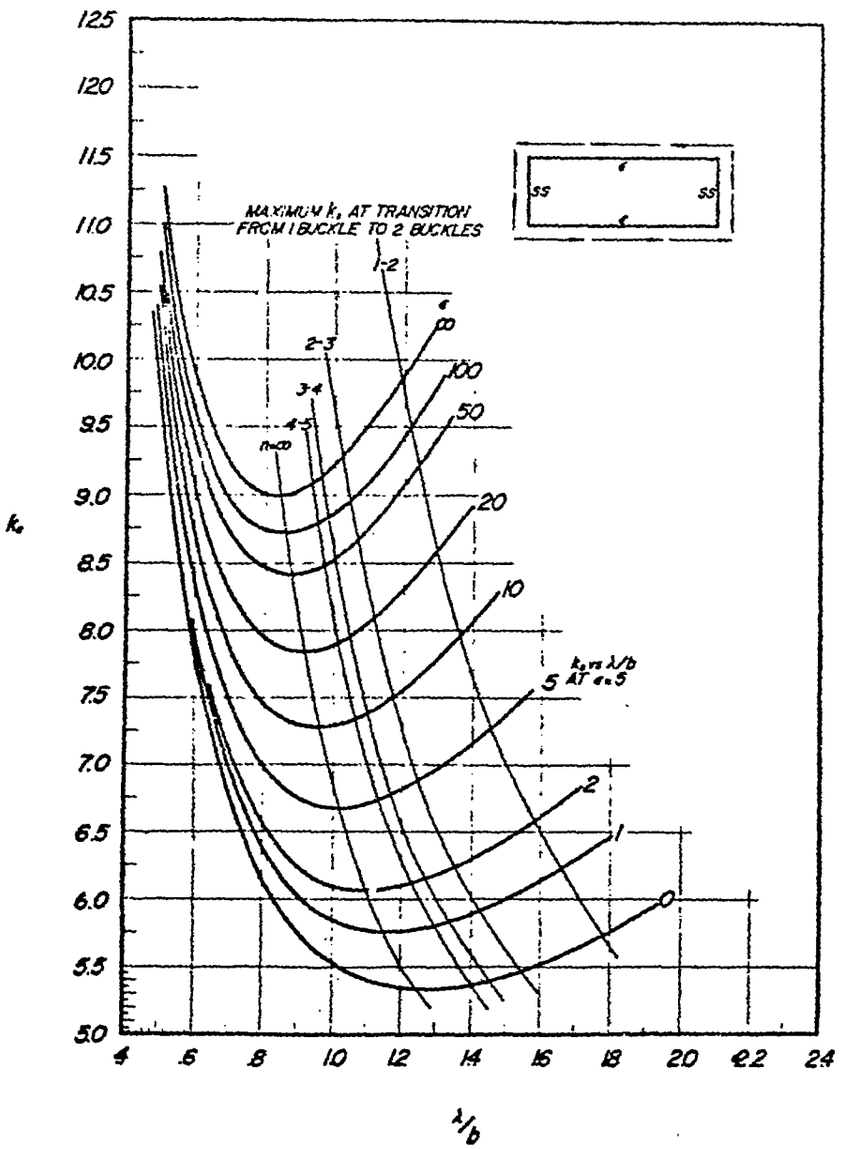

Figure 24.- Shear-buckling-stress coefficient for plates obtained from analysis of infinitely long plates as a function of λ/b for various amounts of edge rotational restraint.

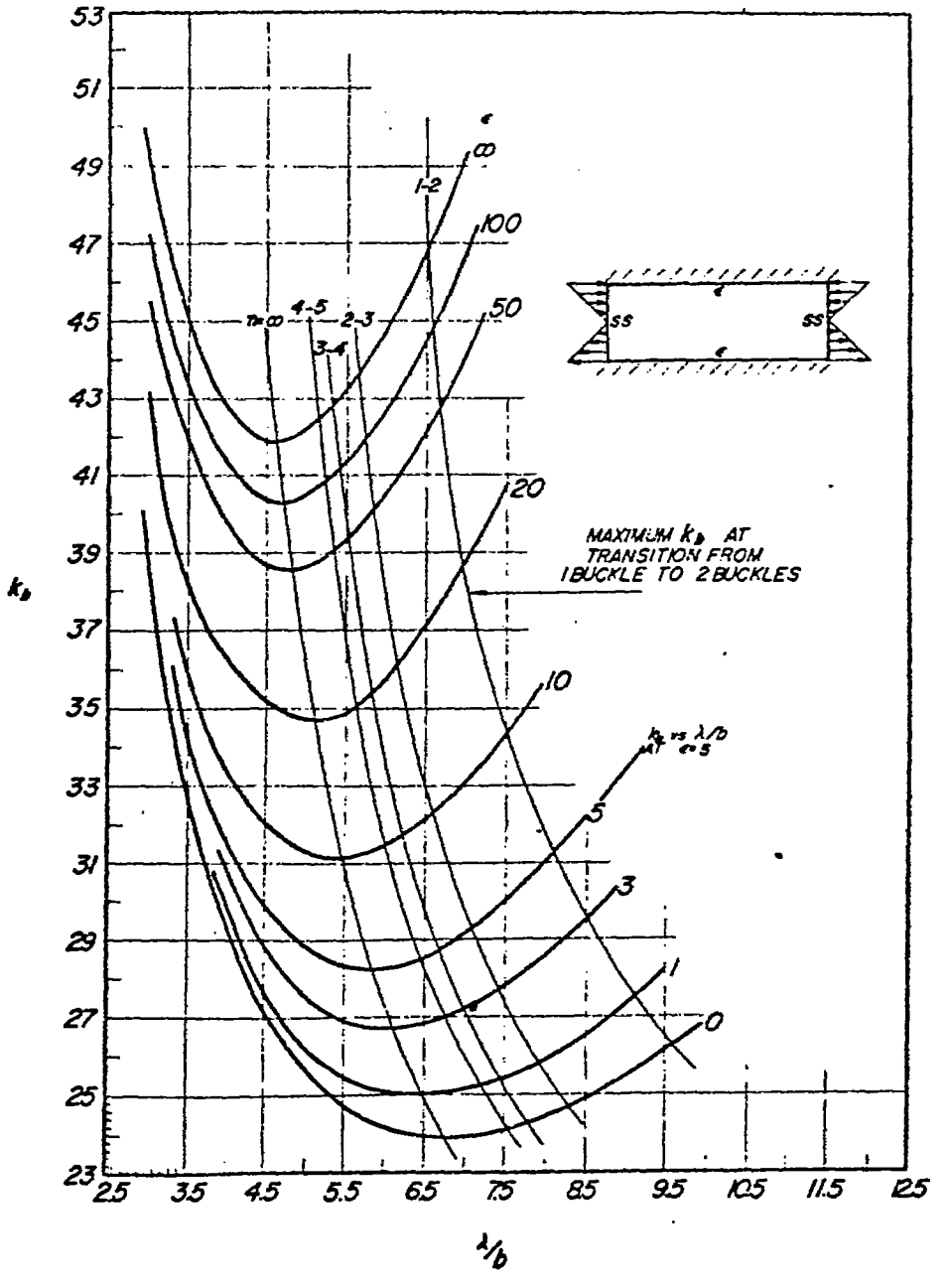

Figure 25.- Bending-buckling coefficient of plates as a function of λ/b for various amounts of edge rotational restraint.

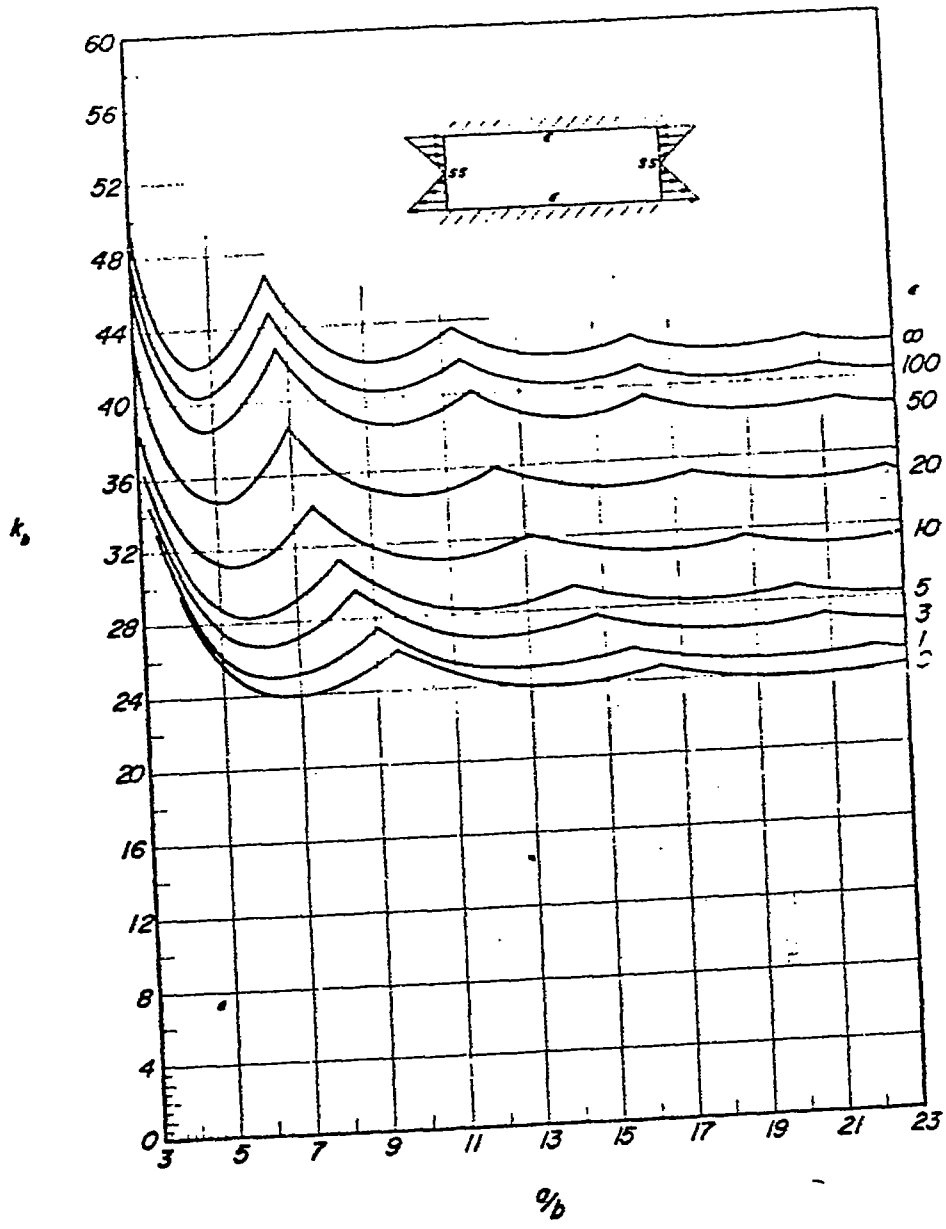

Figure 26.- Bending-buckling coefficient of plates as a function of a/b for various amounts of edge rotational restraint.

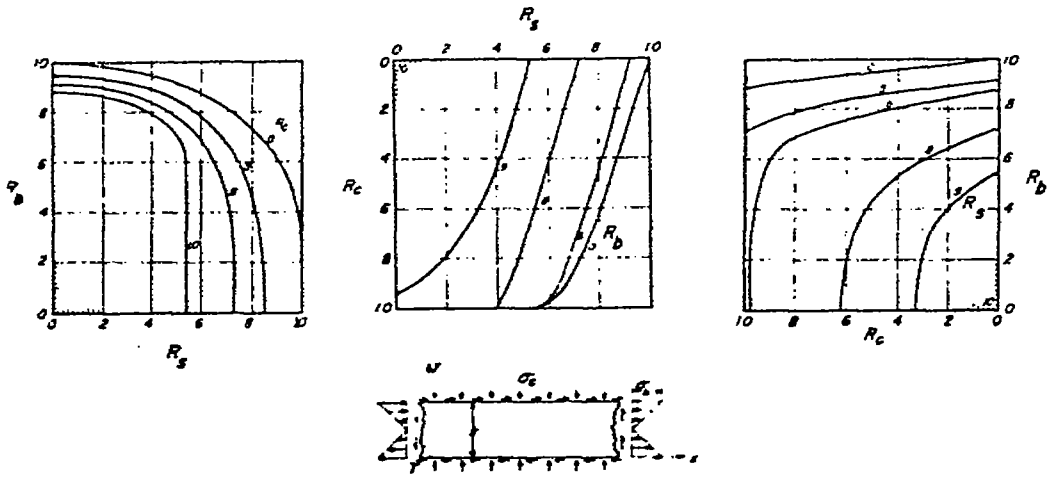

(a) Upper and lower edges simply supported.

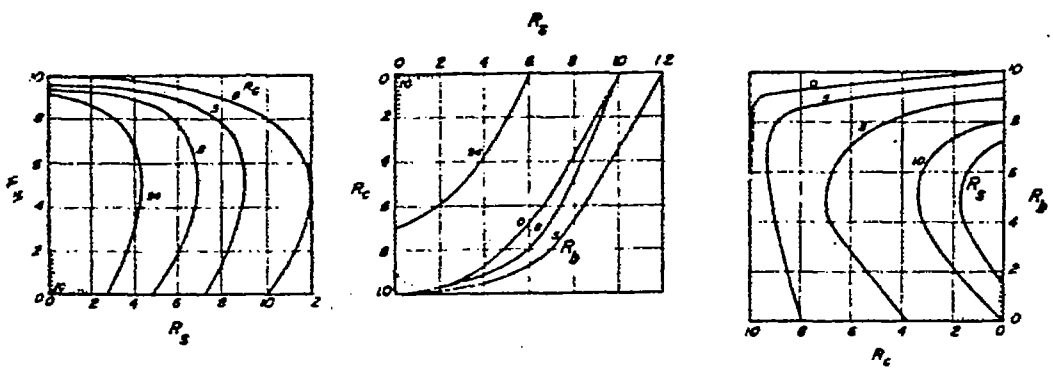

(b) Upper edges simply supported, lower edges clamped.

Figure 27.- Interaction curves for long flat plates under various combinations of compression, bending, and shear.

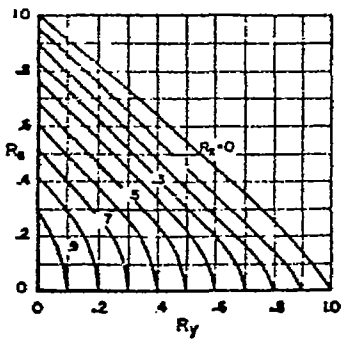

(a) a/b = 0.8.

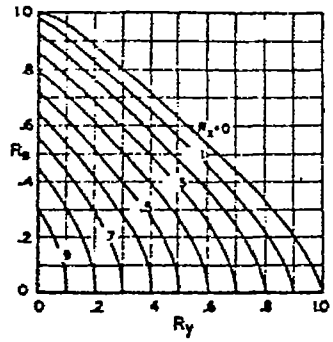

(b) a/b = 1.0.

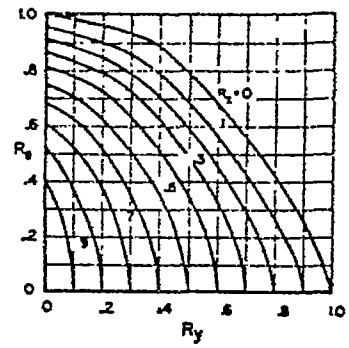

(c) a/b = 1.20.

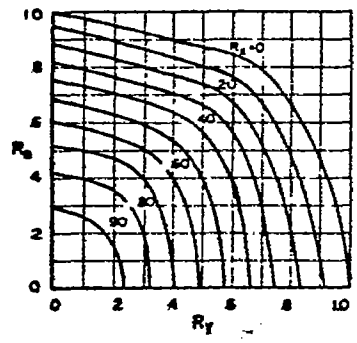

(d) a/b = 1.60.

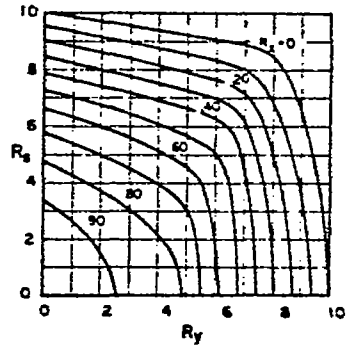

(e) a/b = 2.0.

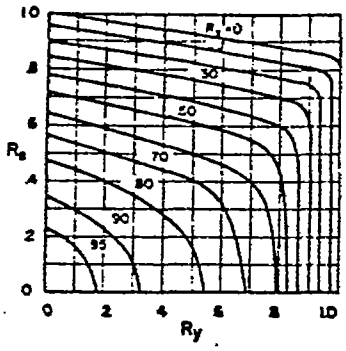

(f) a/b = 3.0.

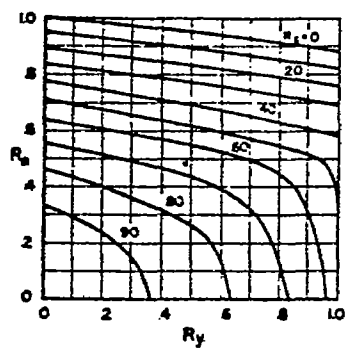

(g) a/b = ∞.

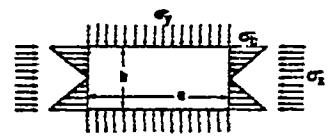

Figure 28.- Interaction curves for flat rectangular plates under combined biaxial-compression and longitudinal-bending loadings. Curves taken from reference 39.

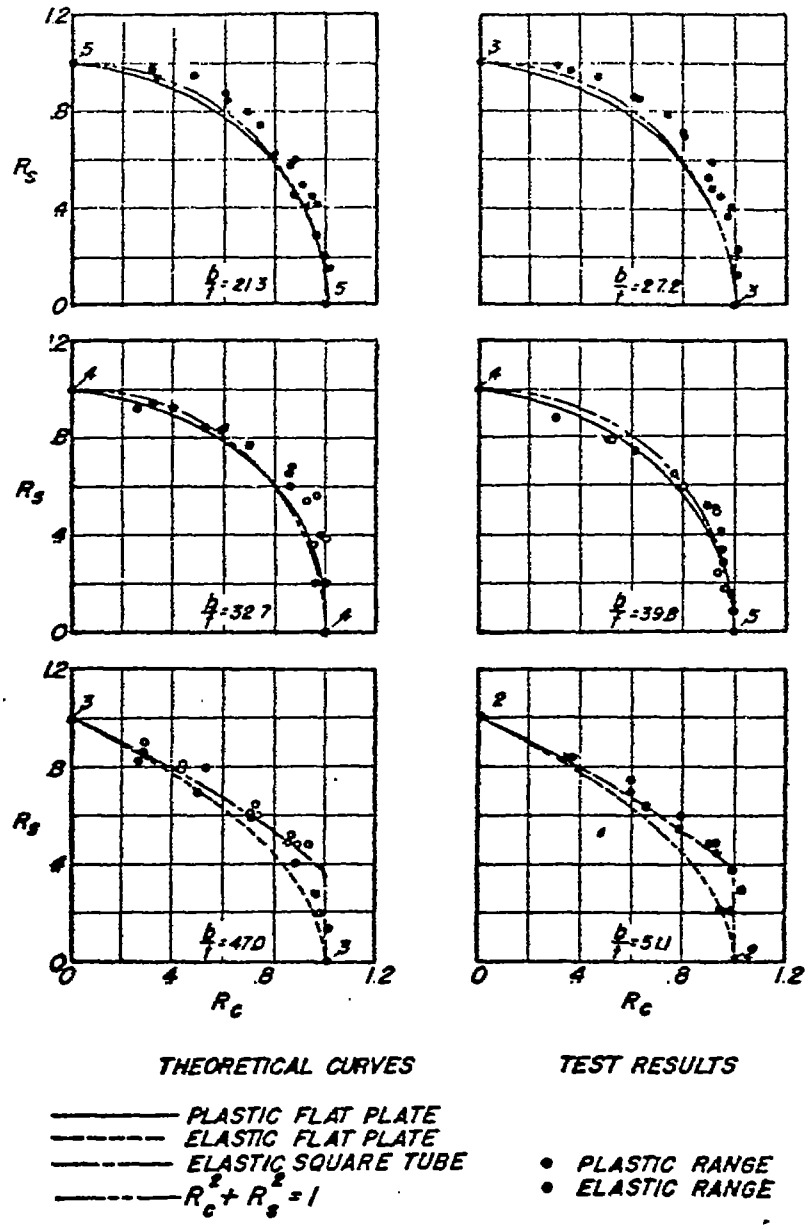

Figure 29.- Comparison of plastic interaction theory and test data for combined axial compression and shear on flat plates. Tests were made with 2014-T6 square tubes.

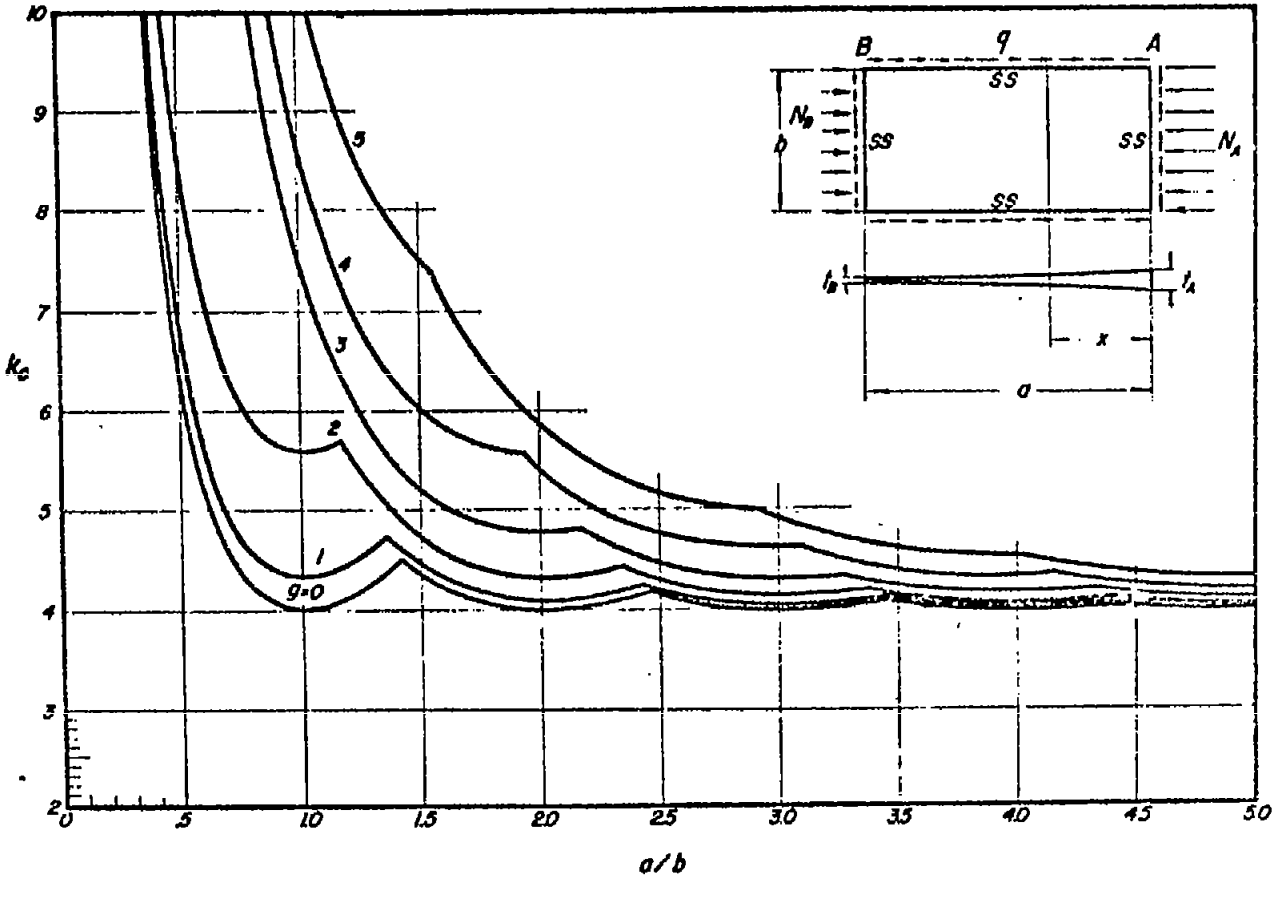

Figure 30.- Compressive-buckling-stress coefficient for a simply supported rectangular flat plate of minimum weight. Thickness and loading vary exponentially along length. $\beta = N_A/N_B$; $g = \log_e \beta$; $N_x/N_A = e^{-gx/a}$; $q/N_A = (gb/2a)e^{-gx/a}$; and $t_x/t_A = e^{-gx/3a}$.

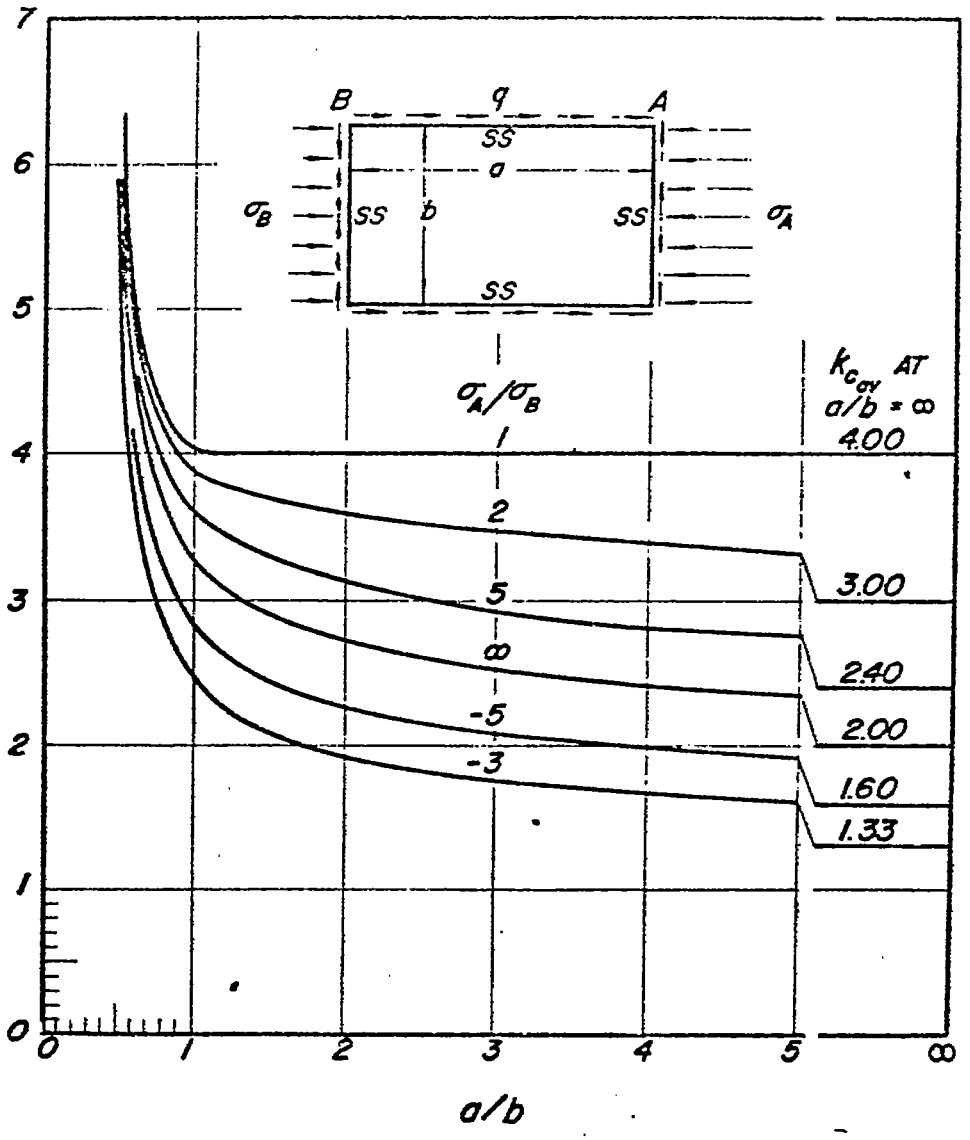

Figure 31.- Average compressive-buckling-stress coefficient for rectangular flat plate of constant thickness with linearly varying axial load. $\sigma_{av} = \dfrac{k_{c_{av}} \pi^2 E}{12\left(1 - \nu_e^2\right)} \left(\dfrac{t}{b}\right)^2$.

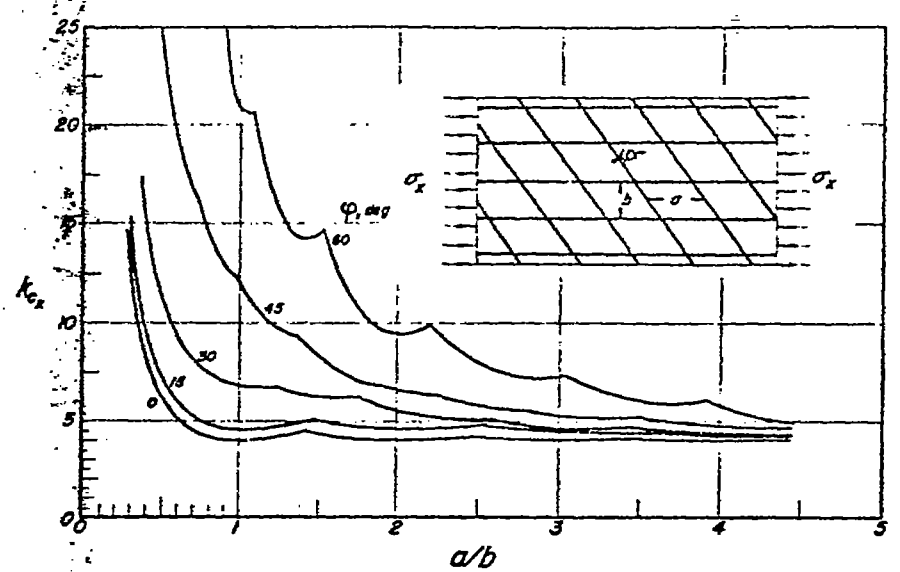

(a) Loading in x-direction.

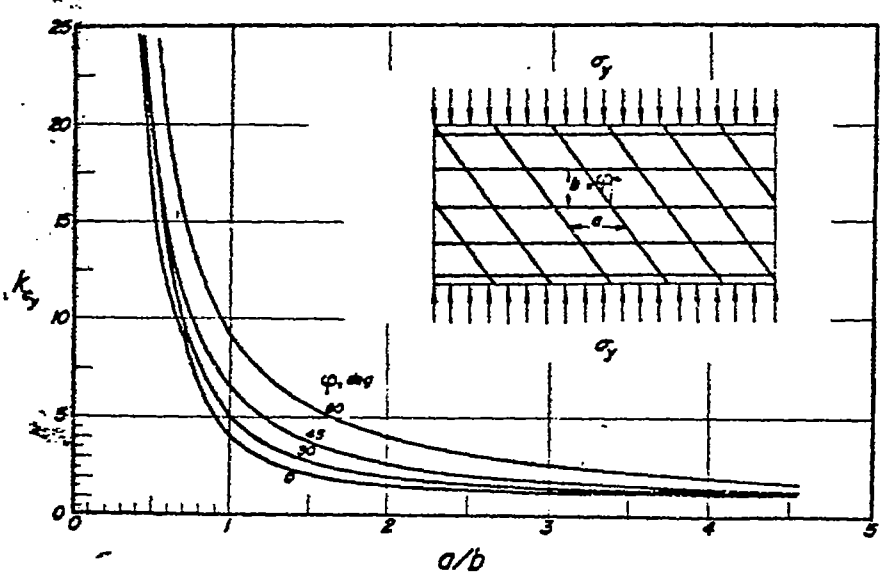

(b) Loading in y-direction.

Figure 32.- Compressive-buckling coefficients for flat sheet on non-deflecting supports divided into parallelogram-shaped panels. All panel sides are equal.

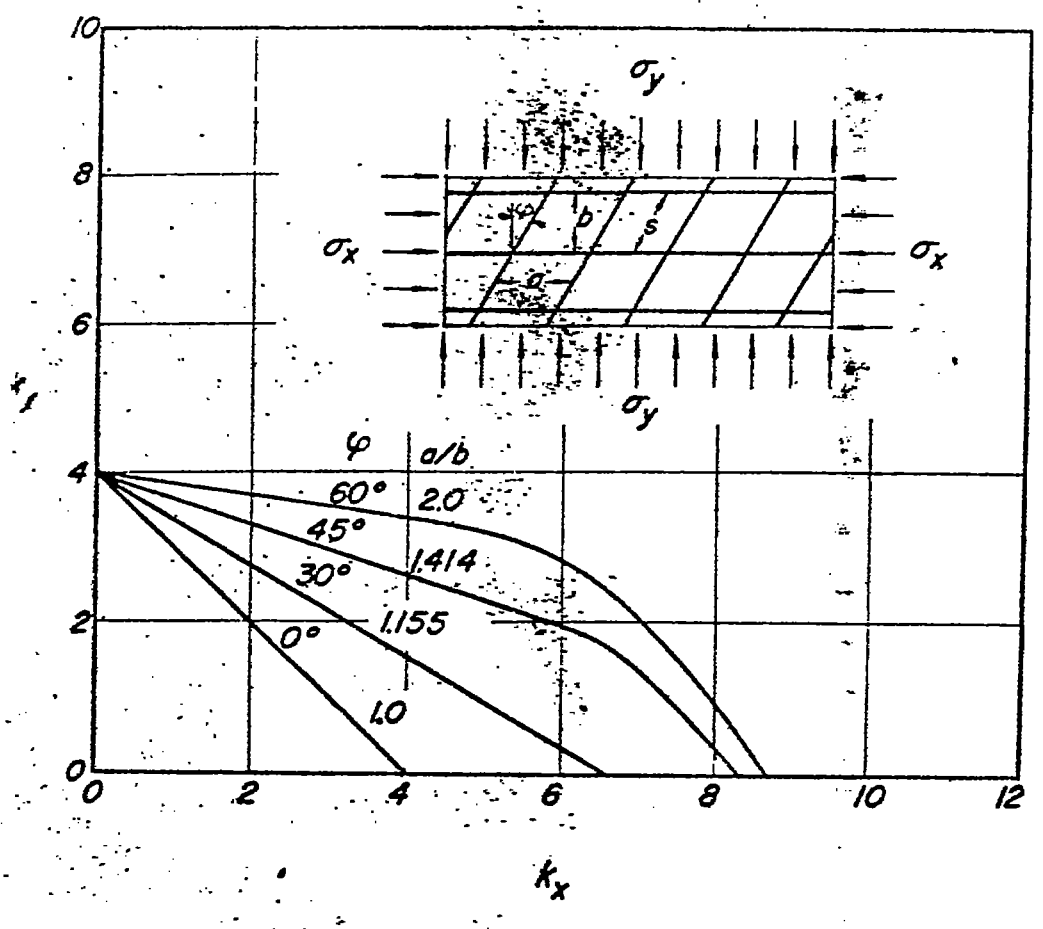

(c) Combined axial and transverse loading.

Figure 32.- Concluded.

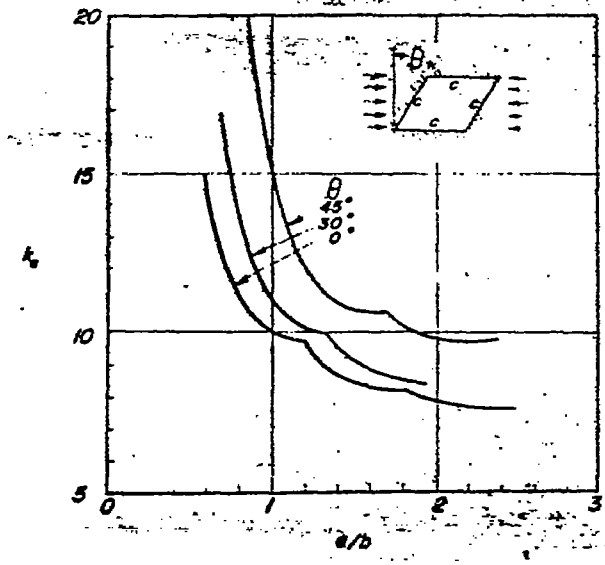

(a) Compressive loading.

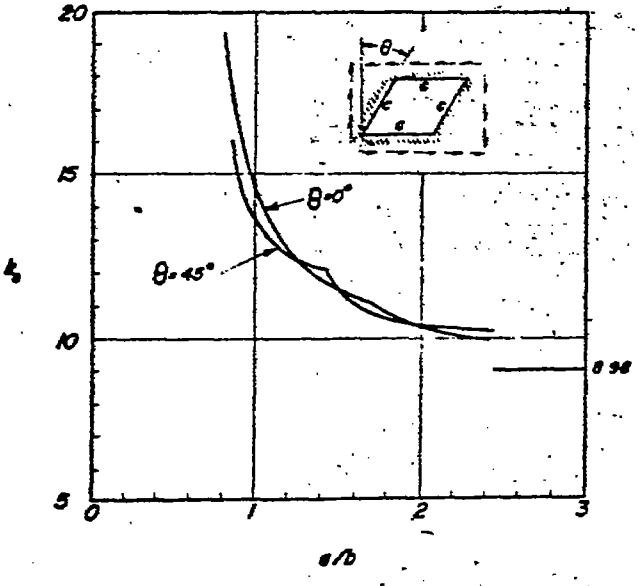

(b) Shear loading.

Figure 33.- Buckling coefficient of clamped oblique flat plates.

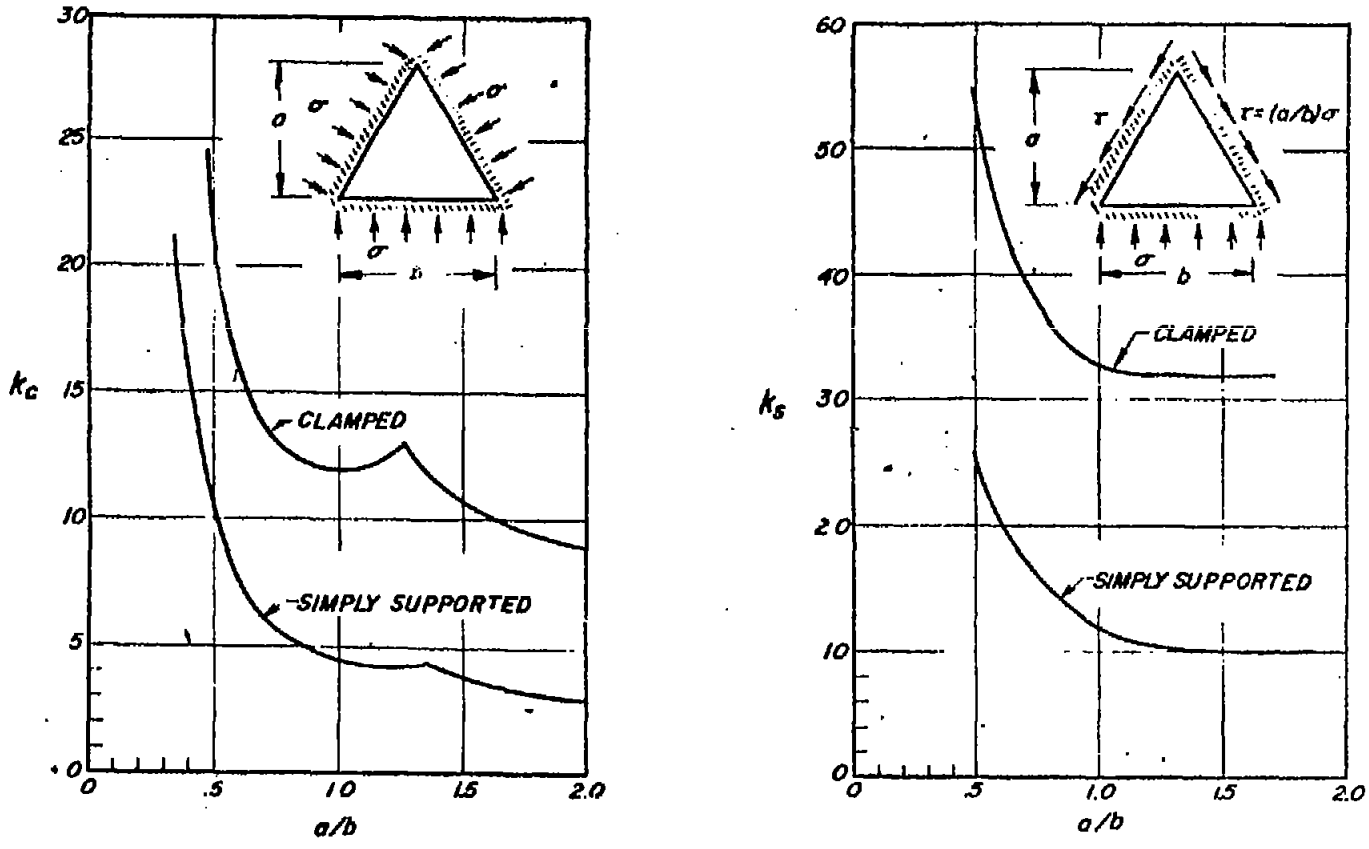

(a) Uniform compression.

(b) Shear

Figure 34.- Buckling coefficients for isosceles triangular plates.

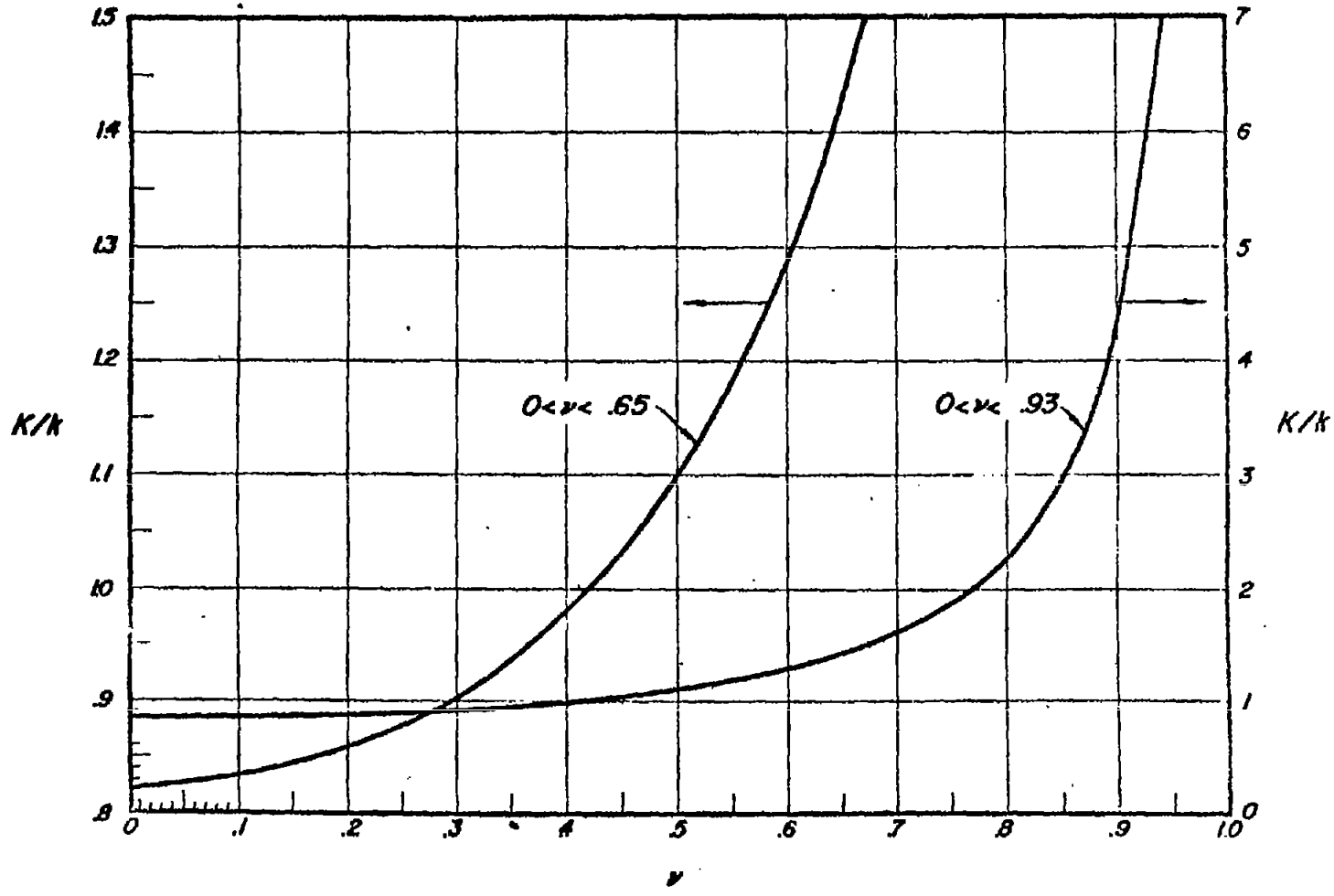

Figure 35.- K/k as a function of Poisson's ratio. $K/k = \pi^2/12(1 - \nu^2)$.